UNIVERSITA' POLITECNICA DELLE MARCHE

FACOLTA' DI INGEGNERIA

Master of Science course in Biomedical Engineering

Curriculum: Engineering of Medical Devices

COST-EFFECTIVE COLLAGEN-BASED 3D-BIOPRINTED SCAFFOLDS AND THEIR POTENTIAL APPLICATIONS AS TISSUE PHANTOMS

Supervisor:

Prof.ssa **Alida Mazzoli**

Co-supervisors:

Prof.ssa **Pasquapina Ciarmela**

Prof.ssa **Francesca Luzi**

Student:

Maria Pia Talozzi

A.Y. 2023/2024

May God bless and keep you always,
May your wishes all come true,
May you always do for others
And let others do for you.
May you build a ladder to the stars
And climb on every rung,
May you stay forever young,
……

May you grow up to be righteous,
May you grow up to be true,
May you always know the truth
And see the lights surrounding you.
May you always be courageous,
Stand upright and be strong,
May you stay forever young,
……

May your hands always be busy,
May your feet always be swift,
May you have a strong foundation
When the winds of changes shift.
May your heart always be joyful,
May your song always be sung,
May you stay forever young,
……

(Forever young, Bob Dylan, 1974)

Introduction

Medical models also defined “phantoms,” have been widely used for medical training. They are increasingly used as medical computational models, for surgical planning, algorithm validation, and for the development of medical devices. Such models not only reproduce the geometric structures of human organs, but also possess the properties and functions of the organ structure. With the rapid advancement of three-dimensional (3D) printing and 3D-bioprinting technologies, these additive manufacturing techniques have been widely explored to fabricate functional medical phantoms for various applications. Realistic phantoms of biological tissues are becoming of high interest in the field of tissue engineering, creating *in vitro* models to better understand tissue development, disease mechanisms, to test and screen drugs, to study tumour behaviours and tumour drug resistance. Since their invention in the 1980s, the techniques for three-dimensional (3D) printing, formally Additive Manufacturing (AM), have been developed and used for various applications by many researchers and industrial companies worldwide. In its early years, 3D printing was primarily a rapid prototyping technique; today, it is radically changing manufacturing and many other industries with new processes, materials, and applications. In addition to plastic prototypes, complex engine components, houses, food, and even human organs can be 3D-printed; medical field represents a major market for 3D printing, a technique showing great potential for personalized medicine and care. Currently most common medical applications of 3D printing include custom-made dentures, hearing aid shells, surgical and medical models, orthotic and prosthetic components, and artificial hip and knee implants *[Wu J. et al., (2017); Banks J. et al., (2013); Klein GT et al., (2013); Gross BC et al., (2014); Zopf D.A. et al., (2013)].*

3D-printing technology is also used for fabrication of phantoms of body parts, useful for doctors when preparing or planning complex medical operations or procedures *[Gross BC et al. (2014)].* Such phantoms can also be effective tools for medical training and patient education purposes.

3D-bioprinting technology has been developed since early 2000s; it consists in deposition, layer by layer, of bioinks made of cells plus a gel media to build up 3D bio-functional structures. The final objective is to use the 3D printing technology for tissue engineering (TE) applications to build tissues, organs and body parts [*Mironov V. et al., (2003); Murphy S.V. et al., (2014)].*

3D-printing technologies overcome the drawback of traditional manufacturing processes and

represent an effective tool for producing patient-specific, high-fidelity, medical phantoms rapidly and at a low cost. Due to the increasing demand for tissue and organ transplantation, and the lack of tissue and organ donors, numerous efforts have been made in the field of tissue engineering to develop biological substitutes for human tissues and organs *[Atala A. et al., (2006); Furth M.E. et al., (2007); Place E.S. et al., (2009)].*

For tissue engineering purposes, biodegradable scaffolds with high porosity and interconnectivity can be employed to provide shape, mechanical support, and microarchitecture for cellular growth and reorganization to improve and accelerate the healing and repairing process *[Furth M.E. et al., (2007); Kao C.T. et al., (2015)].*

Different strategies for creating 3D scaffolds have been proposed and investigated, such as freeze-drying *[Haaparanta A.M. et al., (2014); Campbell J.J. et al., (2017)],* gas foaming *[Rossi E. et al., (2016)]*, phase separation *[Akbarzadeh R. et al., (2014)],* porogen leaching *[Guarino V. et al., (2008)],* and electrospinning *[Gasemi-Mobarakeh L. et al., (2008); Orr S.B. et al., (2015)].* However, a precise control of the porosity and inner microstructure of the scaffold manufactured by these techniques, with the purpose of controlling oxygen, nutrients, and soluble biomolecules for promoting cell growth and differentiation, is still challenging. In addition, the possibility of managing different types of cell growth in tissue engineered scaffolds to form functional complex tissues, remains a major engineering design issue.

Although autologous cell-laden scaffolds with simple structural design have demonstrated their capability of driving the regeneration of multifunctional tissues and organs in vivo *[Atala A. et al., (2006); Raya-Rivera A. et al., (2011); Warnke P.H. et al., (2004)],* advanced strategies for manufacturing acellular or cell-laden bio-scaffolds with higher levels of complexity are still in progress *[Furth M.E. et al., (2007); Bertassoni L.E. et al., (2014); Cheng Y.L. et al., (2016); Yeo M et al., (2016); Ouyang L. et al., (2017)].*

An increasing interest is oriented to the creation of complex and functional 3D bio-scaffolds, with the use of specific biomaterials and cells, to provide a microenvironment similar to native tissue. Many studies have focused their attention on the development of a robotic dispensing system for bioprinting (extrusion-based bioprinting), because it represents an easy-to-use system and for its good compatibility with different bioinks *[Liu W. et al., (2017)].*

Extrusion-based bioprinting allows the manufacture of 3D constructs on a millimetre scale by the pneumatically or mechanically driven dispensation of biopolymers or synthetic polymers in a

layer-by-layer fashion *[Liu W. et al., (2017); Melchels F.P.W. et al., (2014); Akkineni A.R. et al., (2016); Ho C.M. et al., (2017)].*

Spheroids and organoids composed of multiple cellular types can be used as the building blocks for large tissues and organs production: printed using extrusion-based bioprinting *[Mironov V. et al., (2009); Itoh M. et al., (2015)],* can be used as phantom tissues in the field of drug, cancer and disease research.

In tissue engineering strategies, biomaterials are essential components: it is well known that cellular environment (the Extracellular Matrix) and the cell interactions (cell-cell interaction and cell-matrix interaction) play a key role; it is for this reason that it is important to select the proper polymer for a given application. Biomaterials used for this purpose can be natural or synthetic polymers, degradable (in a certain time span) or non-degradable.

Scaffolds can be made by one polymer only or can be composite/blend scaffolds; in any case their physicochemical properties, including biocompatibility, biodegradability, mechanical strength, porosity represent fundamental aspects *[Runxuan Cai et al. (2023)].*

In this thesis, after a short introduction regarding the biological and technological aspects inherent the 3D-bioprinting, will be described the activities, the main aspects to consider in developing a new bioink and the main results obtained in this multi-step work.

The core material selected is collagen, that represents the main structural component of the human extracellular matrices, chosen for its low antigenicity, high biocompatibility, functional activity. Collagen consists in a wide family of fibrillar and non-fibrillar proteins, but in this work has been considered mainly Collagen type I, the most represented in skin, tendons, cartilage, bones, cornea/eyes structures, for its wide potential of application.

Two collagen-based blends have been developed, one obtained blending collagen and alginate, the second one mixing collagen with gelatine and alginate, with the purpose of using the advantages of each component minimizing the respective disadvantages. All the components used are for alimentary use, from bovine source collagen and gelatine, from brown algae alginate; all these products are widely available and largely affordable.

About the cells used to test biocompatibility of the bio-blends, has been used SK-LMS-1 cell line, derived from a leiomyosarcoma of vulva of a 43 years-old white female, mixed with the two

blends developed to form the bioinks and 3D-bioprinted with the pneumatic Cellink Inkredible+ 3D bioprinter.

The aim of this work was to develop and test hydrogels based on the use of cost-effective biomaterials, assessing blend properties, with the purpose of creating a library of biomaterials and bio-scaffolds to be used on large scale as tissue phantom in tissue engineering, in biological and cancer research, for drug development and, for education purpose.

1. Extracellular Matrix (ECM)

In the human body, almost all the cells interact with extra cellular matrices (ECMs), which have tissue and organ-specific composition and architecture. These ECMs not only function as cellular scaffolds, providing structural support, but also play a crucial role in regulating cellular functions: cellular environment (fig.1) is considered the core element for fabricating functional, complex tissue models *in vitro,* reproducing cell-cell interactions and cell-matrix interaction, important for cell behaviour, as migration, proliferation, apoptosis, anoikis.

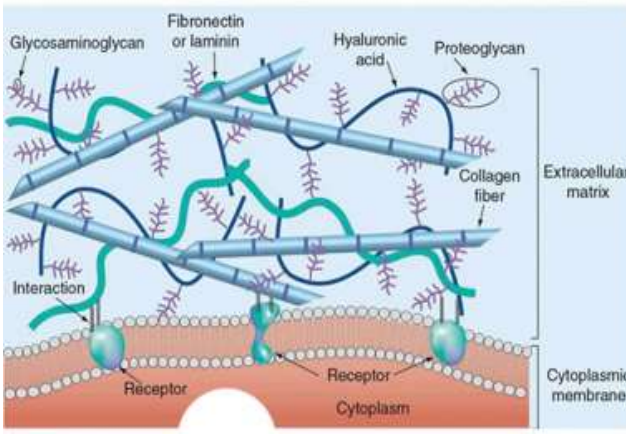

Fig.1: 3D_structure model of the natural ECM *(from Aghmiuni-Khiavi, 2017).*

Cells can react not only to the physical characteristics of their microenvironment, but also to chemical gradients: materials and tissue models with adequate physical and biochemical signals from extracellular matrix (ECM), are essential in tailoring cell-matrix and cell-cell interactions *[Zamir E. and Geiger B., (2001)].*

Although the two-dimensional (2D) cell culture model has significantly contributed to biological research, it has been proved to have poor representations of the cellular interactions that take place in vivo, and this aspect has been demonstrated to be extremely important in cancer research: drugs showing promising cytotoxicity in 2D *in vitro* systems, present weak or no efficacy in real patients with tumours, resulting in a significant delay of anticancer drug development *[van der Worp H.B. et al., (2010)].* To reduce the impact of this problem, the disciplines involved in tissue engineering have directed their interest toward materials and 3D structures able to emulate the ECM and the tumour microenvironment (TME) with the objective to construct highly accurate *in vitro* 3D tissue models, providing a basis for reproducible and quantifiable investigations.

The ECM represents an intricate network composed of an array of multidomain macromolecules organized in a cell/tissue specific manner. The structures and properties of the ECM change from cell to cell *[Yue B., (2014)]: f*or example, the ECM of the cornea is a transparent and soft sheet, while the ECM of the bone is extremely hard. As the natural microenvironment in which cells live, the ECM of each tissue and organ is unique in both physicochemical and biological properties *[Watt F.M and Huck W.T.S., (2013)].*

The ECM provides cells with mechanical support and biochemical signals to promote cell proliferation and differentiation, among other functions *[Gattazzo F. et al., (2014)].*

The native ECM is complex in terms of composition, and it mainly contains collagen, non-collagen glycoproteins (such as fibronectin, laminin, and tenascin), glycosaminoglycans (such as hyaluronic acid), and proteoaminoglycans. *[Choudhury D. et al., (2018); Dzobo K. et al., (2019)].*

Collagen is the most abundant and ubiquitous protein in the body, accounting for approximately 25–30% of the total vertebrate proteins *[Ricard- Blum S., (2011)].* Type I collagen is the dominant fibrillar component of the ECM in mammals. It provides cells with a 3D environment that supports cell growth and influences morphology and function.

With respect to tumour research, it is today clear that three-dimensional (3D) cell culture systems offer an excellent opportunity to recapitulate the real avascular solid tumour, by allowing cancer cells to be cultured, either alone or in co-culture with other cell types, in a spatial manner simulating the structural architecture of the tumour that provides cell–cell and cell–ECM interactions, mimicking the native tumour microenvironment. The cross-talk between the different cells and components of the tumour microenvironment (TME), plays an essential role in tumour growth, progression and metastasis *[Roma-Rodrigues C. et al, (2019)].*

Cancer cells are experts in modifying their surrounding environments: cancer cells can co-opt fibroblasts to obtain growth factors, necessary to sustain their own growth and proliferation. Additionally, tumour cells can interact with the surrounding endothelial cells, promoting the release of soluble factors, like vascular endothelial growth factor (VEGF), to trigger the angiogenic process. Tumour cells can also evade the immunosurveillance systems through different strategies. *[Pitt J.M. et al., (2016)].*

Tumour cells themselves can alter the organization and protein deposition of the ECM, forming a physical barrier that prevents drug penetration into tumour cells *[Najafi M. et al., (2019); Sangaletti S. et al., (2017)],* accumulation, and efficacy, leading to tumour resistance to therapy *[Hanahan, D. et al., (2011)].*

This is the reason why new therapeutic strategies have been developed to target the tumour-promoting microenvironmental factors to block the interaction between tumour cells and the TME *[Roma-Rodrigues C. et al, (2019)].*

Thus, discovery and testing new anticancer drug candidates requires preclinical models more physiological than conventional 2D cultures, capable of recapitulating these TME aspects. In this sense, spheroids provide the appropriate model of the pathophysiologic parameters present in the real tumour, because they replicate the complex multicellular architecture, the barriers to mass transport, and extracellular matrix deposition, which explain their growing use as models for better prediction of drug effects and delivery in the last decades *[Kitaeva K.V. et al., (2020)]*.

2. 3D-bioprinting

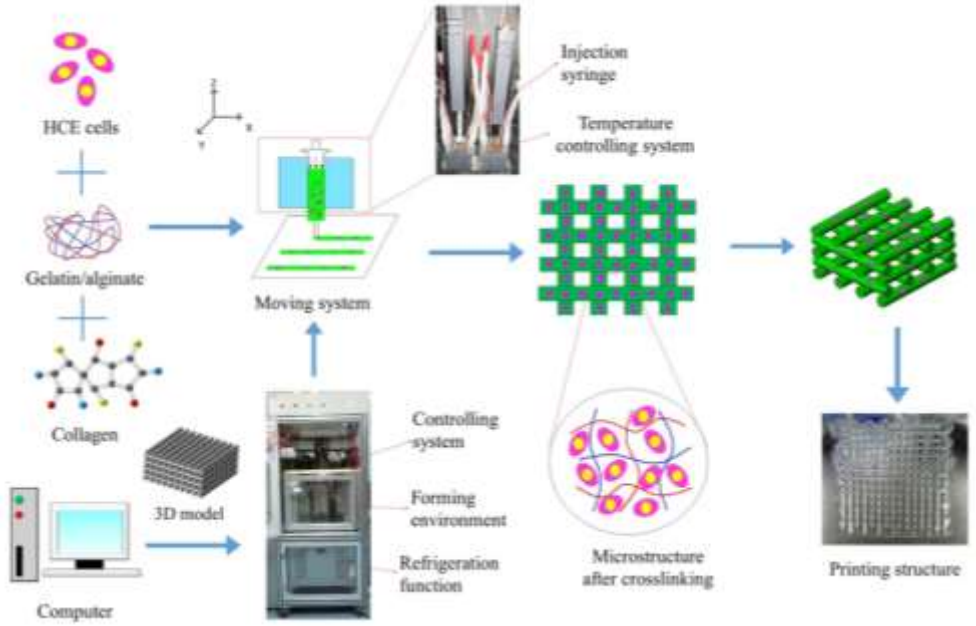

Fig. 2: Schematic illustration of the 3D bioprinting process and optical images of the printing setup and construct (*from Bioprinting three-dimensional cell-laden tissue constructs with controllable degradation Zhengjie Wu, Xin Su, YuanyuanXu, Bin Kong, Wei Sun, Shengli Mi)*

Three-dimensional (3D) printing is a rapid prototyping technology that creates 3D physical objects layer by layer *[Chatterjee K. and Ghosh T.K., (2020)].* Since the invention of the first 3D printing technology, stereolithography in 1983, numerous 3D printing technologies have been developed *[Kulkarni P. et al., (2000)].*

The American Society for Testing and Materials International Standard has classified 3D printing technologies into seven categories on the base of the different principles: 1) material extrusion, 2) powder bed fusion, 3) vat photopolymerization, 4) material jetting, 5) binder jetting, 6) sheet lamination, and 7) energy deposition.

3D printing can quickly fabricate various structures with little waste of material: it is for this reason, together with the gradual reduction of the cost and personalized customization, that 3D printing has become widely used in many industrial fields. As for regards the medical sector it is used for anatomical modelling, custom made prostheses manufacturing and tissue engineering *[Ma D. et al., (2022)].*

An important branch of 3D printing, the 3D bioprinting, is a combination of 3D printing and biology [Munaz A. et al., (2016)], used to replicate in structure and function their natural counterparts, printing bioinks (fig. 2) [Matai I. et al. (2020)].

Bioinks are the natural or synthetic biomaterials loaded with living cells and represent the raw material of 3D bioprinting processes *[Hospodiuk M. et al., (2017)].*

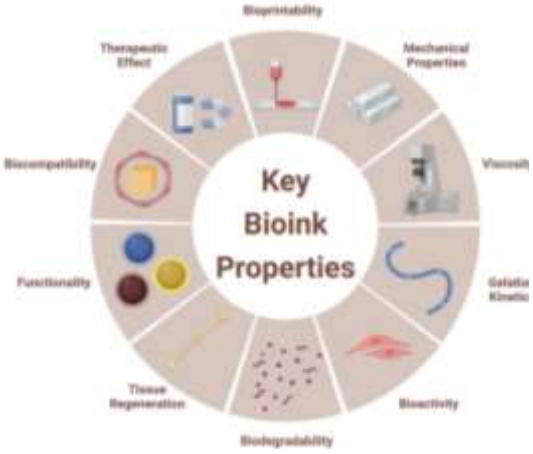

Fig.3: Key properties of the bioink in 3D bioprinting (*from Runxuan Cai et al. (2023)).*

Selection of bioinks is a basic factor in 3D bioprinting; it is important for such materials to present a good printability, biocompatibility, together with mechanical and degradation properties (fig. 3) *[Mao H. et al., (2020)].*

The materials used for 3D bioprinting are generally divided in two categories: naturally derived biomaterials (such as collagen, hyaluronic acid, gelatine) and synthetic biomaterials (such as polylactic acid (PLA), polycaprolactone (PCL), and polyurethane (PU)). These materials present different advantages and disadvantages: the naturally derived biomaterials have good biocompatibility, but their mechanical properties are weak; on the other hand, synthetic biomaterials present lower biocompatibility, but have adjustable properties *[Park S. et al., (2022)].*

When replicating a functional living tissue microenvironment, to obtain a good result, it is necessary to reproduce the composition of the desired tissue or organ. One single material cannot reproduce all the functions of native tissues and organs because, biological tissues, are made of various cell types and their extracellular matrices (ECMs) present different composition. *[Wang H. et al., (2022)].*

2.1 Bioprinting Process. The typical steps in the 3D bioprinting process, include pre-processing, processing and post-processing stages.

2.1.1 The pre-processing step includes the culture of human cells and the design of a scaffold model for 3D bioprinting. The selected cells, need to be expanded *in vitro* to obtain a number sufficient to be mixed with the biomaterials. The creation of a 3D model allows the usage of data generated by computer-assisted design software (CAD, Solidwork) *[Wust S. et al., (2014)]* or

imported data from medical imaging such as MRI and CT scan *[Kang, H.W. et al., (2016)]*. The generation of a 3D model using patient-specific tissue size and morphology enables the creation of a customized 3D construct that is a closer reproduction of the human tissues. The 3D model is converted to a standard tessellation language (.STL) file and then saved as a file format such as G-code. The file format can be easily used by the printer and drives the layer-by-layer deposition of the biological elements *[Chang, R. et al., (2010)]*

2.1.2 The processing step allows to fabricate the 3D cell-laden constructs by 3D bioprinting. The most used bioprinting systems are based on three major strategies: inkjet, laser, and extrusion-based bioprinting. Generally, a three-axis mechanical platform controls the movements of the extruders, printing the biomaterials on the base of the 3D tissue models *[Derakhshanfar S. et al., (2018)]*.

2.1.3 Post-processing involves the maturation of cell-laden constructs to reinforce the development of desired tissues. The optimal nutrition and oxygen delivery, as well as removal of waste, are required to maintain cell viability and functionality. Growth factors are commonly used and play a key role in cell division, matrix synthesis, and tissue differentiation *[Hughes F.J. et al., (2006)]*.

Table I: Comparison of three types of bioprinting techniques.			
Bioprintig technique	**Inkjet-Based Bioprinter**	**Laser-Assisted Bioprinter**	**Extrusion-Based Bioprinter**
Cost	**Low**	**High**	**Moderate**
Material viscosities	3.5-12mPa/s	1-300mPa/s	30 to>6x10^{7}mPa/s
Resolution	10-100µm	~75µm	100µm-mm range
Quality of structure	Poor	Fair	High
Print speed	Fast	Medium	Slow
Cell viability	>85%	>95%	40-80%

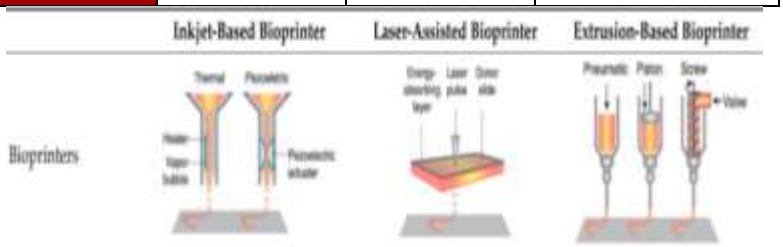

Fig. 4: comparison of 3 types of bioprinting techniques *(modified from Malda J. et al., 2013)*

2.2 Bioprinting Techniques. Several additive manufacturing techniques have been used to fabricate 3D scaffolds *[Bose S. et al., (2013)]*. Among them, inkjet-based, laser-assisted, and extrusion-based bioprinting (fig. 4), are the most used to fabricate 3D cell-laden scaffolds for human tissues. Each bioprinting technique presents specific strengths, weaknesses and limitations. In Table I, is presented a comparison of three approaches.

The bioprinting method selected, depends on the considerations of biological issues and their complexity, resolution and cell structure.

2.2.1 Extrusion-Based Bioprinting. The extrusion-based bioprinting technique, combines both a fluid-dispensing system and an automated robotic system for extrusion and printing respectively *[Mironov, V. et al., (2003)].* The fluid-dispensing system can be driven by a pneumatic- or mechanical- based power source. By applying a continuous force during the bioprinting process, bioink is printed as a continuous cylindrical filament rather than a single bioink droplet. Recently, the trend of extrusion-based bioprinters is a multi-head tissue construction. One of the main advantages of extrusion bioprinters is their ability to print a wide range of biomaterials with different viscosity including hydrogels, biocompatible copolymers, and cell spheroids from 30 to 6×10^7 mPa/s (Table I) *[Jones, N., (2012)].*

3. Bioink

Definition. A bioink is a material suitable for use in an extrusion based dispensing system, known as a bioprinter, that allows the printing of living cells and growth factors. Often bioinks possess shear thinning characteristics but this property is not necessary for every bioink. Viscosity of bioinks can range from water-like to a paste-like consistency: a wide diversity of bioinks exists (*Paige Ford, 2019).*

The selection of proper bioink is crucial for successful bioprinting, because it will provide the required properties for adequate printing fidelity and mechanical properties to ensure printability and long-term functionality following deposition *[Murphy S.V. et al., (2014)].*

3.1 Thickening agents can improve the printability of a bioink; a thickening agent can increase the viscosity or change the rheometric properties of a biomaterial, without significantly changing other characteristics. Additionally, these thickening agents can stabilize emulsions, (*Paige Ford, 2019)* for instance allowing crosslinking. In fact, in the last three decades, low viscosity biomaterials such as collagen, fibrinogen and matrigel have been developed and have similar viscosity to water prior of crosslinking or self-assembly. These materials are not bioprintable on their own because they cannot form continuous filaments, so thickening agents are added to stabilize a bioink. Common thickening agents in bioprinting include nanofibrillar cellulose, alginate, bentonite, PEG/PEO, Xanthan, Gellen.

A further advantage in the use of thickening agents is represented by the great reduction of the costs because of the lower quantities of the expensive biomaterial to obtain the same result, without any increase of the biomaterial concentration. These thickeners can either be permanent components of a bioprinted construct or be eliminated after bioprinting. An ideal bioink-filler would be degraded by the cells. Thickeners may also be used to soften or stiffen the bioprinted filament by a disrupting or crosslinking process. Additionally, certain thickeners can reduce the sensitivity of a bioink to temperature changes or drying out, improving the effective “printability window” *[Malda J. et al., (2013)]*.

3.2 Bioink composition. Biomaterials, cells and bioactive molecules have always been considered the important components of bioinks, which are used to print structures like natural tissues *[Yang et al., (2020)].*

3.2.1 Biomaterials. Human tissues have complex structure, and a single biomaterial cannot usually meet all mechanical and functional requirements, which are essential to produce biomimetic tissue-like constructs [Ashammakhi et al., (2019)]. One of the most important strategies to solve this problem is the use of multimaterial bioinks. ECM biomimetic bioinks with high performance, have been generated by blending other materials with unique properties and by the inclusion of fillers and additives with distinct properties.

The materials commonly used for constructing bioinks are divided into two categories: synthetic polymers, such as polycaprolactone (PCL), polylactic acid (PLA), polylactic acid-glycolic acid (PLGA), polyethylene oxide terephthalate-co-butylene terephthalate (PEO/PBT), and natural polymers such as collagen, gelatine, alginic acid, hyaluronic acid, decellularized extracellular matrix, agarose, and nanocellulose *[Agarwal et al., (2021)].* Natural biological materials, have the advantages of biological activity, non-toxic degradation products, high similarity and excellent biocompatibility with the ECM. Synthetic biomaterials are less restrictive in 3D printing because their structure and properties can be adjusted according to needs.

3.2.1.1 Natural Polymers. Collagen is widely found in all tissues; it is the most abundant and ubiquitous protein in the body, accounting for approximately 25–30% of the total vertebrate proteins *[Ricard-Blum S., (2011)].* Collagen is highly heterogeneous: it represents a family of collagen proteins which differ in characteristic, location, molecular and spatial structure. The two main collagen groups are fibrillar and non-fibrillar collagen *[Ricard- Blum S., (2011); Sorushanova A. et al., (2019)].* Fibrillar collagen forms fibrils, constituting about 90% of all collagen present in the human body. It is encoded by 11 genes and is made of three polypeptide chains with an α-helix structure, separated by short non-helical fragments called telopeptides. The spatial structure of fibrillar collagen is cross-striated with transverse bands repeating every 64–67 nm (Fig. 5a,b). Non-fibrillar collagen is different in terms of

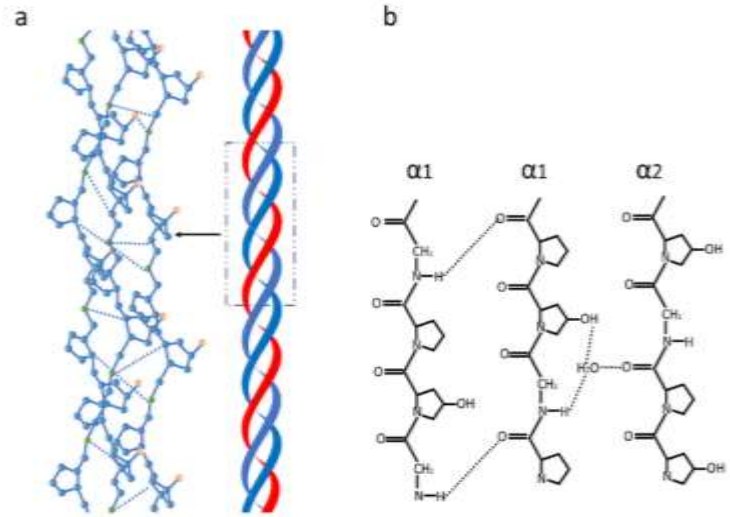

Fig. 5: (a) the triple helix of type I collagen. (b) Hydrogen bonds of the collagen model (*from Zhang et al. Journal of Leather Science and Engineering (2020)).*

structure, distribution and properties. Although it represents only the 10% of all the collagen in the human body, it is a vital part of many organs *[Gelse K. et al., (2003); Holmes D. et al., (2018)].*

Collagen is the dominant element of connective tissue extracellular matrix (ECM). Due to its physicochemical properties, collagen is responsible for the integrity, strength and elasticity of tissues. Collagen plays an important role in the healing process, tissue growth, regeneration but, also participates in the processes of cells adhesion, growth and differentiation. These collagen functions take place mainly due to the specific structure of its fibres. Its spatial structure, called a superhelix, provides the beneficial properties of collagen, especially very high mechanical strength *[Meyer M., (2019); Birk D.E. et al., (2015); Brodsky B. and Ramshaw J., (1997)].* Collagen is one of the most widely used biomaterial in tissue engineering, included in the 3D bioprinting. However, collagen is temperature-sensitive and prone to degradation during most sterilization processes, so collagen scaffolds often need to be cross-linked or used in combination with other materials. The 3D collagen scaffolds, with high porosity, permeability and biocompatibility, could facilitate the formation of new tissues *[Cheng et al., (2021)].* Although collagen has good biocompatibility, it is difficult for collagen to form a bioink with appropriate viscosity. The formed scaffold has low strength, and the pH needs to be adjusted before using collagen as a biomaterial, because the fibres formed under neutral pH conditions give a physical gel within 30 min at room temperature, and at low concentration *[Mazzocchi et al., (2018)].*

Gelatine is another commonly used 3D bioprinting material; it is a natural protein derived from collagen hydrolysis. Gelatine is non-cytotoxic, water-soluble, presents high water absorption and no immunogenicity; it is biocompatible, and promotes cell adhesion. Gelatine can replace collagen in 3D bioprinting due to better physical properties but can also be used as additional material to form a blend. Like collagen, gelatine must be treated with acid or alkali before its use *[Yue et al., (2015)].*

Constructs containing gelatine, can be crosslinked by the glutaraldehyde, but this approach reduces the biocompatibility of the scaffold. Based on this characteristics, pure gelatine is usually used as a sacrificial material in 3D bioprinting, as it is conducive to the transmission of oxygen and nutrients. In order to retain the biocompatibility of gelatine and enhance its mechanical strength, the modification of gelatine and the use of UV cross-linking have been considered by a large number of researchers *[Billiet et al., (2014)].*

Alginate is a natural, seaweed-derived, and ion-sensitive anionic polysaccharide *[Neufurth et al., (2014)].* It is biodegradable, and non-immunogenic; it has been widely used in tissue engineering application as biomaterial for bioink, because of its low toxicity, good biocompatibility, fast crosslinking and the shear thinning properties. *[Bouhadir et al., (2001); Rastogi and Kandasubramanian, (2019)].* The main disadvantage of alginic acid hydrogel is the low bioactivity. Alginate can provide a cytoprotective effect against processing pressure stress and can form a hard gel with the use of a crosslinking agent as calcium chloride ($CaCl_2$), a chelating agent applied immediately after the 3D printing, able to crosslink alginate via sodium–calcium ion exchange reaction at room temperature *[Demirtaş et al., (2017)].* The limitation of alginate is the short cell-binding domain on the polymer chain, and calcium ions may cause inflammation in the body *[Chan G. and Mooney D.J., (2013)]*.

3.2.2 Cells. The selection of the cell type is crucial for 3D bioprinting and depends on the biological tissue under study and to replicate. Not all tissue-specific cells can be isolated and cultured *in vitro*, and not all cells can maintain their biological activity after undergoing a 3D bioprinting process. Therefore, how to optimise cell separation, culture and enhancement of proliferation technology have always been the focus of exploration and improvement of 3D bioprinting.

Stem cells have a broad application potential in the fields of cell repair, developmental biology and pharmacology. The 3D bioprinted scaffolds containing live macrophages and antibiotics demonstrated to promote the clearance of Staphylococcus aureus associated to craniotomy biofilm infections *[(Aldrich A.et al., (2019)].*

The neuron is the most basic structural and functional unit of the nervous system, and its function is to receive stimulation, generate and conduct excitation. Neuron damage, which often causes irreversible damage to patients, has always represented a major clinical difficulty. By formulating specific neural tissue bioinks, printing neuronal structures and precisely controlling the microenvironment in 3D space, may represent a new therapy in the future *[Knowlton S. et al., (2018)].*

Cancer cells can spontaneously assemble into spheroids in 3D culture environment that privileges cell–cell and cell–ECM interactions over cell–substrate interactions, as typical of 2D culture environment *[Białkowska K. et al., (2020)].* These predominant cell–cell and cell–ECM interactions result in the formation of a 3D structure able to reproduce the spatial organization and environment

of avascular solid tumours, where cells can proliferate, aggregate and differentiate *[Białkowska K. et al., (2020)].*

Spheroids have a diameter of 200µm or more, generally with a spherical shape, and display three concentric zones of heterogeneous cell populations (Fig. 6), recapitulating many characteristics of the *in vivo* solid tumours, such as nutrient and oxygen gradients, the morphology and polarity of the cells, as well as gene expression and activation of cell signalling pathways *[Pinto B. et al., (2020)].* These features make spheroids a promising model for the study of cancer biology, cancer initiation, invasion and metastatic processes, as well as drug testing *[Imamura Y. et al., (2015)].* On the base of the composition of the bioblends, the spheroids formed will be different in shape, dimension and number.

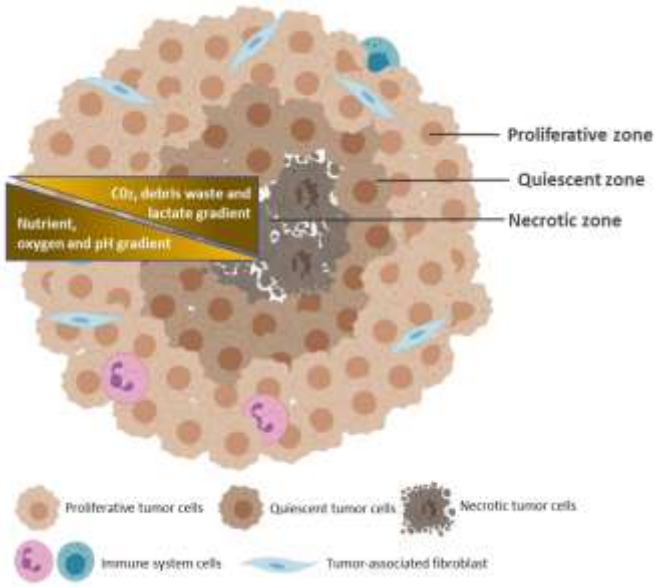

Fig. 6: Typical structure of a multicellular tumour spheroid. The geometric rearrangement of the cells within the spheroid forms three concentric zones of cell populations: an external proliferating zone (Proliferative zone); a middle zone of quiescent cells (Quiescent zone), and an internal zone of necrotic cells (Necrotic zone). These cell layers are due to the gradients of nutrients, oxygen, and pH, from the outside to the centre of the spheroid (Necrotic zone) and by the gradients of CO_2 and lactate, from the centre to the outside *(from Pinto B. et al., (2020)).*

3.2.2.1 Gompertzian cell growth model. Gompertz's equation represents the most important model of tumour cell growth as this model presents a good fit to data and simplicity. The key assumption in the Gompertz model is that the cell growth rate decreases as function of time (t). Because of this decrease of the growth rate, the dimension of the tumour mass reaches an asymptotic value (carrying capacity). *[Alzahrani E.O. et al., (2014)].* Many other models followed the Gompertz's model equation, but in this section, will be just described the deterministic formulation of Gompertz cell growth model introduced by Benjamin Gompertz in 1825, and the typical sigmoidal curve describing the model. The dependence of the size x(t) of the growing tumour on time (t) is well described by the differential Gompertzian equation

$$dx/dt = a*n - b*n*\ln(n) \quad (1)$$

where *a*, is the rate of growth of the tumour, a parameter related to the initial mitotic cellular rate, and *b* is the damping factor of growth, mainly represented by antiangiogenic processes.

The objective is to find the right-hand side of equation (1), f(x) of the general equation

$$dx/dt = f(x) \quad (2)$$

that describes the corresponding growth. This model considers cell growth not tumour emergence, this means that if originally, no tumour mass is present (x = 0), there is nothing to grow, so we should have f(x) = 0. In other words, the desired function f(x) should have the property f(0) = 0 *[Olague P. B. and Kreinovich V., (2016)].*

Now, integrating starting from the initial condition $x(0)=x_0$, given *a* and *b*, can be obtained:

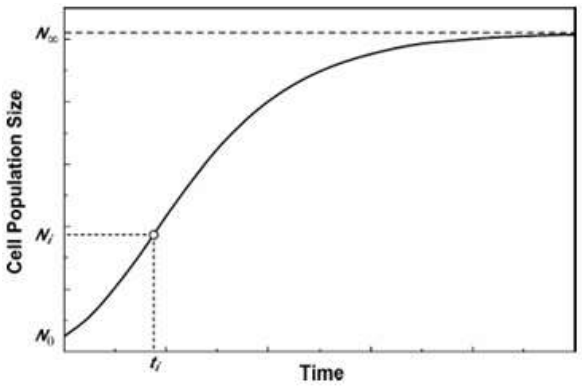

Fig. 7. Typical Gompertz sigmoidal growth curve. N_0 is the initial number of cells, N^∞ is the maximal number of cells (carrying capacity), and N_i is the population size at the inflection point achieved at time (t_i) (*from Kozusko F., Bajzer Z., (2003))*

$$\int_{x_0}^{x} \frac{dx}{x(a-b\ln x)} = \int_0^t \quad (3)$$

$$\left[-\frac{1}{b}\ln(a-b\ln x)\right]_{x_0}^{x} = t \quad (4)$$

$$-\frac{1}{b}\left(\ln(a-b\ln x) - \ln(a-b\ln x_0)\right) = t \quad (5)$$

$$\ln\left(\frac{a-b\ln x}{a-b\ln x_0}\right) = -bt \quad (6)$$

$$a - b\ln x = (a-b\ln x_0)\, e^{-bt} \quad (7)$$

$$\ln x = \frac{a}{b} - \left(\frac{a}{b} - \ln x_0\right) e^{-bt} \quad (8)$$

$$x(t) = e^{\frac{a}{b}} e^{-(\frac{a}{b} - ln x_0)e^{bt}} = x_0^{e^{-bt}}\, e^{\frac{a}{b}(1-e^{-bt})} \quad (9)$$

Considering $x_0=1$, the exponential term is not relevant. Fig. 7, shows the curve describing the present model: it shows an increase until to the inflection point after which the rate of growth slowly decreases reaching a plateauing behaviour for N^{∞} [(*)] *[Kozusko F., Bajzer Z., (2003)].* [(*)] (*N ≡X*).

3.2.3 Growth Factors and Bioactive Molecules. The bioactive molecules applied in 3D bioprinting are mainly growth factors, enzymes, antibodies, antigens, plasmids, DNA. These bioactive molecules can be selected according to the type of tissues to be repaired and the functions to be achieved in 3D bioprinting. Enzymes are proteins or RNAs produced by living cells that are

highly specific and catalytically efficient for their substrates. (Steier et al., 2020). Growth factors, as a class of substances able to regulate cell growth and development, have been widely used in tissue engineering and 3D bioprinting. DNA is an essential biological macromolecule for the development and normal operation of organisms. It is widely used in modern biology and biochemistry, mainly in the field of genetic engineering; it can also be applied in 3D bioprinting to prepare gene-active bioinks and combine with bone marrow mesenchymal stem cells, providing a new idea for the treatment of bone defect regeneration *[Cunniffe G.M. et al., (2017)].*

4. Analysis techniques

In the evaluation of bioinks for extrusion printing, various approaches can be distinguished, particularly based on how they are related to the different stages of the printing process. It is necessary to emphasise that any assessments of the cell-free bioink may not hold complete relevance for the equivalent bioink containing cells, as cells have an impact on the rheological properties of the mixture.

During the development of a bioink, a suitable gelation mechanism, homogeneity of the materials in terms of cell/fibre distribution, cytocompatibility, swelling/degradation behaviour need to be investigated and optimized. Generally speaking, to assess printability, can be useful the evaluation of the rheological properties of the bioink as predictors of the potential shape fidelity. Moreover, as hydrogel filaments are the basic elements in extrusion bioprinting, their formation, planar orientation and stacking during the layer-by-layer printing process can also be evaluated. The quality and mechanical stability of these filaments is a primary indicator of printing accuracy, shape fidelity, and resolution that can be achieved.

4.1 Blend characterization

4.1.1 Tube inverting test. It is a simple method to qualitatively assess the gelation of a sample and the time necessary for such sol-> gel transition. The sample state is controlled at different times just inverting the tube (fig. 8). When this method is used, it is necessary to consider variables such as the amount of sample introduced into the tube and the diameter of the test tube because both factors can affect the result of this test.

Fig. 8: Tube inverting test technique.

4.1.2 Swelling test. Swelling is the change in volume of a gel as it absorbs a compatible solvent, such as water for hydrogels. Swelling is possible because the solid component of the hydrogel, which is typically a polymer network, is both elastic and hydrophilic, enabling enough water to be absorbed to increase the volume, but creating elastic tension within the networked

polymer chains that prevents total dissolution (Fig. 9). During the past decades, hydrogels have attracted the attention from the research community and the polymer industry to their wide range of applications as in manufacturing contact lenses, hygiene products, tissue engineering, drug delivery systems, wound dressings, etc. Swelling rate is one of the most important technical features of hydrogels. To measure the swelling rate, the profile of swelling capacity versus time of a hydrogel sample is often obtained by performing free-absorbency capacity measurements at consecutive time intervals *[Zhang et al., (2020)].*

4.1.3 Degradation test. Performing the swelling test, it is possible to check the degradation of the hydrogels: often a reduction in weight during a swelling test, is due to a degree of degradation with reduction of the mass of construct.

4.1.4 Dehydration test. Dehydration is the change in volume of a gel as it loses its content of water, during the drying (Fig. 9).

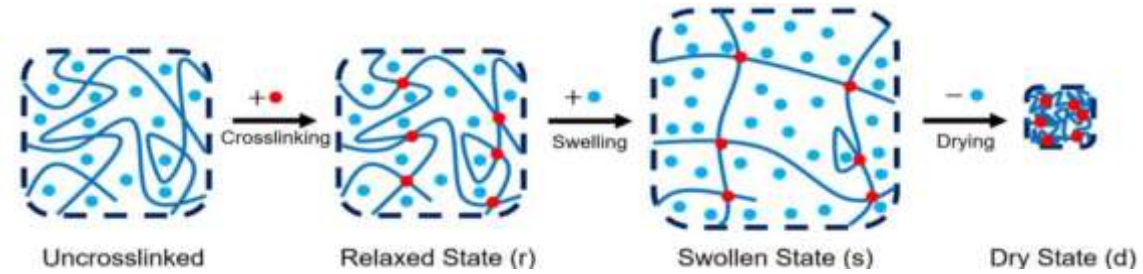

Fig. 9: Swollen stages *(from The Swollen Polymer Network Model. Nate Richbourg, 2023)*

4.2 Rheometer and rheological properties. Rheology is a branch of physics that describes the deformation and flow behaviour of materials under the influence of applied forces *[Malda J. et al., (2013)].* The term originates from the Greek word "rhei" (ῥεῖ) meaning "to flow". Rheometry is the measuring technology used to determine rheological properties *[Introduction to rheology, D. Vader, H. Wyss].*

Rheometers can be identified as "strain controlled" and "stress controlled" rheometers: in the first case, can be applied a rotation ω (strain) and it is possible to measure a torque M (stress); in the second case applying a torque M (stress), it is possible to measure a rotation ω (strain) (Fig. 10). Stress-controlled rheometers have better torque sensitivity; strain-controlled rheometers can probe higher frequency; but nowadays, feedback loops are fast enough so that most rheometers can operate well in both modes *(Introduction to rheology, D. Vader, H. Wyss).*

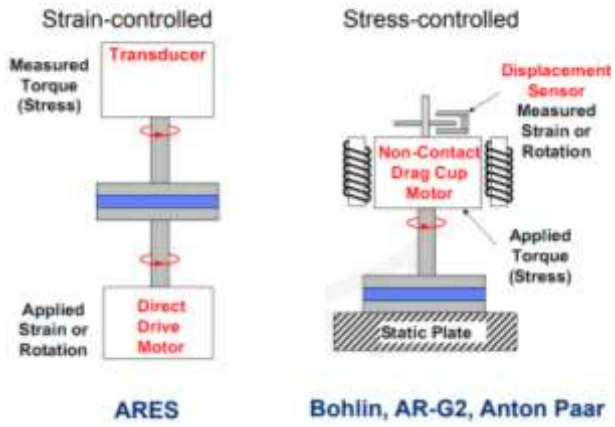

Fig. 10: comparison between strain- and stress-controlled rheometers. *(from Introduction to rheology, D. Vader, H. Wyss)*

On the base of the geometries of the measuring systems, rotational rheometers are defined as cone-plate, plate-plate and concentric-cylinder rheometers (Couette cell) (Fig. 11). Cone-plate presents uniform strain/strain rate and a fixed gap height; plate-plate geometry presents non-uniform strain, adjustable gap height. This geometry represents a good method for testing boundary effects like slip. Concentric–cylinder, presents a good sensitivity for low-viscosity fluids (*Introduction to rheology, D. Vader, H. Wyss).*

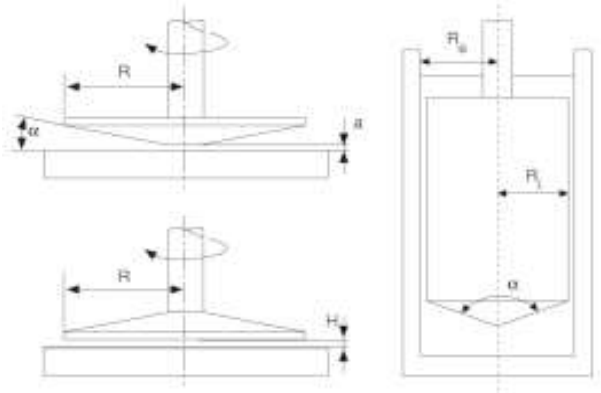

Fig.11: measuring systems: cone-plate (with radius R, cone angle α, truncation a); plate-plate (with radius R, distance between plates H); concentric cylinders (with bob radius R_i, cup radius R_e, internal angle α at the tip of the bob). *(from Introduction to rheology, D. Vader, H. Wyss).*

4.2.1 Rheological properties. Rheological properties have a large influence on hydrogels printability. In 3D extrusion-based processes, a bioink presents at the beginning, a bulk resting state, then undergoes a transition to a high shear condition while passing through the nozzle, and finally reaches a new resting state. The main rheological properties describing these transitions are viscosity, viscoelastic shear moduli, elastic recovery, and shear stress (fig.12) *[Ribeiro A. et al., (2018)].*

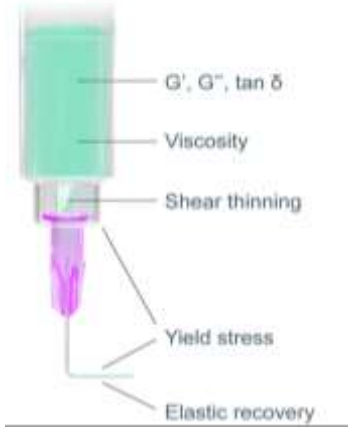

Fig.12: Rheological properties affecting printability and shape fidelity. Interplay of rheological properties in extrusion-based printing *(from Schwab A. et al., 2020).*

4.2.1.1 Viscosity is the resistance of a fluid to flow under the application of a stress and has a great influence on the printing fidelity. Generally, higher viscosities result in higher printing fidelity, but it also leads to increased shear stress, which can affect the cells suspended in the bioink. The main factors determining the viscosity of polymers in solution are molecular weight, concentration and presence of additives *[Cowie J. and Arrighi V., (2007)]*. Viscosity is defined as the ratio of the shear stress to the shear rate. Fluids exhibiting deviations from linearity, with change in the ratios are defined non-Newtonian. Non-Newtonian fluids can be classified into time-independent (shear-thinning and shear thickening) and time-dependent fluids (thixotropic or rheopectic) *[Cheremisinoff N., (1993)]*. Shear-thinning is the most common type of time-independent non-Newtonian fluid behaviour, where the increase of the shear rate $\dot{\gamma}$, results in a decrease of viscosity *[Mezger T. G., (2011)].* Some of the non-Newtonian viscous fluid models often used include (13):

- Bingham-Green visco-plastic: presents a solid behaviour at low stress, flows at high stress (it is necessary to exceed a yield stress to flow).
- Shear thinning or pseudo-plastic: does not present yield stress, flow well at high stress (as blood, paints).
- Shear-thickening fluids or dilatant: flow well at low shear, present solid behaviour at high shear (example is maizena).

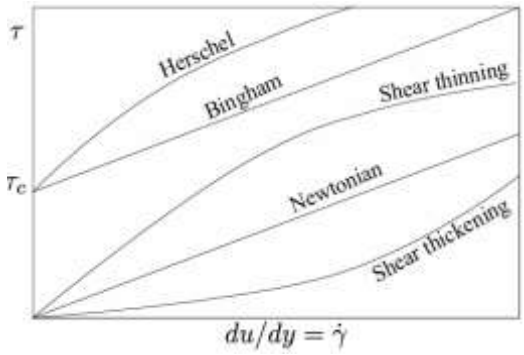

Fig.13 Rheological models for non-Newtonian fluids *(modified from ACS Omega 2022, 7, 33, 28708-28722)*

- Herschel-Bulkley visco-plastic: is a generalization for non-Newtonian viscous fluids.

4.2.1.2 Viscoelasticity. Bioinks for extrusion printing, show both viscous flow and elastic shape-retention properties. These properties are known as viscoelasticity. This behaviour is described by two parameters: the storage (or elastic) modulus G' and the loss (or viscous) modulus G".

$$\text{The storage modulus } G'(\omega) = \int_0^\infty \omega G(s) \sin(\omega s) ds \qquad (1)$$

$$\text{The loss modulus } G''(\omega) = \int_0^\infty \omega G(s) \cos(\omega s) ds. \qquad (2)$$

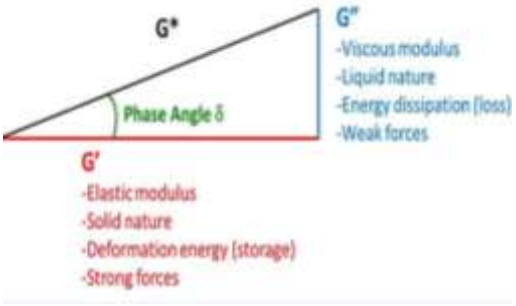

Fig.14 diagram illustrating the relationship between complex modulus G*, storage modulus G', loss modulus G'' using the phase angle δ. The elastic behaviour is presented on the x-axis and the viscous portion on the y-axis *(from Science Exchenge).*

The storage modulus G' is a measure of the energy elastically stored during deformation and is associated with elastic shape retention; the loss modulus G'' measures the energy dissipated by the material and is linked to the viscous flow (Fig.14). Viscoelastic properties can be measured via oscillatory rheology, while viscosity is measured under rotation. G' and G" are measured as a function of the frequency and amplitude of the oscillation *[Mezger T. G., (2011)].*

It is also possible to define the complex viscosity, representative of the viscous behaviour:

$$\eta^* = G^*/i\omega = (G' + iG'') / i\omega = G''/\omega - iG'/\omega = \eta' - i\eta'' \qquad (3)$$

where G* is the complex modulus. So

$$|\eta^*| = |G^*| / \omega \qquad (4)$$

(S. Milner, Journal of Rheology, 40, 303 (1996))

It is possible to notice that the imaginary part of the complex modulus is related to the real part of the complex viscosity, and vice versa, generating a phase shift δ between deformation and stress in viscoelastic materials, that can be computed using a polar definition of the complex modulus:

$$G^* = G' + iG'' = |G|e^{i\delta} = |G|\cos(\delta) + i|G|\sin(\delta) \qquad (5)$$

$$\Rightarrow \frac{G''}{G'} = \frac{|G|\sin(\delta)}{|G|\cos(\delta)} = \tan(\delta) \qquad (6)$$

$$\Rightarrow \delta = \tan^{-1}\left(\frac{G''}{G'}\right) \qquad (7)$$

The G”/G’ ratio (eq. 6) represents the damping factor or tan(δ). Shape retention can also be defined in terms of yield point or yield stress, that is the stress to exceed to obtain a deformation (Fig.15). Both elastic modulus and yield point are correlated to the number of cross-links within the bioink *[Mezger T. G., (2011)].*

The following tests represent a short overview of the most common types of analysis performed at the rheometer to assess the rheological properties of biomaterials.

4.2.1.3 Amplitude sweeps *is* an oscillatory test that uses an increasing amplitude (energy input) to probe sample properties such as rheological stability. The amplitude sweep test (Fig. 15), is an important assay to properly determine the Linear Viscoelastic Region (LVE) to define rheological stability within either a % strain or stress value that is a critical input parameter for subsequent frequency-based assays and for other oscillatory tests performed at the same temperature, to ensure that the rheological integrity remains intact. It is important to underline that the LVR can change with temperature *[Whitcomb, KJ., (2021)].*

4.2.1.4 Frequency sweeps generate a rheological "fingerprint” of a material. It is used to probe viscoelastic properties such as stiffness (complex modulus, G*), solid nature (elastic or storage modulus, G'), liquid nature (viscous or loss modulus, G"), solid or liquid tendency (phase angle), complex viscosity, and tan(δ) (G"/G' ratio) across a frequency range. This assay is useful to probe polymer and biomolecule viscoelastic behaviour and structure in diverse matrices. It is important that this assay is performed within the LVR (Linear Viscoelastic Region) determined with an amplitude sweep test (Fig. 15). In this case (assay performed within the LVR), the same result can be obtained with both methods if the sample does not change during the test period. The results of frequency sweeps are usually represented in a diagram with the angular frequency (ω) plotted on the x-axis and storage modulus G' and loss modulus G'' plotted on the y-axis, with both axes on a logarithmic scale *[Faith A. Morrison, Understanding Rheology (2002)].*

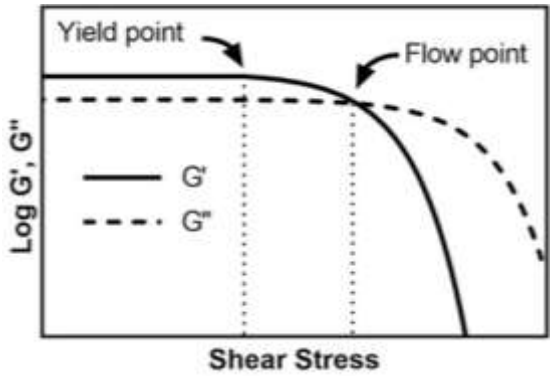

Fig.15: Amplitude sweeps of a viscoelastic substance represented as a function of the shear stress, showing the yield point as the limit of the linear viscoelastic region and the flow point, e.g., the stress at which the viscous modulus G’’ is above the elastic modulus G’ and therefore flow can occur. *(from Schwab A. et al., (2020)).*

4.2.1.5 Yield point and flow point. Amplitude sweeps can also be used for determining the yield point and the flow point (Fig. 15). The yield point τ_y – also called yield stress – is the value of the shear stress at the limit of the LVR. This point is also called the linearity limit. The flow point τ_f – also called flow stress – is the value of the shear stress at the crossover point G' = G'' (fig. 15). At higher shear, the viscous portion dominates and the sample flows. In conclusion, if a sample shows G'' > G' in the LVR and, therefore the character of a fluid, it may have a yield point but not a flow point because it is always liquid *[Mezger T. G., (2011), Schwab A. et al., (2020)].*

4.2.1.6 Loss factor or damping factor: tan(δ) = G''/G' (tangent delta), is a dimensionless quantity or 1. This factor is given by the ratio of the two components of the complex modulus G* (eq. 6). The graph of the tan(δ) is displayed in addition to the curves of G' and G'', when there is a phase transition in the sample. This is also called the sol/gel transition point or simply the gel point. It means that the sample has changed its properties during the measurement, passing from the liquid or sol state to the solid or gel state and vice versa. For practical applications, a liquid is said ideally viscous if tan(δ) > 100:1 = 100, while a solid material is defined ideally elastic if tan(δ) < 1:100 = 0.01. *[Mezger T. G., (2011)].*

Many other parameters can affect rheological properties of a material, as environmental pressure (e.g. overpressure up to 1000 bar = 100 MPa), magnetic field or electric field strength, UV light rays with controlled intensity *[Mezger T. G., (2011)].*

It is also important to consider the rheological properties of a blend after mixing with cells. Important phenomena to be considered include volume exclusion, alteration of viscoelastic properties due to the cells in suspension, and potential interference of cells with chemical processes. The extent of these effects depends also on the metabolic state of the embedded cells, their subtype, and the volume occupied, with potential differences when single cells, spheroids, or complex aggregates are processed *[Schwab A. et al., (2020)].*

4.3 Imaging techniques in the blend and scaffold development. During the development of functional tissue constructs, factors needed to be controlled are:

- ECM proteins (Composition, amount, fibre size and spatial orientation);
- Cells (Cell number, viability, growth, morphology, differentiation, cell-cell and cell–matrix interactions);
- Scaffold (Surface topography, inner structure, particle distribution in composites).

4.3.1 Scaffold transparency is a major issue in the imaging of constructs *[Lee J. et al., (2008)].* Most scaffolds possess a high degree of opacity that could derive from high porosities (e.g. fabrication by particulate leaching or gas foaming), multiple internal surfaces (multi-layered or multi-surface architectures), incorporation of micro- and nanoparticles (nanocomposites) or highly diffracting components such as in biopolymer-based hydrogels. Some scaffolds become highly opaque as result of increasing mineralization during maturation (bone TE constructs). Light in the UV and visible range (300–700 nm) used for microscopy imaging penetrates such opaque materials only superficially *[Georgakoudi I et al., (2008)]* and seeded cells further enhance light diffraction. For this reason, traditional imaging methods rely on physical sectioning (histology) to obtain images of the inner micro-architecture, thereby destroying the constructs.

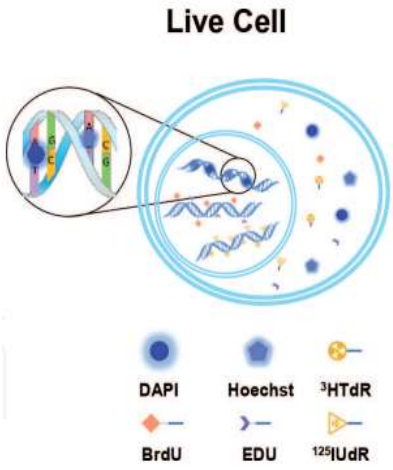

Fig. 16: Methods for DNA analysis in live cells (*modified from Xu J., Chen X., Rui J,Yu Y., Gu D, Ruan JJ, Ruan BH. Cell Growth Measurement).*

Each of the following methods discussed, presents its strengths and limitations and allows imaging within certain spatiotemporal boundaries. The techniques differ largely not only in their invasiveness to the biological material, their imaging speed and ability to create three-dimensional views, their biological specificity, imaging depth and resolution, but also in terms of costs and time.

4.3.2 Transillumination and fluorescence microscopy. The most traditional tool to image cells and tissues is optical microscopy, with many techniques available. Common to these techniques is their resolution window which is determined by the wavelength of the illumination light. Light microscopes use a transmitted white light spectrum for image generation. White light microscopy is primarily used for routine analysis (monitoring cell number and morphology after scaffold bioprinting, spheroids formation, number and dimension of spheroids)

and for imaging histological stained tissue slices *[Kiernan J. (1999)]* with various stains such as Haematoxylin and Eosin, Von Kossa, trichrome *[Boos A.M. et al., (2012)].* The limitations of white light microscopy are low contrast and low specificity in unstained samples. Opaque scaffolds cannot be examined with transillumination microscopy.

In fluorescence microscopy, a sample is illuminated by light in the near UV or lower visible spectrum to excite fluorophores within the sample. These are either extrinsically applied or intrinsically present as auto fluorescent molecules. The fluorophores are detected based on their fluorescence excitation and emission capabilities. The emission light has a larger wavelength (lower energy) than the excitation light and is separated and collected by appropriate beam splitters, dichroic mirrors and emission filters. Unspecific background due to cellular autofluorescence is an important problem that needs to be controlled.

DNA content can be analysed after fluorescent staining or labelled nucleic acid incorporation. As shown in Fig. 16, DAPI and Hoechst dyes penetrate the membrane and are commonly used to label live cells. DNA in active proliferating cells can be labelled by the fluorescent-labelled bromodeoxyuridine (BrdU) and 5-Ethynyl-2'-deoxyuridine (EDU).

4.3.3 Confocal Fluorescence Microscopy (CFM). A huge increase in image contrast is gained using laser scanning Confocal Fluorescence Microscopy *[Smith L.E. et al. (2010); Muller M., (2006)].* The reduced light intensity is overcome by sensitive photomultiplier detectors. The major concern about CFM is the issue of photobleaching and phototoxic effects to cells (invasiveness) due to high laser intensities in the focal plane and ever-present out-of-focus excitation which complicates long-term imaging. The other major limitation is the low tissue penetration of only around 100 mm *[Oheim M., (2001)].*

Fluorescence and confocal microscopy are powerful tools used to get an overview of cell distribution and cell morphology of scaffold containing cells (figure 2b) *[Marelli B. et al., (2011)].* Another application of CFM is the imaging of collagen gel networks *[Mickel W. et al., (2008)].*

4.3.4 Electron Microscopy. Electron microscopy techniques are very good methods to characterise spheroids, because they provide high resolution at nanoscale levels.

High-resolution images of the inner structures can be generated by transmission electron microscopy (TEM) while high-resolution images of the surface of spheroids can be achieved by scanning electron microscopy (SEM) *[Ma, H.L. et al. (2012)].*

The TEM technique provides information on cell–cell interaction in the spheroids, such as cell junctions, and ECM deposition, as well as information on treatment outcomes such as apoptosis, cell shrinkage and organelle swelling *[Tesei A. et al., (2013)].* Importantly, TEM is mostly used to analyse the distribution of drugs or nanoparticles into the spheroid *[Huang K. et al, (2013)].*

5. Materials and Methods

5.1 Materials

5.1.1 Biomaterials, tools for blend preparation at the bench: natural polymers for alimentary use have been utilised. Follows a list of materials used in this experimental work.

Collagen

Vital Proteins
Collagen Peptides
Bovine Collagen
Powder-Neutral

Gelatine

FunCakes
Gelatin Powder:
Bovine Gelatin,
Bloom150

Alginate

Saporepuro
Sodium-Alginate
Thickening additive
product for
alimentary use

Chemical Crosslinker:

home-made $CaCl_2$ (80mM) at the bench.

$CaCl_2$ (50mM) in the printing lab (CellInk solution).

Fig. 17. Tools used at the bench for blend printing

Fig. 18. Magnetic rotating/heating plate with stirrer

Fig.19: analytical balance

5.1.2 Cells mixed to the biomaterials for bioinks preparation were **SK-LMS-1 Cell Line (HTB-88™) ATCC**. SK-LMS-1 is a cell line exhibiting fibroblast morphology (Fig. 20) isolated from the vulva of a 43-year-old, white female patient with leiomyosarcoma. This product has applications in cancer research.

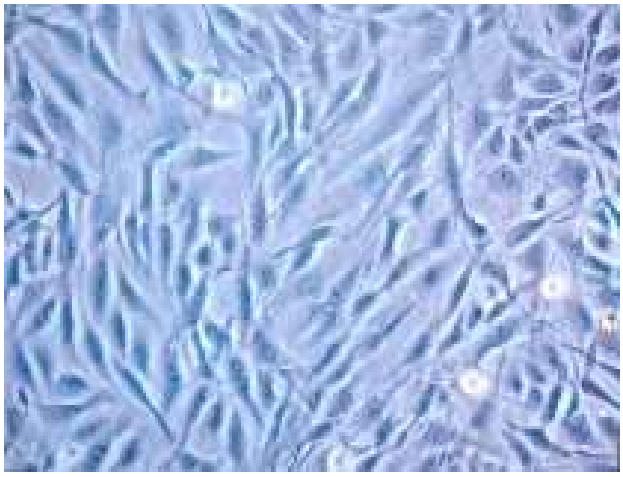

Fig.20: SK-LMS-1 Cell Line exhibiting fibroblast morphology when in culture

Morphology: fibroblast

Growth properties: Adherent

Growth Conditions: Temperature 37°C

Fig. 21: LUNA II cell counter

LUNA-II™ cell counter. The cells mixed to the bio-blends to form the bioinks for 3D bioprinting, have been counted with the use of the LUNA-II™ (Fig. 21), an automated cell counter. Live cells are tagged with green circles and dead cells are tagged with red circles, making it easy to verify the accuracy of each count.

5.1.3 CELLINK INKREDIBLE+ pneumatic 3D Bioprinter (two print-heads)

The bioprinter used in this work is CELLINK INKREDIBLE+ (Fig. 22), a pneumatic 3D bioprinter with two printheads. The printing pressure ranges between 5 to 400 kPa; using an external air supply such as a compressor, a maximum of 700 kPa of pressure can be provided to the INKREDIBLE+. *(from Nicole Witzleben,2020).*

Technical specification is reported as table.

Fig.22: CellInk INKREDIBLE+ bioprinter

Table II. Technical specification of CellInk INKREDIBLE+ bioprinter	
Outer dimentions (LxWxH)	370 x 330 x 430 mm
Weight	15kg
Build volume	130 x 80 x 100 mm (printbed has inserts for P100 petri dish and multi-well plates)
Build surface compatibility	Multi-well plates, petri dish, glass slides
Resolution xy	10µm
Layer resolution	100µm
Pressure range (external air supply)	5-400kPa
Printheads	2
Printbed Temperature range	Room temperature
Printhead Temperature range	Room temperature
UV-sterilization	None
Calibration options	Manual
User interface	Disply, desktop application
Desktop OS compatibility	Windows, Mac OS
Connectivity	SD card, USB B
Supported file formats	.gcode (.stl, .obj, with software)

Fig. 23: Sterile standard conical bioprinting nozzles, length and inner diameter according to the colour.

Fig.24: Falcon 6-well-plate, flat bottom

5.1.4 Further devices used for this work: Rheometer, Incubator and different microscopes

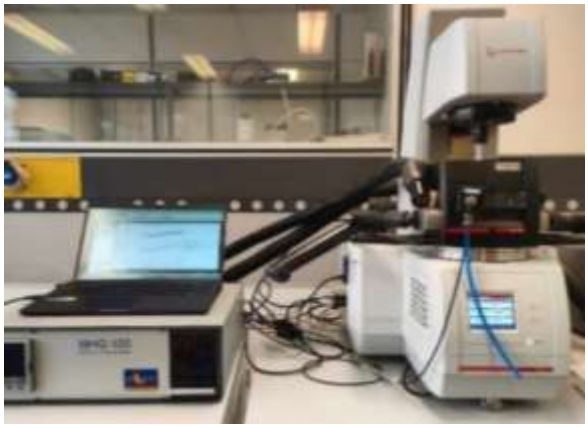

Fig. 25: Rheometer MCR 702e MultiDrive SERIES ANTON PAAR, plate-plate modality

Fig. 26: CELBIO incubator, at 37°C, 5% CO_2.

Fig.27: Olympus BX-51 fluorescence microscope for blend analysis

Fig.28: Inverted optical microscope (Nikon).

Fig.29: Optical Microscopy: haematoxylin/eosin staining observation.

Other materials used include:

Culture medium and disposable materials as tips, flasks, falcon, serological pipette.

5.2 Methods: A Bioprinting Protocol, which provides instructions for bioprinting with the bioink using the INKREDIBLE+ has been followed (Table III). It covers steps from pre-print mixing with cells, 3D bioprinting and post-printing processes of crosslinking. This protocol has been optimized using the CellInk INKREDIBLE+ pneumatic printhead. The following protocol can be performed at room temperature (RT), intended a temperature between 20-25°C.

Table III. Bioprinting Protocol provides instructions for bioprinting with the INKREDIBLE+ bioprinter.

Step	Activity	Material	Description
1.	Blend preparation	Collagen+alginate Collagen+gelatine+alginate	Load bioink in a cartridge at room temperature. (**If not printed with cells, go to step 3)**.
2.	Mix blend with cells	- 3 ml syringes with luer lock connections - Prewarmed blend - Cell suspension in syringe	Mix blend with cell suspension, taking care do not introduce air bubbles to the mixture.
3.	Fill the cartridge with bioink and load the cartridge	clear cartridges (3cc) loaded with bioink (blend with cells) sterile conical bioprinting nozzles	Place the room tempered bioink in the printhead and cap with the conical nozzle of choice: blue conical nozzle, size 22G, 410µm inner diameter has been selected. **Note:** decrease the nozzle diameter to achieve smaller filaments, increases the risk of the bioink clogging and cell damage.
4.	Printing	Bioprinter INKREDIBLE+ 6-well plate	Print structures according to the selected parameters onto a 6_well plate. If printability is not as desired, adjust the pressure up/down by 1 kPa to extrude more/less material. **Note**: it is necessary do not wait too long between extrusions because the bioink can dry in the nozzle causing it to clog. If this occurs, replace with new nozzle.
5.	Crosslinking	Crosslinking solution ($CaCl_2$) Cell culture medium	Crosslink the scaffold bio-printed with $CaCl_2$ crosslinking solution. Cover the cell-laden scaffolds with crosslinking solution as long as needed, depending on construct size and molar concentration of the crosslinker. Remove crosslinking solution and rinse constructs with basal culture media once.
6.	Incubation	Cell culture medium	After crosslinking and washing, add the desired medium to the scaffolds and place them into incubator. Incubate the scaffolds in cell culture medium in standard culture conditions (37°C, 5% CO_2 and 95% relative humidity).

5.2.1 Blend development. Ingredients: Vital Proteins-Collagen Peptides-Bovine Collagen Powder Neutral; FunCakes Gelatine Powder-bovine gelatine (Bloom150); Saporepuro-Sodium Alginate (SA) powder from brown algae, product for alimentary use; Calcium Chloride Anhydrous, distilled water. The blends were prepared by dissolving collagen powder into distilled water through magnetic stirring for few minutes at room temperature. Subsequently, gelatine was gently added to the solution enhancing the temperature of the magnetic plate to 38°C, mixing to obtain a completely transparent blend. After that, sodium alginate powder was added and mixed till to complete dissolution in the medium. 6 Collagen/Gelatine/SA solutions were prepared at different concentration for the experiment. The 80mM $CaCl_2$ was prepared by dissolving calcium chloride anhydrous in water, stirring for 5 min. The same procedure was followed for the second blend; the only difference was that after collagen, sodium alginate powder was added. Also in this case, different solutions of the blend at different concentration of the components were prepared. The concentration ratios were selected based on the results of hand-printing tests at the bench, performed using a kit made of a large syringe, a nozzle with an inner diameter of about 400µm and home-made $CaCl_2$ 80mM as crosslinker. The selected blends, where tested for repeatability: each blend, in the same environmental conditions, was prepared at the selected concentration with the purpose to obtain the same result at the hand-printing test, that was a scaffold able to maintain the shape after crosslinking, well adherent to the Petri dish, transparent enough to see through it and resistant to degradation test performed after hand-printing. The blends that passed the previous tests, were considered eligible for printability test at the CelliInk Incredible+ bioprinter (without and with cells mixed). After blend preparation and before final printing, biomaterials were mixed with cells to form the bioinks used for scaffold 3D-bioprinting on 6-well plates.

5.2.2 Bioprinting Process The bioprinter used in this investigation was the Pneumatic two-headed CellInk Incredible+ 3D Bioprinter (CellInk, Goteborg, Sweden). Before starting the bioprinting process, the characteristics and parameters of the desired scaffold were fixed and a G-code defined (Fig. 30). The scaffolds were printed into 6-well plates (Falcon flat bottom); equivalent filament shape was extruded for each change of coordinate (mm E); feed rate was fixed at 600 mm/min (F); printing pressure was manually optimised for each material, with a pressure range between 2kPa and 7kPa. The print-head used, was kept at the room temperature of 22°C for all samples. The bioink blends were extruded from a syringe connected to an air compressor; the conical nozzle used for both blends had an inner diameter of 410µm, a length of 22G. The printed scaffolds, made of 2 layers

with a height 0.4 mm per layer, had a size of 10.0 x 10.0 x 0.8 mm and a line-space of 2 mm. The printing process started from the B1 well.

Before starting the bioprinting process, the bioprinter was initialized and the distance of the nozzle above the collector plate was found by measuring the 'zero' of the z-axes and of the x-y plane, representing the position at which the conical nozzle is in contact with the collector plate and then raising the nozzle to leave a space sufficient for a sheet of paper to pass through. During the bioprinting, this distance was further optimised to create well-attached, round, consistent filaments.

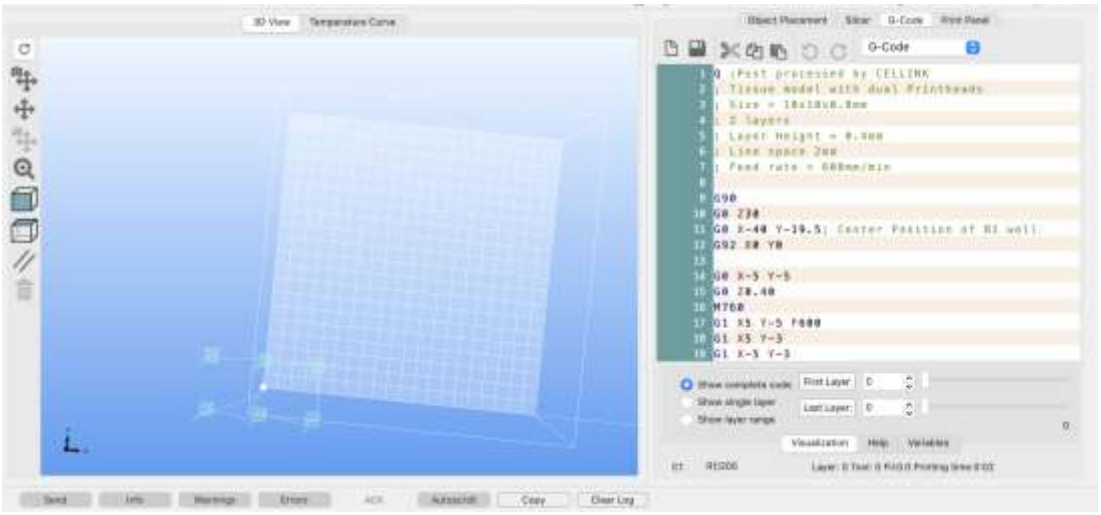

Fig. 30: G_code and image of the 6well plate for printing the scaffolds created with the Cellink HeartWere software.

Where poor attachment or inconsistency was observed, the initial height was lowered, while flattened, squashed filaments indicated the printing height needed to be raised. To optimise the extrusion parameters, the pressure was initially set by observing the flow of material out of the nozzle in a stationary position. The starting pressure was considered the pressure able to produce a steady filament flow. For each blend, two 6-well plates were bioprinted, one containing cell free scaffolds and, the other one containing scaffods made of blend + cells (Figg. 31,32). After the printing process, scaffolds were covered with calcium chloride ($CaCl_2$) solution (50mM) for a time sufficient for crosslinking the constructs and then washed away. As a following step, the crosslinked scaffolds, covered with Dulbecco's Modified Eagle Medium (DMEM-F12), were put into the CELBIO incubator, at 37°C, 5% CO_2 until the scaffold detachment and preparation for the different microscopy analysis.

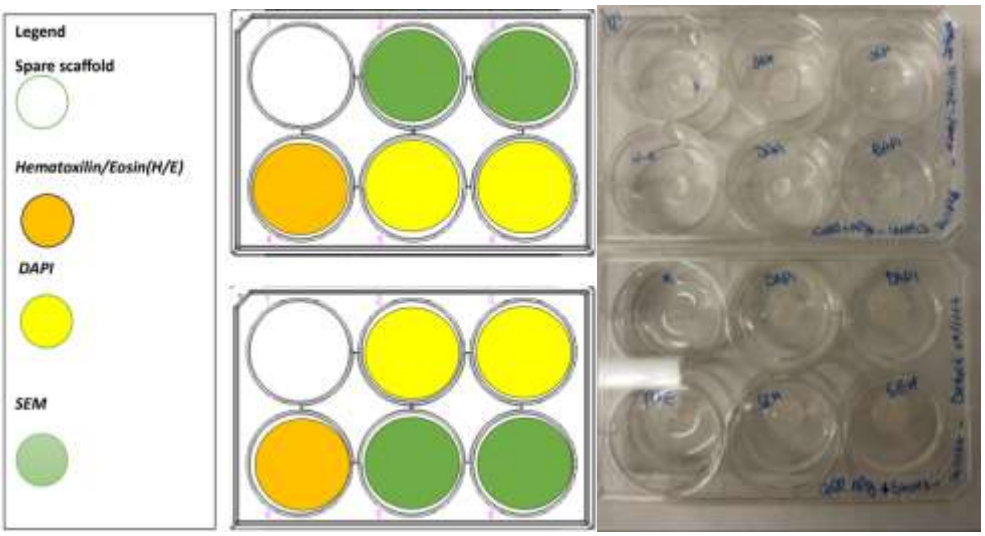

Fig.31: collagen+alginate: two 6well-plates containing scaffolds bioprinted without (above) and with (below) SK-LMS-1 cells (ATCC), covered with crosslinker ($CaCl_2$).

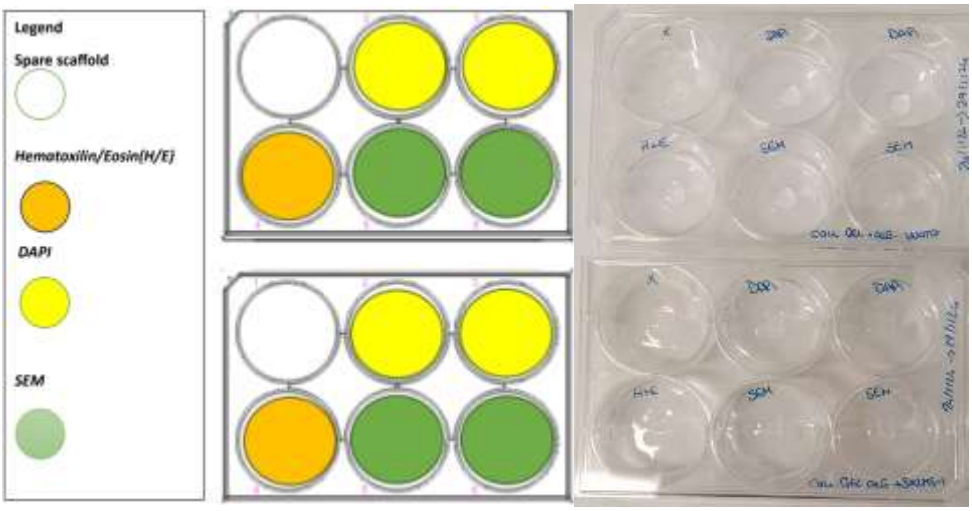

Fig.32: collagen+gelatine+alginate: two 6well-plates containing scaffolds bioprinted without (above) and with (below) SK-LMS-1 cells (ATCC), covered with crosslinker ($CaCl_2$).

When the 4 6-well plates (2 for each material, cell-free and cell-laden) were ready, two scaffolds from each plate were stained with Haematoxylin and Eosin for optical microscopy observation, two scaffolds for each plate underwent the inclusion protocol for FE_SEM observation and, one scaffold for each plate was stained with DAPI for cell control at the inverted optical fluorescent microscopy.

5.2.3 Blend characterization. After the initial development of blends, the materials underwent different test for characterization. Later on, are described the tests performed on the blends.

5.2.3.1 Blend analysis with the OLYMPUS BX-51 microscope, to check homogeneity of the blends, filament formation, reticulation and crosslinking development. To these purpose, disks of the materials developed were prepared as described before and were cross-linked for 30 min with 80mM home-made $CaCl_2$. Slices of these bulks were cut after crosslinking and observed at the Olympus BX-51 microscope.

5.2.3.2 Tube inverting test: The samples examined during the tube inverting test were prepared at the same concentration of those studied for swelling and dehydration assay. To obtain an indication of the time necessary for sol-> gel transition, the sample condition was checked at different times just rotating the tube starting from t_0=*0'* till to the final time of control *tfin* (Fig.33). To control the presence of fluid, it was sufficient to incline the tube.

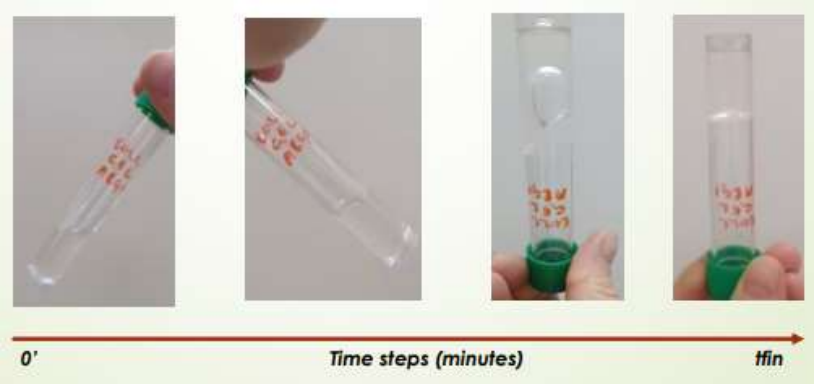

Fig.33: tube inverting test.

5.2.3.3 Swelling and dehydration tests: Swelling is the change in volume of a gel as it absorbs a compatible solvent, such as water for hydrogels, while dehydration test evaluates the loose of water content in time. For swelling, degradation and dehydration tests, have been used 4 samples, 2 for each material. To evaluate the swelling ratio of the blends, that means the capability of absorption from the surrounding environment of the samples, weight was measured immediately after the sol-gel transition (t_0), and then at fixed intervals, after 1hour, 24hours, 48hours and 72hours for Collagen_Alginate blend while, for Collagen_Gelatine_Alginate blend, a further control of weight was performed at 96 hours.

Dehydration test was performed by leaving the samples in the open air, at room temperature, weighting the samples at fixed intervals as for swelling test. The formulas used to compute the swelling ratio percentage (SR%) and the dehydration ratio percentage (DR%) are the following:

$$SR\% = \frac{W_t - W_d}{W_d} \; X100$$

$$DR\% = \frac{W_t - W_d}{Wt} \; X100$$

- ***wt***= sample weight (g) swollen/dried at a certain time step.
- ***wd*** = initial sample weight (g) of the gel (t=0).

5.2.3.4 Rheological measurements. The rheological properties of the two blends developed (Collagen Alginate and Collagen Gelatine Alginate), were investigated at 25°C by using a MCR 702e Anton-Paar rheometer (Graz, Austria); the tests were performed with a plate–plate geometry, with the diameter of the upper plate of 25 mm, a gap of 1 mm (Fig. 34).

Fig. 34: Rheometer MCR 702e MultiDrive SERIES ANTON PAAR, plate-plate geometry

The amplitude sweep test was performed as function of the strain γ (%), from 0.01% to 100%.

The oscillatory shear measurements were performed as a function of the oscillation frequency (ω), from 0.1 rad/s to 100 rad/s, for a constant strain (γ) of 0.1% (in the linear range of viscoelasticity).

The elastic/storage (G') modulus and the viscous/loss (G'') modulus were determined in oscillatory shear conditions as a measure of the stored and dissipated energy during one cycle of deformation.

The damping factor or loss/tangent (tan(δ) = G''/G'), gives information about the viscoelastic characteristics of the samples.

The shear viscosity (η) of the blends was determined as a function of shear rate ($\dot{\gamma}$) in stationary shear flow conditions, for $\dot{\gamma}$ varying in the range 0.01 s^{-1} – 1000 s^{-1}.

5.2.4 Cell characterization. To assess cell biocompatibility and cell behaviour in the scaffolds, several techniques to characterise spheroids, either in viable or fixed mode were used. These techniques allowed to study formation, organization, size, shape and migration of spheroids.

5.2.4.1. Optical Microscopy was used for monitoring spheroid formation, spheroid number, morphological changes such as size and shape over time, taking images then analysed by appropriate software. In this work, the difference in number, size and total area of spheroids were analysed with an inverted-phase contrast microscope, to evaluate the characteristics of the different scaffolds. The images taken were used to build up the curves of growth of the number of spheroids present into each well of the 6well plate: 6 random photos per well, per day of control (day1, day2, day5 and day6), for a total number of 36 images per plate, per day of control, were taken for the computational analysis.

Scaffolds without and with spheroids were also processed for histological sectioning and underwent a Haematoxylin and Eosin staining procedure for morphological analysis. The 3D-bioprinted scaffolds, (without and with spheroids) were fixed with Paraformaldehyde 4% (Sigma-Aldrich, St. Louis, MO, USA) and embedded in paraffin. The paraffin sections were rehydrated by using both xylene and a descending-graded series of ethyl alcohol. After washing with the 50% alcohol, the sections were kept for five minutes in distilled water. Then, they were stained with haematoxylin (Bio-Optica, Milan, Italy) for 2 min, washed in distilled water, and then stained with Eosin (Bio-Optica) for 2 min; subsequently, they were washed in distilled water. Finally, they were dehydrated through an ascending graded series of ethyl alcohol and xylene and were mounted with Eukitt Solution (Orsatec GmbH, Kindler GmbH and Co., Bobingen, Germany). *[Greco S. et al., (2023)].*

This staining method with Haematoxylin/Eosin, a histochemical stain used in morphology, made it possible to evaluate the presence of spheroids in the matrices, distinguishing the pyknotic nuclei and eosinophilic cytoplasm in spheroid sections and, the surrounding eosinophilic matrix formed by the blends.

5.2.4.2 Fluorescence microscopy. DAPI staining was used to assess presence of spheroids, proliferation, apoptosis in the spheroids. For DAPI staining, sterile PBS (Corning) was used to dilute the 4',6-diamidino2-phenylindole (DAPI) solution (ThermoFischer) to the final concentration of 300 nM. Firstly, the scaffolds containing the spheroids were washed 1–3 times with sterile PBS and then were coated with the fluorescent dye solution of DAPI (300 nM) and incubated for 1–5 min, covered with silver paper to protect them from light. Finally, the solution was removed by washing 2–3 times with PBS and images were acquired by using a Nikon Fluorescent, phase contrast light microscope *[Greco S. et al., (2023)].*

5.3 Statistical Analysis. Non-parametric Kruskal-Wallis test was performed to determine the difference between the groups of data, followed by a post hoc test. The results obtained have been displayed as bar chart per column, representing the number of spheroids per day of control, while the minimum/maximum *box and whisker plot* has been used for the area of the spheroids, where the median value is indicated by the continuous horizontal line inside each box. Asterisks (∗) indicate statistical significance: *p < 0.5; **p<0.01; ***p < 0.001; ****p < 0.0001. 'ns' = "not significant."

5.4 Informatic tools. GraphPad PRISM 9 (version 9.5.0) was used for statistical analyses. Microsoft Excel spreadsheet-Office Home Student 2019 and MatLab R2023a (Academic use) were used for further data analysis and graphical representations.

6. Results

6.1 Blend development: preliminary experiments at the bench.

The materials available were tested, mixed at different concentrations and manually printed into petri dishes at the bench to assess hand-printability. The blends that gave a stable construct, were selected and underwent a test of repeatability: each blend was prepared and hand-printed four times. The blends that allowed the hand-printing of a stable scaffold for four times, were selected. In the following images (Fig. 35a., 35b., 35c.) are reported few examples of the work done.

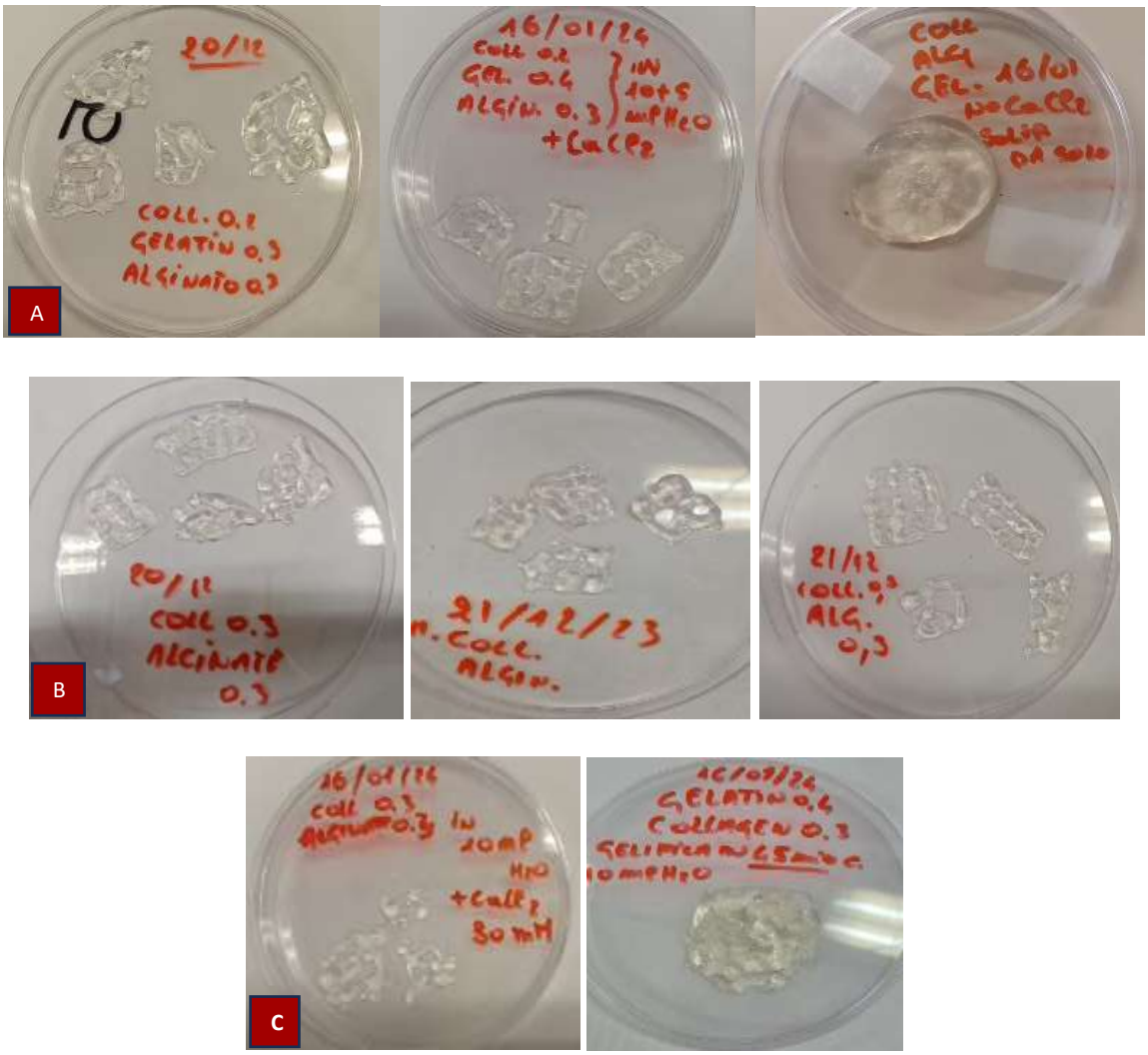

Fig.35: Scaffolds handprinted at the bench**. Line a**. handprinted scaffolds made of collagen gelatine alginate at different concentrations and crosslinked with $CaCl_2$, plus a bulk of the same blend also crosslinked. **Line b.** handprinted scaffolds made of collagen-alginate, prepared in different days, crosslinked with $CaCl_2$. **Line c.** handprinted scaffold and relative bulk made of collagen-gelatine non chemically crosslinked. This blend developed at the bench has been eliminated because of the not availability of a chemical crosslinker; the only crosslinker available for this 3° blend, was the glutaraldehyde, not biocompatible. These trials have been performed to find the right ratio of the different component for the blend, to perform analysis of transparency, capability of maintaining a shape, repeatability of the test of hand-printing, to assess the tendency of lose water content in time).

6.2 Blend characterization.

6.2.1 Olympus BX-51 Fluorescence Microscope: analysis of blends.

After the development procedure, Collagen-based bio-blends were selected. Immediately after preparation, slices of the bulk were observed at the Olympus BX-51 microscope (Figg. 36-39) for analysis of homogeneity of the blends, fibre formation and crosslinking of the constructs. In Fig. 37, it is possible to notice in real time, the formation of fibres after preparation of the blend not yet crosslinked.

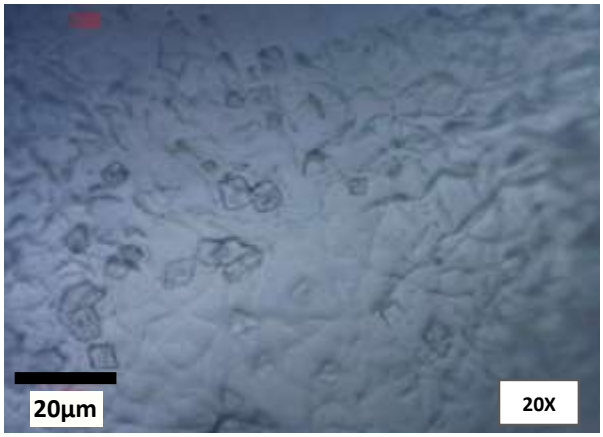

Fig. 36: Collagen+Alginate blend: slice of bulk after crosslink with $CaCl_2$.Relevant the presence of crosslinked fibres (20X), (Olympus BX-51 microscope).

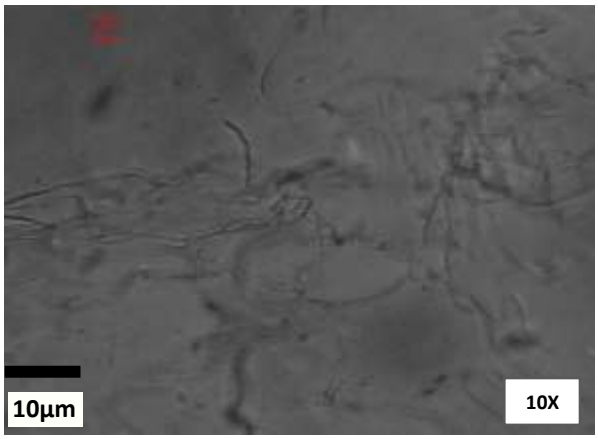

Fig. 37: Collagen+Gelatin+Alginate blend observed before sol->gel transition. First stage of fibre formation ((10X) Olympus BX-51 microscope).

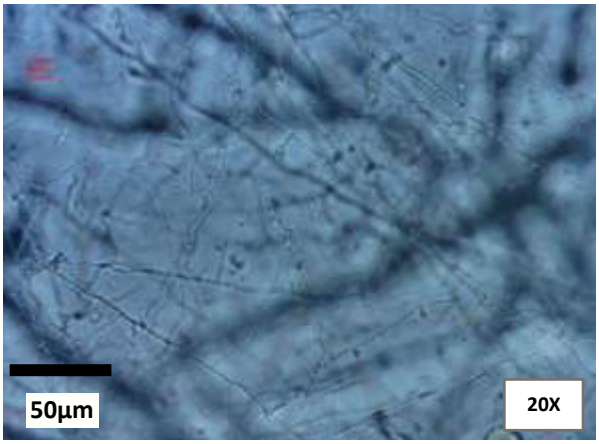

Fig. 38: Collagen+Gelatin+Alginate blend crosslinked with $CaCl_2$. Slice of bulk. It is evident the important presence of crosslinked fibres. (20X), (Olympus BX-51 microscope).

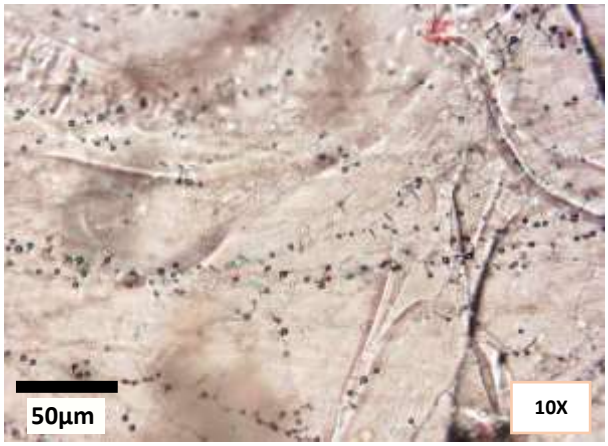

Fig. 39: Collagen+Gelatin+Alginate blend crosslinked with $CaCl_2$. Slice of bulk. It is evident the important presence of crosslinked fibres and reticulation. The black dots are small babbles trapped into the bulk. (10X), (Olympus BX-51 microscope).

6.2.2 Tube inverting test

This test allows the evaluation of sol-gel transition of the blends. Collagen-Gelatine blend presented a sol→gel transition in about 45 min. (Fig. 40, 41(left side of each image); this product was eliminated because the only chemical crosslinker available was glutaraldehyde, not biocompatible). The gelling time for Collagen-Gelatine- Alginate (Fig. 42) was about 1.30 hours, while Collagen-Alginate blend took the longest time, with a sol→gel transition of about 4 hours (Fig. 41 (right side)).

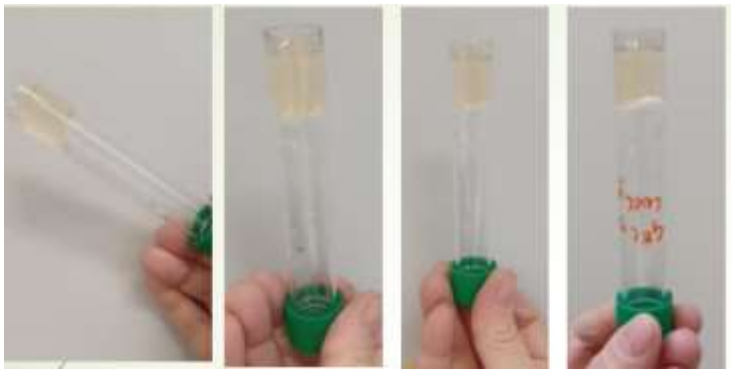

Fig.40: Collagen+Gelatine presents a sol→gel transition in about 45 min (eliminated).

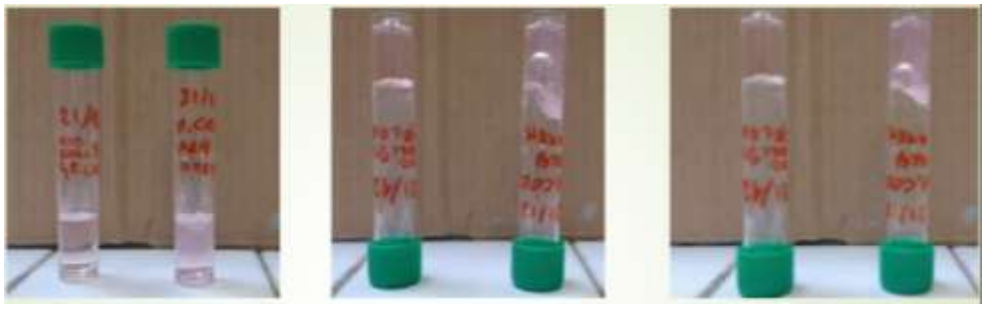

Fig.41: Collagen+Gelatine (on the left) vs Collagen+Alginate (on the right), both in DMEM, at time 0, 3hr, 5hrs after preparation. Collagen+Gelatine, (blend eliminated), presents a sol->gel transition in about 45 min, while Collagen+Alginate takes more than 4 hours at the concentrations prepared, at room temperature (19°C).

Fig. 42: Collagen+Gelatine+Alginate blend: control at time 15min, 1hr, 1.30hrs.

6.2.3 Collagen Alginate blend-swelling and dehydration tests

Fig.43: collagen + alginate blend. Samples used for swelling, degradation and dehydratrion tests.

TableIV: Swelling test. Weights(g) taken at fixed times.

Time (hours)	Weight (g)
0	11.32
1	13.38
24	12.80
48	14.04
72	20.07

TableV: Dehydration test. Weights(g) taken at fixed times.

Time (hours)	Weight (g)
0	11.64
1	9.45
24	8.35
48	8.19
72	8.10

Material characterization: collagen + alginate blend (swelling test)

Material characterization: collagen + alginate blend (dehydration test)

Fig. 44: collagen + alginate blend. Samples used for swelling and dehydration test weighted at 0, 1, 24, 48 and 72 hrs (the results are reported in the Table IV and Table V above).

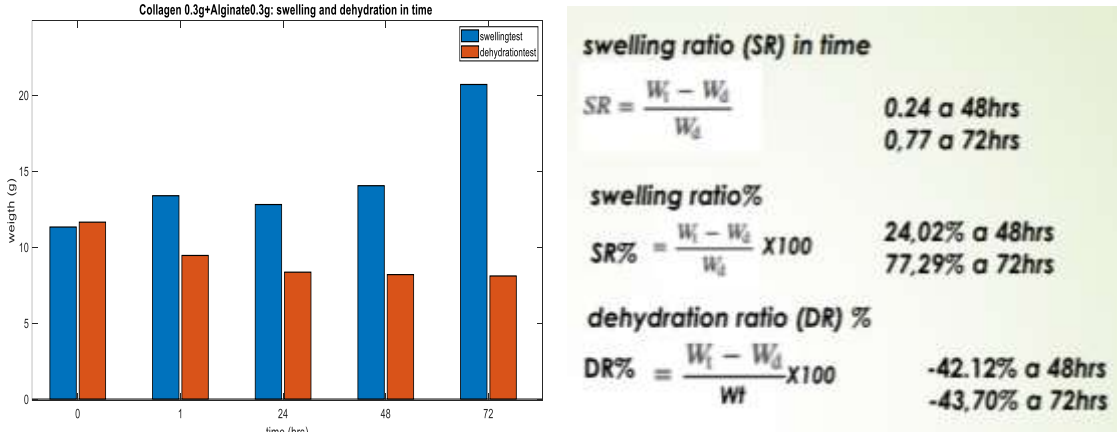

Fig. 45: collagen_alginate blend. Pictorial and numerical representation of the results of swelling and dehydration tests expressed as swelling ratio, swelling ratio %, dehydration ratio %.

6.2.4 Collagen Gelatine Alginate blend

swelling and dehydration tests

Fig.46: collagen+gelatine+alginate blend. Samples used for swelling, degradation and dehydratrion test.

TableVI: Swelling test. Weights(g) taken at fixed times.

Time (hours)	Weight (g)
0	9.55
1	10.96
24	9.45
48	11.93
96	15.01

TableVII: Dehydration test. Weights(g) taken at fixed times.

Time (hours)	Weight (g)
0	10.60
1	10.60
24	10.57
48	10.52
96	10.44

Material characterization: collagen+gelatine+alginate blend (swelling test)

Material characterization: collagen+gelatine+alginate blend (dehydration test)

Fig. 47: collagen_gelatine_alginate blend. Samples used for swelling and dehydration tests, weighted at 0, 1, 24, 48 and 96 hours (the results are reported in the Table VI and Table VII above).

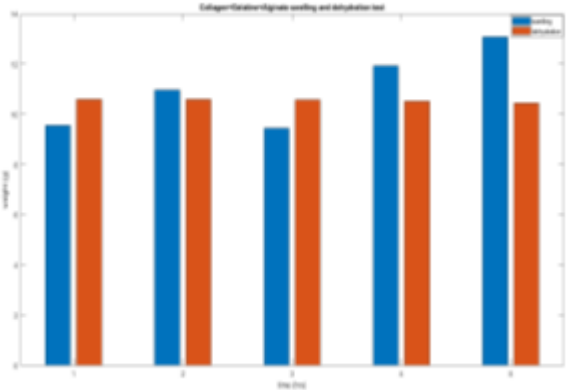

swelling ratio (SR) in time

$$SR = \frac{W_t - W_d}{W_d}$$

0,25 a 48hrs
0,57 a 96hrs

swelling ratio % (SR%) in time

$$SR\% = \frac{W_t - W_d}{W_d} \times 100$$

24,92% a 48hrs
57,17% a 96hrs

dehydration ratio (DR) %

$$DR\% = \frac{W_t - W_d}{Wt} \times 100$$

= -0.76% a 48hrs
-1.53% a 96hrs

Fig. 48: collagen_gelatine_alginate blend: results of swelling and dehydration tests. In this test, the last control was at 96 hrs to check the behaviour of the material because of its stability in time.

In Fig. 45 and Fig. 48, are reported pictorially and numerically, the results of the swelling and dehydration tests.

It is interesting to notice that the swelling ratio % of the two blends at 48 hours are comparable, with SR% = 24,02% of the collagen-alginate blend and SR% = 24,92% for collagen-gelatine-alginate. The result is completely different in the following controls: it is possible to notice that collagen-alginate, at 72hrs has a SR%=77,29% while collagen-gelatine-alginate blend, at 96hrs presents a SR%=51,17%, remaining stable in time.

About the dehydration ratio%, collagen-alginate presents a loose of water content equal to 42,12% at 48 hours, reaching a 43,70% at 72hrs, while collagen-gelatine-alginate blend maintains a constant weight during the whole dehydration test, presenting a loose of water content of 0,76% at 48 hours, that becomes 1,53% at 96 hours. This means that the second blend was able to maintain its content of water and did not dehydrate when left at room temperature in the open air. This stability in water content can be observed also looking at the fig.47, in which it is evident a constant dimension of the bulk prepared for the test, while the sample for the swelling test shows an evident increase of its dimension and a change in shape but it does not present loose of substance (degradation).

6.2.5 Rheometer analysis

The sweep tests were performed using both amplitude and frequency sweep. The same viscoelastic behaviour of the two blends was observed using amplitude (fig. 49) and frequency sweep tests (Fig. 51); Collagen-Gelatine-Alginate blend is characterised by solid-like behaviour (G'>G") in both the sweep tests (Fig. 49 and Fig. 51). The amplitude sweep tests were performed as function of the strain γ (%), from 0.01% to 100%: G' and G'' showed constant plateau values within the limit of linear viscoelastic region (LVR). For G' > G'' in the LVR, the sample presents a gel-like or solid structure (Collagen-Gelatine-Alginate up to the value of γ=10%, reversing the behaviour). For G'' > G' in the LVR, the sample is fluid (Collagen-Alginate). The LVR limit was fixed at 0.1 % of strain (Fig. 49). In Fig. 50, is shown a comparison between the G' functions of the two collagen-based blends.

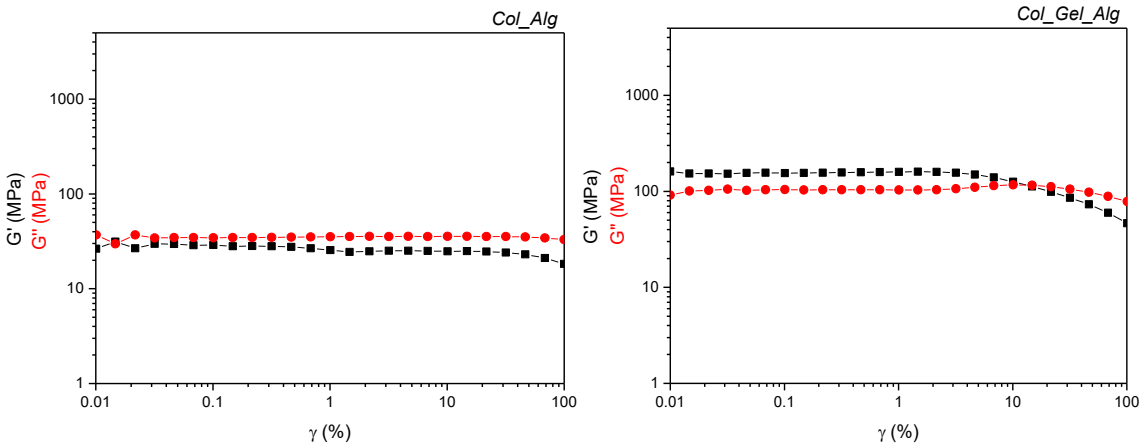

Fig. 49: Amplitude sweep tests: G' and G'' moduli are given as function of the strain γ (%) for Collagen-Alginate and Collagen-Gelatine-Alginate blends.

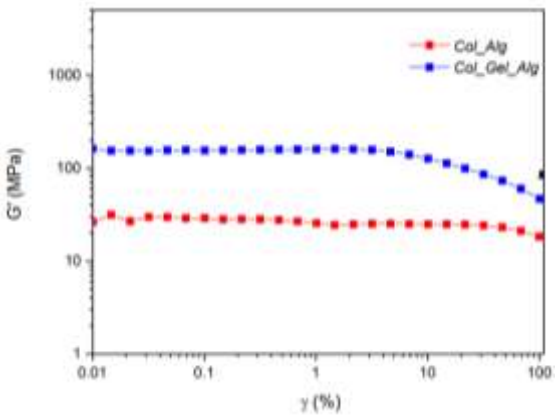

Fig.50: Amplitude sweep test: Comparison between the G' moduli as a function of the strain γ (%) of Collagen-Alginate and Collagen-Gelatine-Alginate blends. The LVR limit is fixed at 0.1 % of strain.

The elastic/storage (G') modulus and the viscous/loss (G'') modulus were also determined in oscillatory shear conditions as a measure of the stored and dissipated energy during one cycle of deformation. The oscillatory shear measurements were performed as a function of the oscillation frequency (ω), from 0.1 rad/s to 100 rad/s, for a constant strain γ (%) of 0.1% (in the linear range of viscoelasticity).

Fig. 51, shows a comparison of G' and G'' as a function of (ω) for Col_Alg and Col_Gel_Alg blends. For Col_Gel_Alg sample, the elastic modulus (G') presents higher values as compared with the viscous modulus (G'').

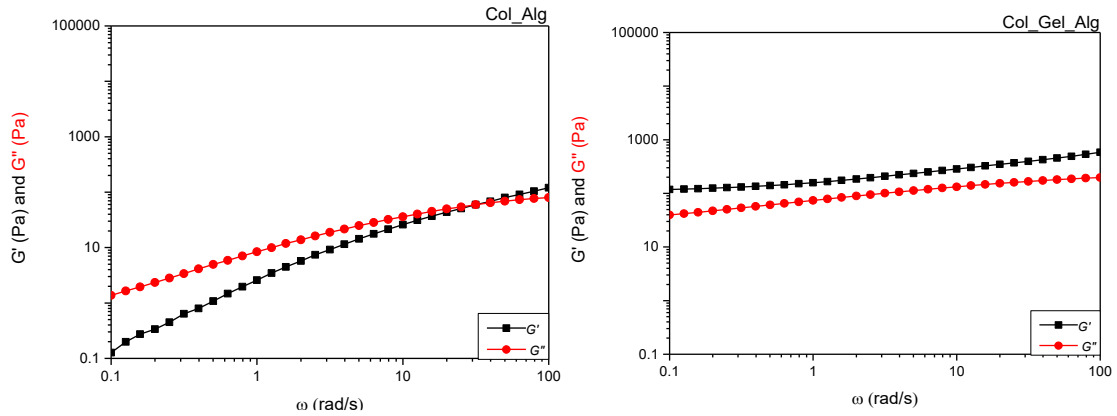

Fig. 51: Frequency sweep tests: Comparison of G' and G'' as a function of (ω) for Collagen-Alginate and Collagen-Gelatine-Alginate blends.

Fig. 52, presents a comparison of the viscoelastic parameters (G'(a), G''(b), tanδ(c)) as a function of the oscillation frequency (ω) of the collagen-based blends used in Cellink Incredible+ 3D-Bioprinter.

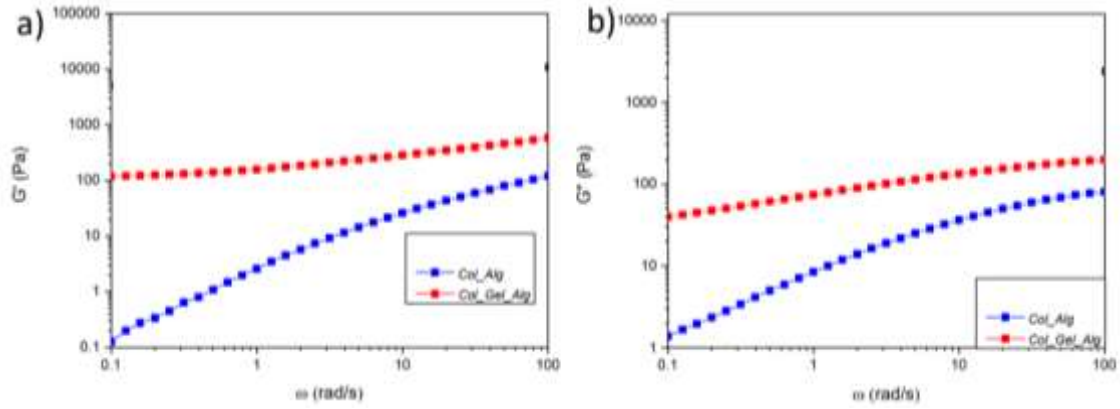

Fig.52: Comparison of G' (a) and of G''(b), as function of (ω), of Collagen-Alginate and Collagen-Gelatine-Alginate blends.

Fig. 52(c), shows a comparison of tan(δ) as a function of the oscillation frequency (ω) of the collagen-based blends. Can be observed that tan(δ) for collagen-gelatine-alginate blend is minor than 1.

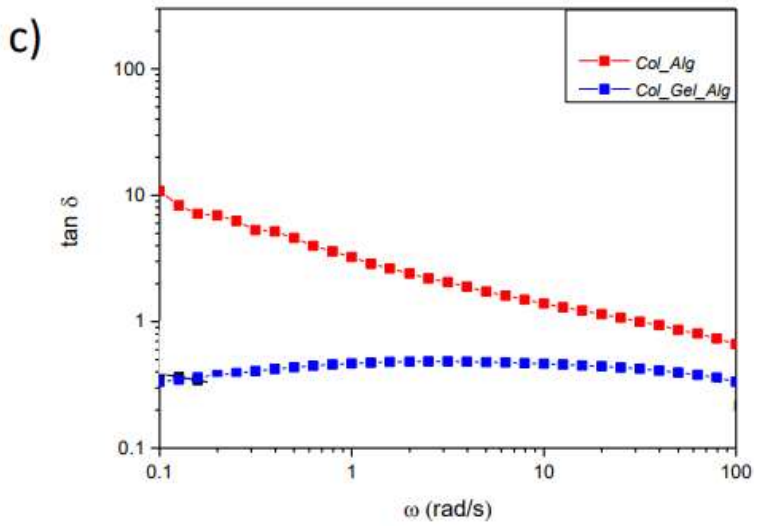

Fig.52 (c): Comparison of tan(δ) as a function of ω of Collagen-Alginate and Collagen-Gelatine-Alginate blends.

The shear viscosity (η) of the two collagen-based blends was determined as function of the shear rate (γ̇) in stationary shear flow conditions, for γ̇ varying in the range 0.01 s^{-1} – 1000 s^{-1}.

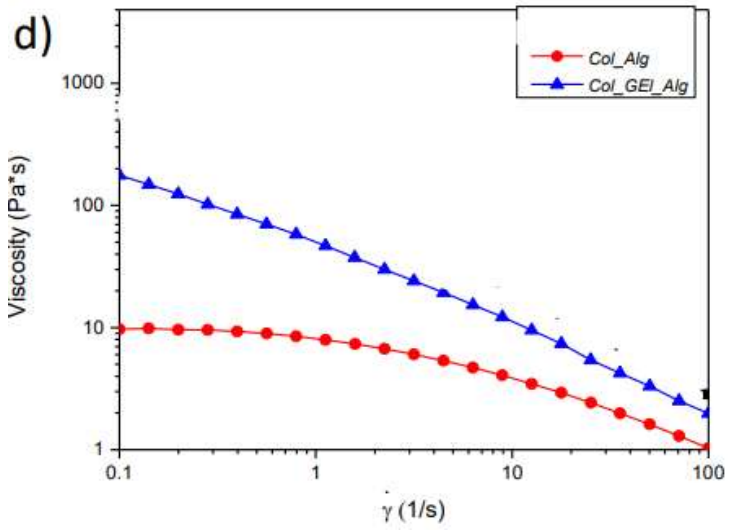

Fig. 52(d) Comparison of the shear viscosity (η) determined as function of shear rate (γ̇) in stationary shear flow conditions, of Collagen-Alginate and Collagen-Gelatine-Alginate.

The blends can be easily extruded for shear stress values (σ_y) above the yield stress (Table VIII), when the viscosity suddenly decreases, and the material starts to flow. The yield stress parameter mainly reveals the resistance of the fluid to flow during the extrusion process; additionally, this value is also directly correlated to the strength required to each layer of the scaffold, to support the following 3D printed layers.

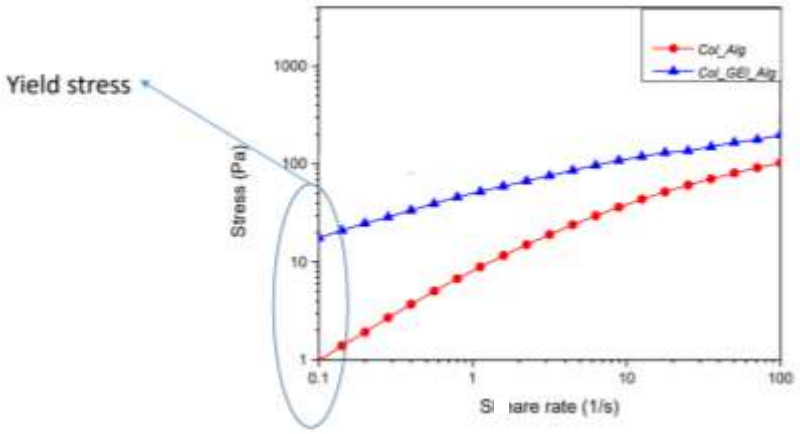

Fig.53: Comparison of yield stress (σ_y) as function of shear rate ($\dot{\gamma}$), of Collagen-Alginate and Collagen-Gelatine-Alginate.

Table VIII summarises the Rheological characteristics of the two Collagen-based blends at 25 °C.

Table VIII. Rheological characteristics of the Collagen-based blends at 25 °C						
	G' (Pa) 1 rad/s	G" (Pa) 1 rad/s	G' (Pa) 100 rad/s	G" (Pa) 100 rad/s	σ_y (Pa)	η_y (Pa*s)
Col_Alg	2.6±0.2	8.4±0.5	120.3±9.4	82.1±2.6	1.1±0.1	9.9±0.2
Col_Gel_Alg	172.5±13.4	80.5±7.8	615.1±21.2	207.1±17.1	20.4±0.3	204.2±2.9

G' and G'' values at 1 rad/s and 100 rad/s were considered.
σ_y - yield stress.
η_y - the viscosity corresponding to the yield stress (σ_y).

In conclusion, Collagen-Alginate blend is a non-Newtonian fluid showing liquid-like behaviour (G">G' and tan(δ)>1), while Collagen-Gelatine-Alginate shows a solid-like behaviour (G'>G" tan(δ)<1), on the base of the angular frequency values (ω).

6.3 Cell characterization

6.3.1 Collagen_Alginate_SK-LMS-1 cells bioink. Cell characterization at optical observation with inverted phase contrast microscope. Images taken at day 1, day 2, day 5, day 6 of control and cell count to build up the curves of growth: were evaluated the formation of spheroids, the number of spheroids and the area of spheroids per day of observation (Fig. 54).

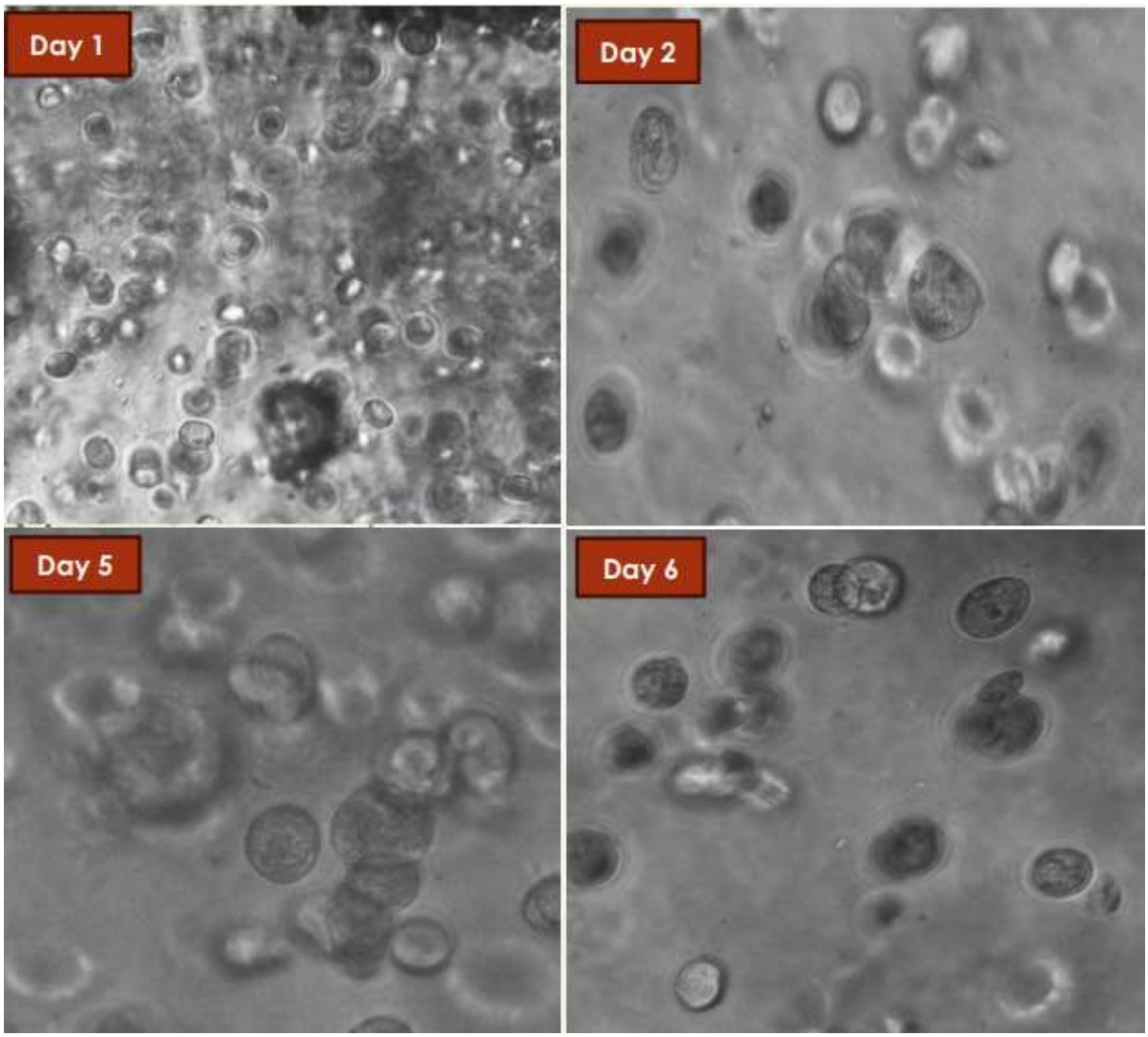

Fig. 54: Images taken with the inverted phase contrast microscope at day 1, 2, 5, 6 of observation.

6.3.1.1 Curves of growth: number and area of spheroids

Collagen Alginate based blend: the graph in Fig. 55, represents the curve of growth of the number of spheroids in time, starting from day1. In each day of control (day1,2,5,6), the count of spheroids has been performed by taking randomly 6 images from each well of the 6-well plate for a total of 36 photos per plate per day of control.

The graph in Fig. 56, represents the curve of growth of the area of spheroids in time, expressed in day of observation, starting from day1.

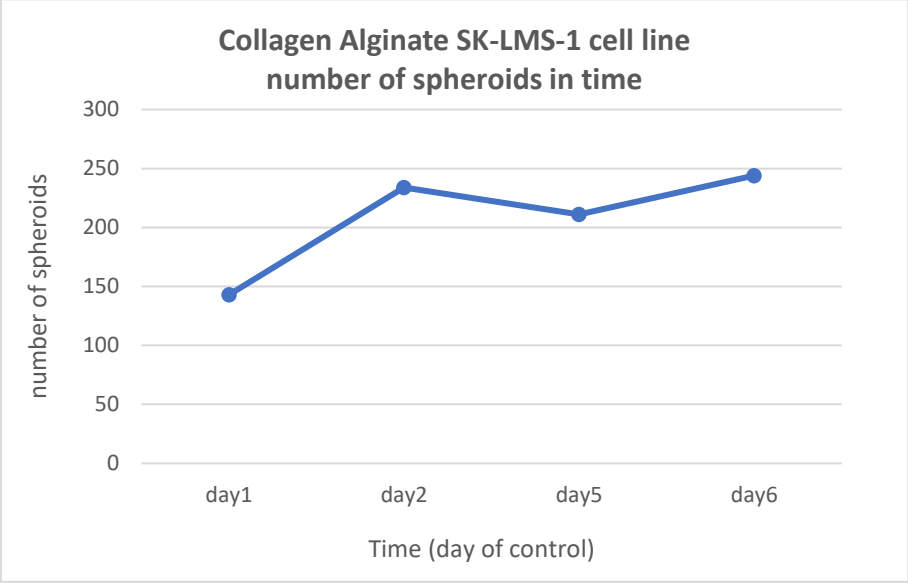

Fig. 55: Collagen Alginate SK-LMS-1 cell line: number of spheroids in time (day of control)

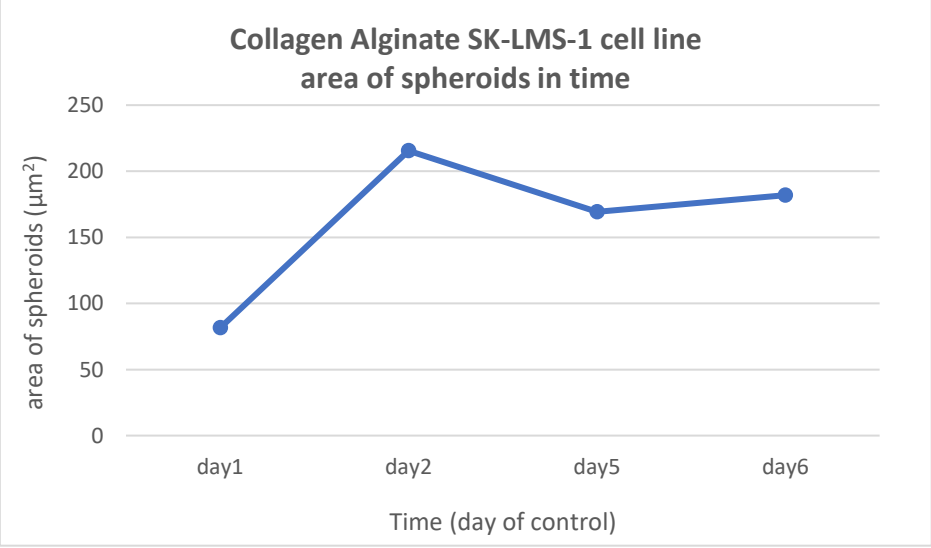

Fig.56: Collagen Alginate SK-LMS-1 cell line: area of spheroids in time (day of control).

6.3.1.2 Statistical analysis: number of spheroids

The graph in Fig. 57 represents the statistical analysis of the number of spheroids per day of control. It can be observed a statistically significant increase of the number of spheroids from day 1 compared to day 2 (p=0.0172) and compared to day 5 (p= 0.0074) and day 6 (p=0.0013) indicating an increased spread.

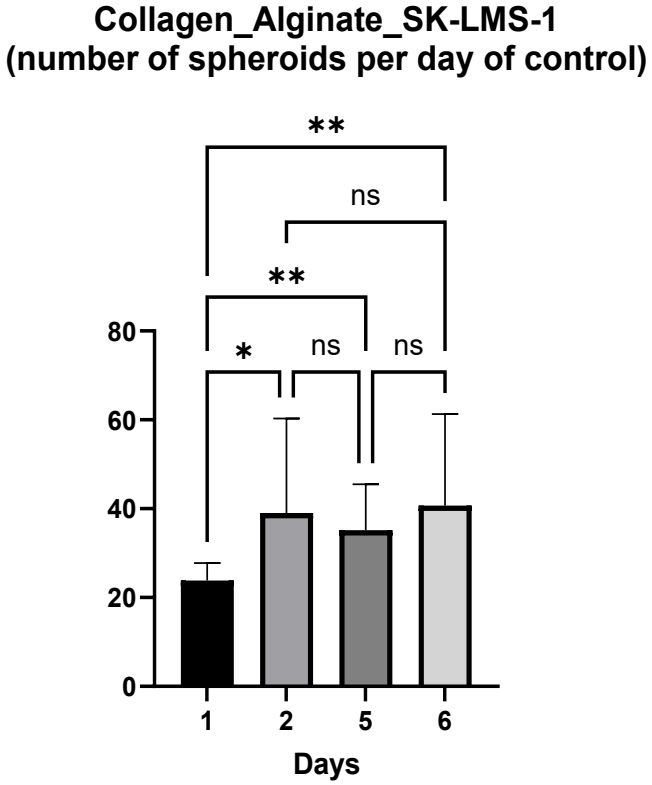

Fig.57: Collagen Alginate SK-LMS-1 cell line. The bar chart by column shows the number of spheroids per day of control (from day1 to day 6).

6.3.1.3 Statistical analysis for area of spheroids

The graph in Fig. 58 represents the statistical analysis of the area of spheroids per day of control (from day 1 to day 6). It can be observed a statistically significant increase of the area of spheroids from day 1 compared to day 2 ($p<0.0001$) and compared to day 5 ($p<0.0001$) and day 6 ($p<0.0001$) indicating an increase in size of spheroids.

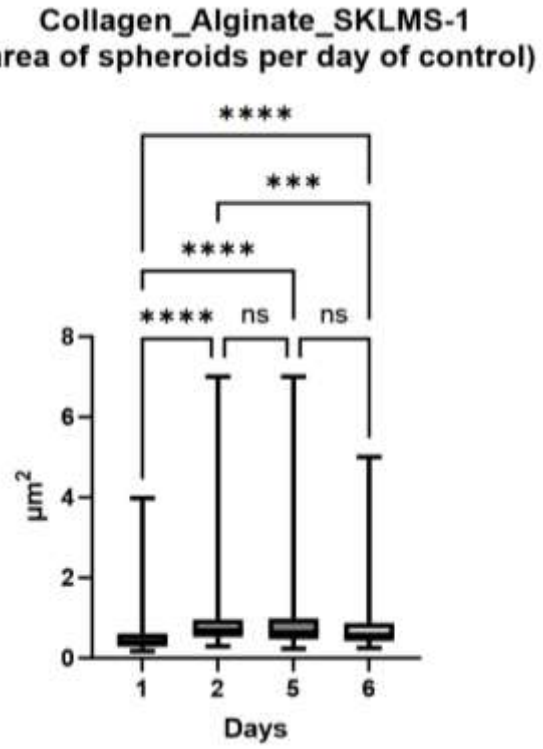

Fig.58: Collagen Alginate SK_LMS-1 cell line. The minimum/maximum *box-and-whisker plot* shows visually the area of spheroids per day of control (from day 1 to day 6).

6.3.2 Collagen_Gelatine_Alginate_SK-LMS-1 cells bioink: optical observation with inverted phase contrast microscope. Cell characterization at optical observation with inverted phase contrast microscope. Images taken at day 1, day 2, day 5, day 6 of control and cell count to build up the curves of cell growth: were evaluated the formation of spheroids, the number of spheroids and the area of spheroids per day of observation (Fig. 59).

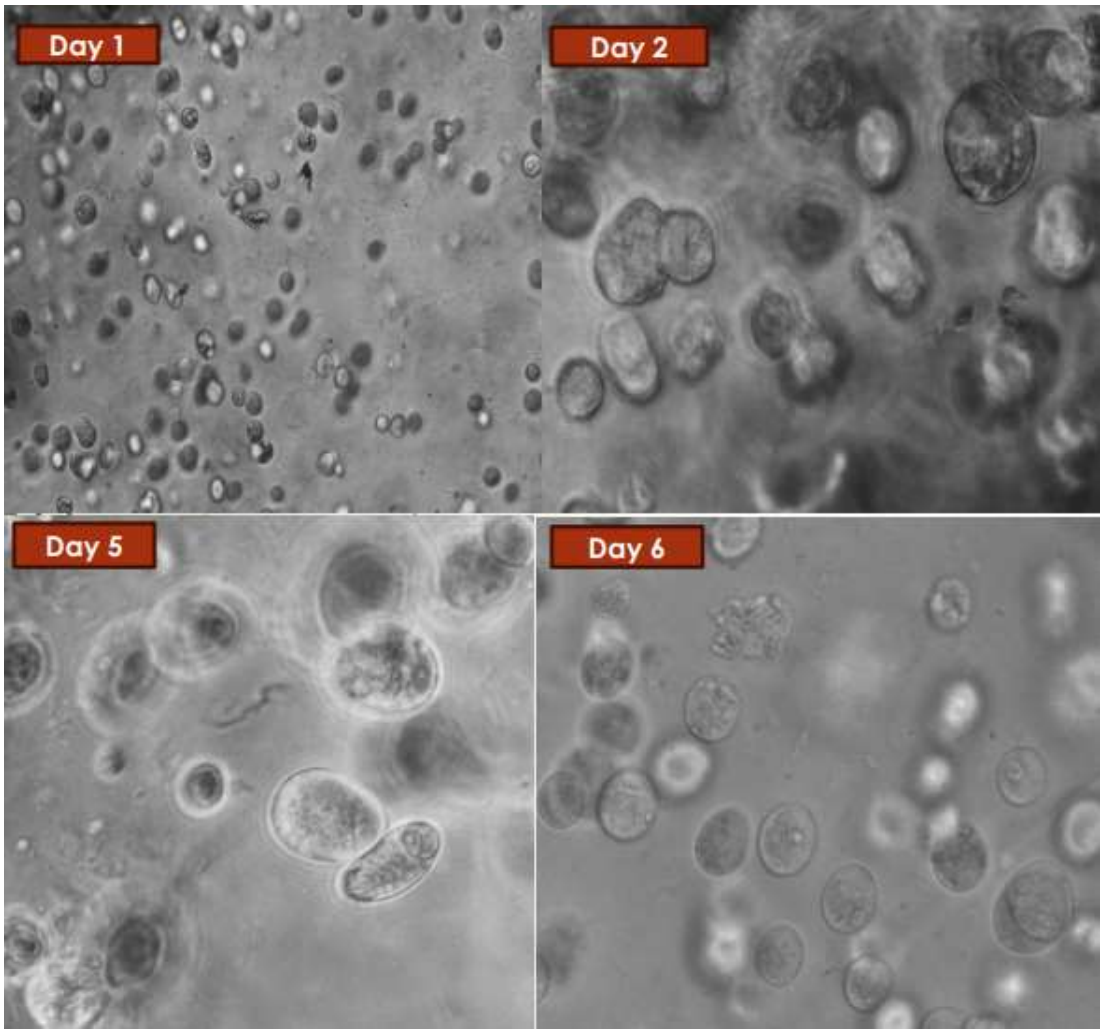

Fig. 59: Images taken with the inverted phase contrast microscope at day 1, 2, 5, 6 of observation.

6.3.2.1 Curves of growth: number and area of spheroids

Collagen Gelatine Alginate-based blend: the graph in Fig. 60, represents the curve of growth of the number of spheroids in time, expressed in day of observation, starting from day1. In each day of control (day1,2,5,6), the count of spheroids has been performed by taking randomly 6 images from each well of the 6-well plate for a total of 36 photos per plate per day of control.

The graph in Fig. 61, represents the curve of growth of the area of spheroids in time, expressed in day of observation, starting from day1. It can be observed that, the trend of the area of spheroids follows a Gompertzian model of growth *[Alzahrani E.O. et al., (2014)].*

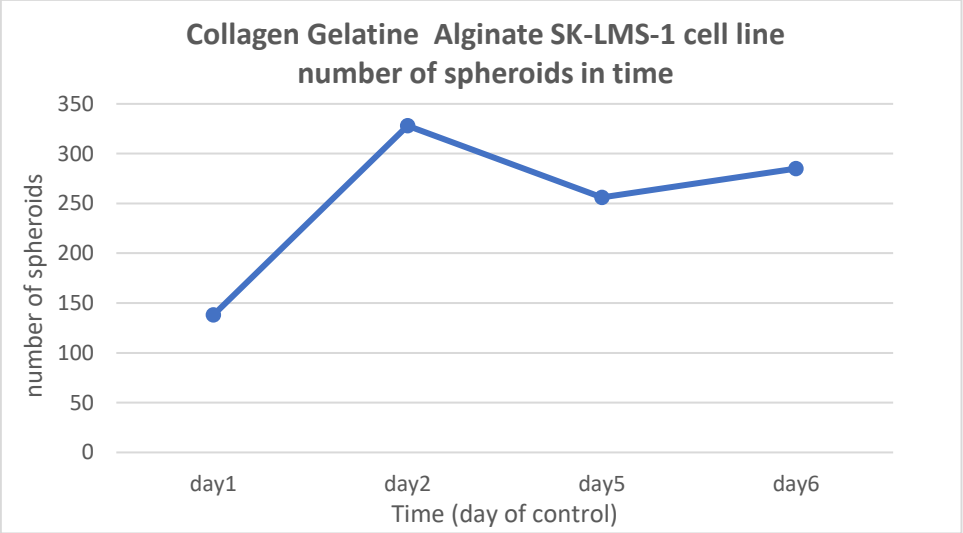

Fig. 60. Collagen Gelatine Alginate SK-LMS-1 cell line: number of spheroids in time (day of control).

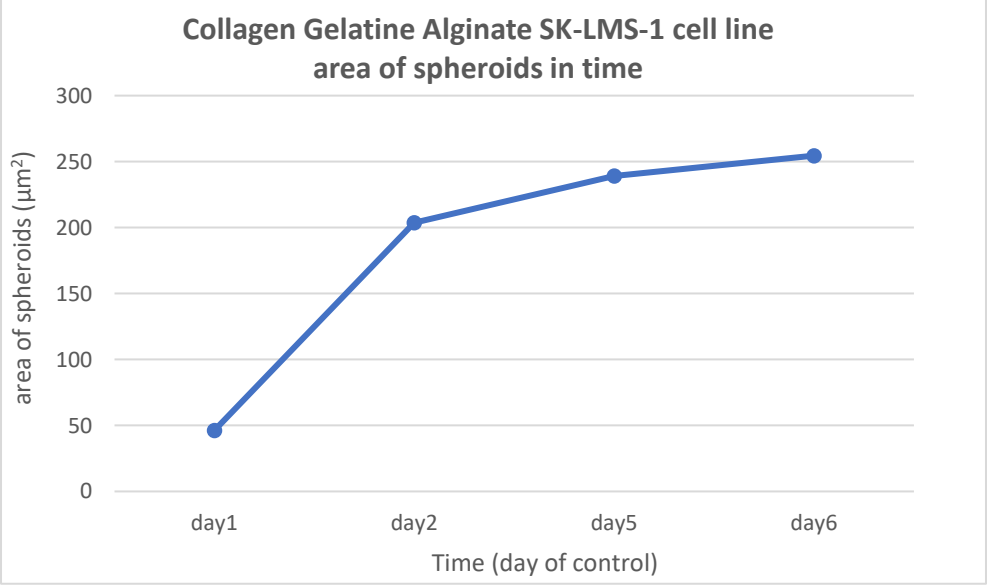

Fig.61: Collagen Gelatine Alginate SK-LMS-1 cell line: area of spheroids in time (day of control).

6.3.2.2 Curves of growth overlapped: comparison of the curves of number of spheroids (Fig. 62) and area of spheroids (Fig. 63) from the scaffolds obtained with the two bioinks.

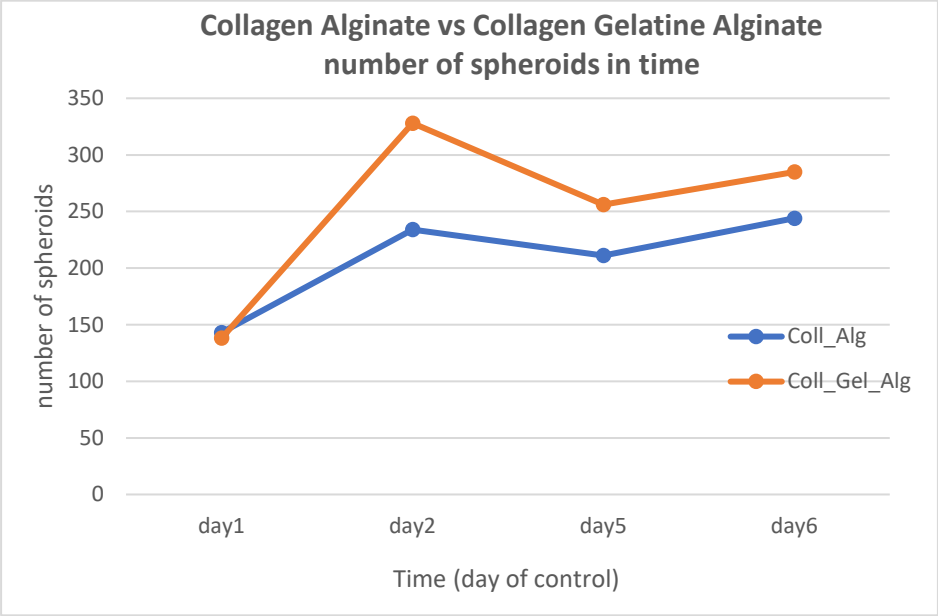

Fig. 62: Collagen Alginate vs Collagen Gelatine Alginate: number of spheroids in time (day of control)

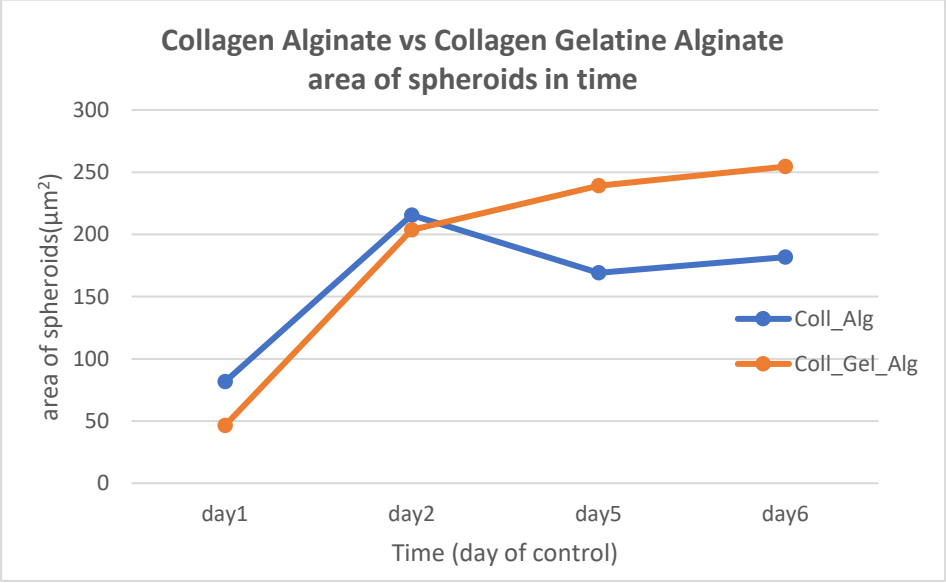

Fig.63: Collagen Alginate vs Collagen Gelatine Alginate: area of spheroids in time (day of control).

6.3.2.3 Statistical analysis: number of spheroids

The graph in Fig. 64 represents the statistical analysis of the number of spheroids per day of control (from day 1 to day 6). It can be observed a statistically significant increase in the number of spheroids from day 1 compared to day 2 ($p<0.0001$) and compared to day 5 ($p<0.0001$) and day 6 ($p=0.0006$) indicating an increased spread.

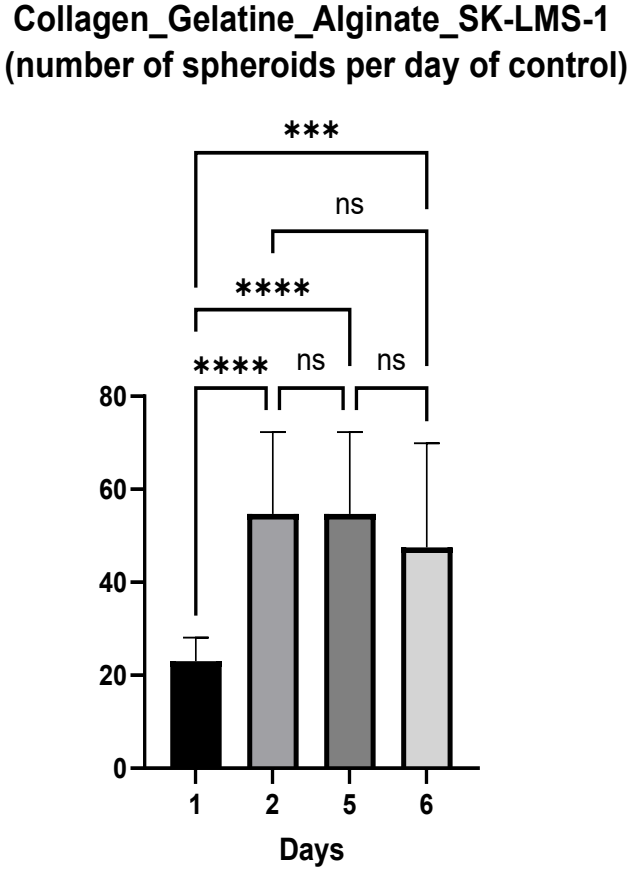

Fig. 64: Collagen Gelatine Alginate SK-LMS-1 cell line. The bar graph by column shows the number of spheroids per day of control (from day 1 to day 6).

6.3.2.4 Statistical analysis for area of spheroids

The graph in Fig. 65 represents the statistical analysis of the area of spheroids per day of control (from day 1 to day 6). It can be observed a statistically significant increase of the area of spheroids from day 1 compared to day 2 ($p<0.0001$) and compared to day 5 ($p<0.0001$) and day 6 ($p<0.0001$) indicating an increase in their size.

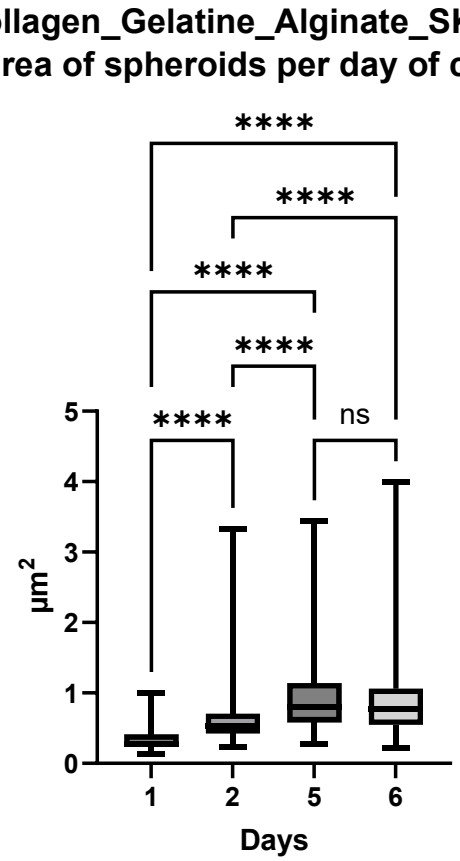

Fig.65: Collagen Gelatine Alginate SK-LMS-1 cell line. The minimum/maximum *box-and-whisker plot* shows visually the area of spheroids per day of control.

6.3.3 Optical Microscopy analysis: Haematoxylin & Eosin staining

6.3.3.1 Collagen Alginate blend

In Fig. 66, is shown a collection of images of the cell free matrix formed with the Collagen Alginate blend developed, treated with Haematoxylin & Eosin histochemical staining.

In Fig. 67, is shown a collection of images of the cell laden matrix obtained with Collagen Alginate SK-LMS-1 cell-line bioink, treated with Haematoxylin & Eosin histochemical staining. It is possible to observe the presence of eosinophilic multinucleated spheroids.

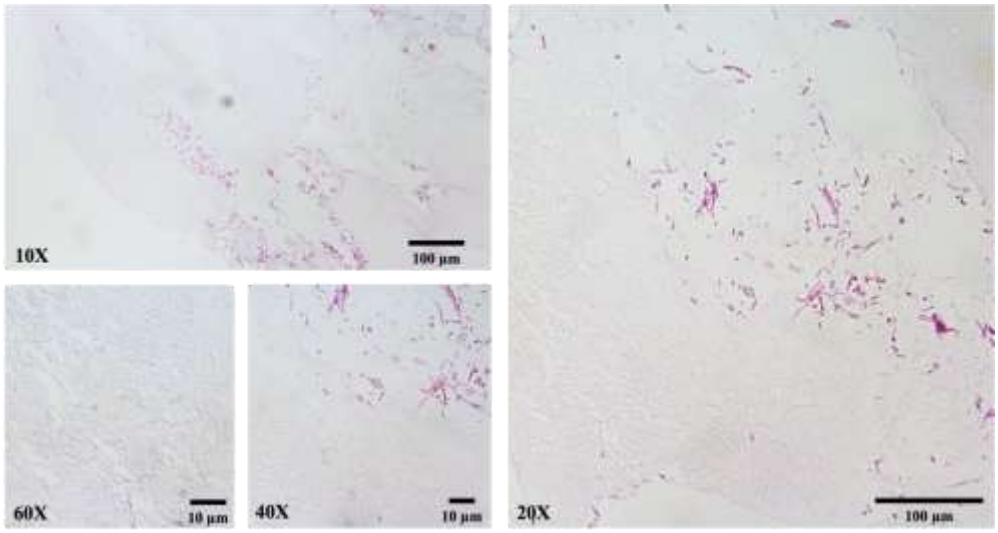

Fig.66: Collagen Alginate blend: optical microscopy of cell free matrix stained with Haematoxylin/Eosin

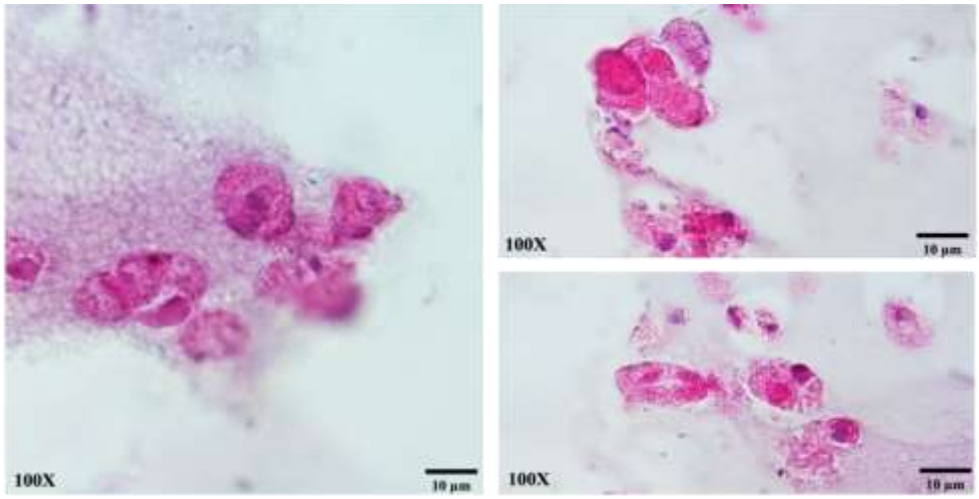

Fig. 67: Collagen Alginate blend: optical microscopy of cell laden matrix stained with Haematoxylin/Eosin

6.3.3.2 Collagen Gelatine Alginate blend

In Fig. 68, is shown a collection of images of the cell free matrix formed with the Collagen Gelatine Alginate blend developed, treated with Haematoxylin & Eosin histochemical staining.

In Fig. 69, is shown a collection of images of the cell laden matrix formed with the Collagen Gelatine Alginate SK-LMS-1 cell-line bioink, treated with Haematoxylin & Eosin histochemical staining. It is possible to observe the presence of eosinophilic multinucleated spheroids.

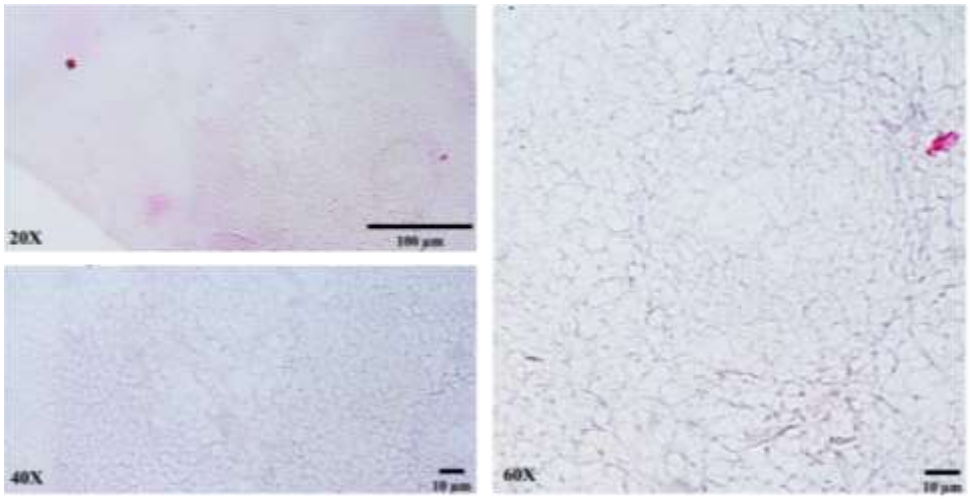

Fig.68: Collagen Gelatine Alginate blend: optical microscopy after Haematoxylin & Eosin staining (matrix only)

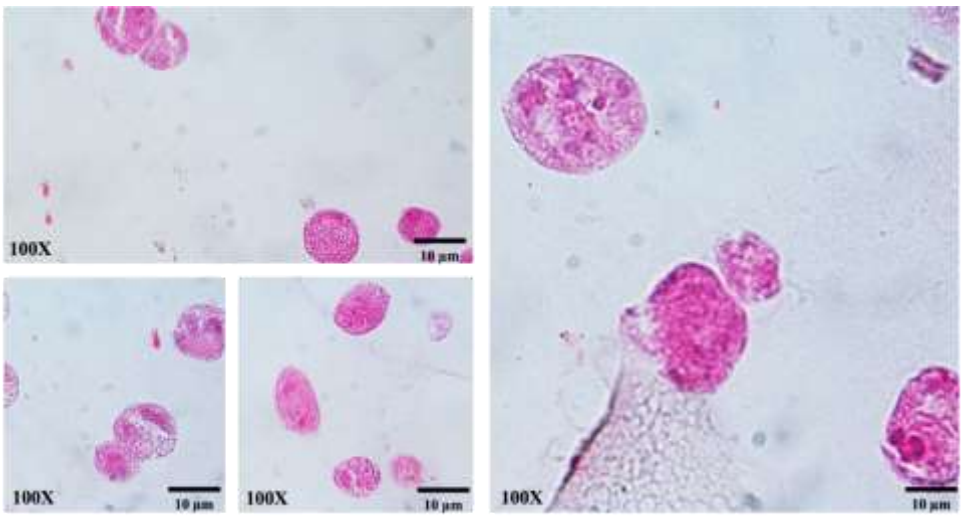

Fig. 69: Collagen Gelatine Alginate blend: optical microscopy after Haematoxylin & Eosin staining (matrix+SKLMS-1 cell line)

6.3.4 Fluorescence Microscopy analysis: DAPI staining

In this section are reported the images acquired after DAPI staining. Both the cell free matrices (Fig. 70, 72) and both matrices with spheroids (Figg. 71, 73) were stained with DAPI. It is possible to observe an excellent growth of spheroids in both matrices, validating the data.

6.3.4.1 Collagen Alginate blend

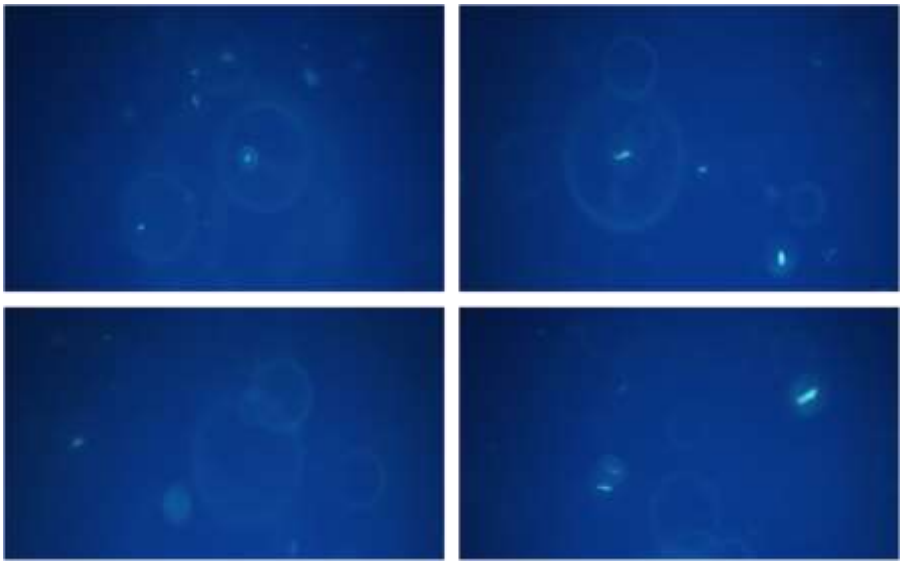

Fig. 70: Collagen Alginate blend. Optical fluorescence observation (DAPI): matrix only

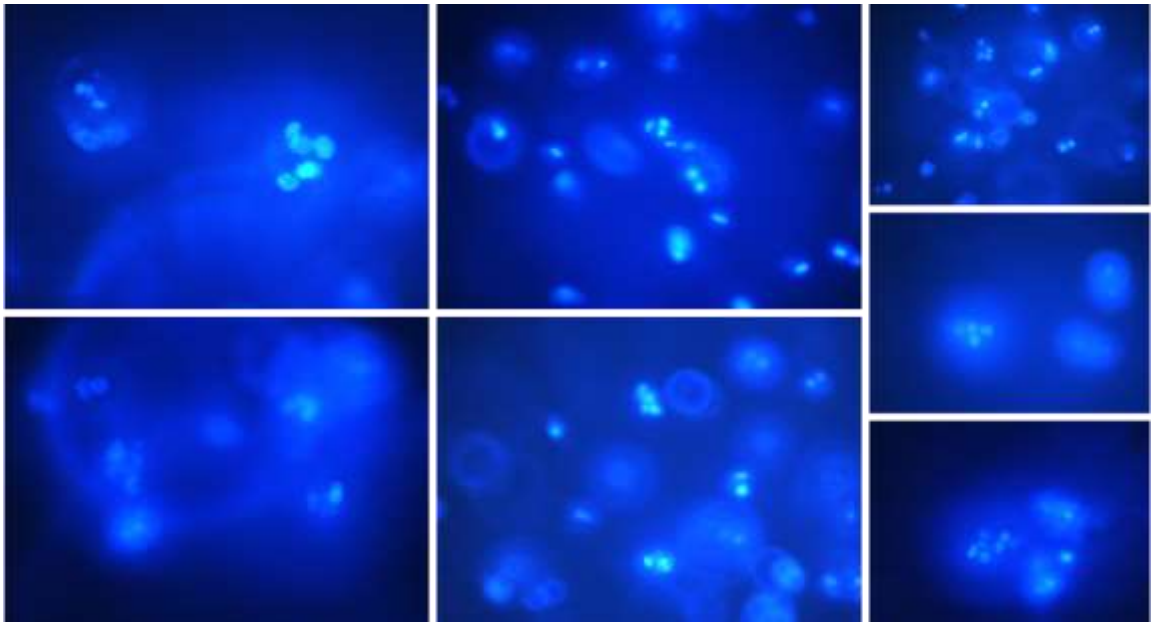

Fig. 71: Collagen Alginate SK-LMS-1 cell line-bioink. Matrix + spheroids after DAPI staining

6.3.4.2 Collagen Gelatine Alginate blend

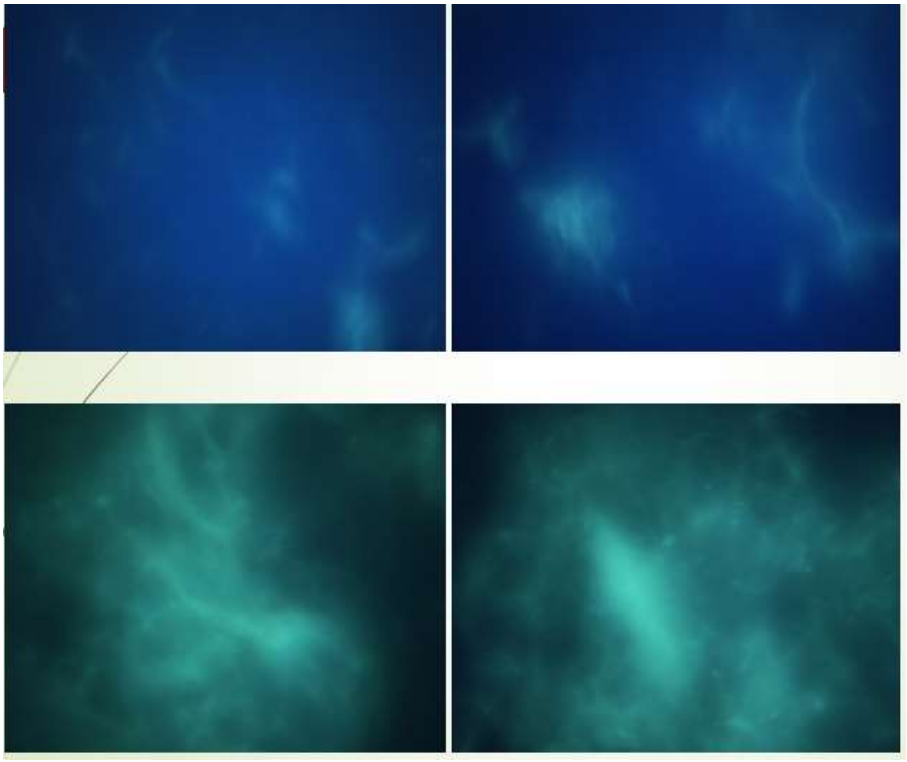

Fig. 72: Collagen Gelatine Alginate blend. Optical fluorescence observation (DAPI): matrix only

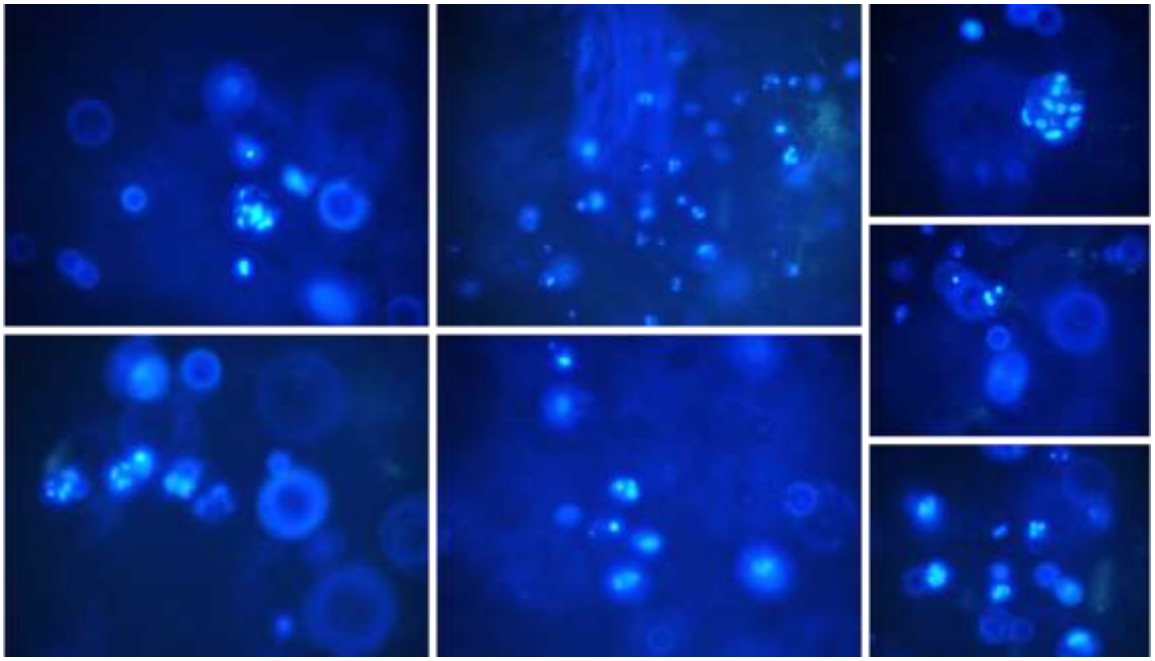

Fig. 73: Collagen Gelatine Alginate SK-LMS-1 cell line-bioink. Matrix + spheroids after DAPI staining

7. Discussion

In biological applications, the mechanical properties of bioinks based on natural polymers such as collagen and gelatine, depend on the concentration, crosslinking mechanism and the crosslinking conditions of the materials. In addition, the combination of multiple natural materials into blend/composite materials, can further facilitate mechanical properties: many experimental studies showed that a single biomaterial as component of a bioink is more restrictive, and the scaffold obtained are not able to achieve ideal performance. It is for this reason that one of the current trends in biomaterial development for 3D bioprinting is the construction of blend-bioinks *[Zhang J. et al., (2021)],* and this is the reason why, after a few trials performed with the single materials available, has been decided to develop blend-bioinks for the present work, selecting as core material Collagen type I.

Although type I collagen has been widely used in 3D bioprinting, it presents limitations, such as poor mechanical properties, low viscosity, and long gelation time *[Sorushanova et al., (2019)]*. In recent years, researchers have used different strategies to improve the printing properties of collagen, including chemical modification of collagen, adjustment of pH and temperature, change in collagen concentration, and mixing collagen with other materials *[Kim Y.B. et al., (2016)].* Keeping in mind these aspects, the strategies used in this work to improve the structural properties of the collagen-based bio-blends developed were diverse, including change in concentration of collagen, mixing collagen with thickener agents as gelatine, change of the pH of collagen solution, addition of sodium alginate to the blend, easily crosslinked with $CaCl_2$, a chemical crosslinker quite biocompatible. The best results obtained are represented by the two blends developed and tested in this work.

The rheological properties of blends/bioinks are very important to obtain satisfactory 3D bioprinting *[Pramod D. et al., (2021)].* The ideal extrusion bioink should be shear thinner and able to achieve low viscosity in the high shear environment of the printing nozzle. Normally, the higher viscosity materials provide structural support for the printed construct and lower viscosity materials provide a suitable environment for maintaining cell viability and function; encapsulated cells exposed to higher stresses present a reduction of cell viability during bioprinting *[Murphy S. V. and Atala A. (2014)].* In fact, due to the mechanical requirements for structural stability after extrusion, the bioink is usually quite viscous, about 10–300 Pa*s, with problems of high shear force and low

cell survival rate *[Blaeser A. et al., (2016); Kang D. et al., (2018)].* In addition, due to the mechanical limitation of extruding viscous materials through small nozzles, the diameter of the nozzles used is limited, which further limits the resolution of extrusion printing *[Bedell M.L. et al., (2020)].* On the other end, according to certain authors, biomaterials with liquid-like behaviour are not suitable for extrusion bioprinting process because they are not able to maintain shape after extrusion, showing the tendency to modify their shape overtime *[Wu D. et al., (2018); Nacu I. et al., (2023)].*

This aspect can be overcome using, after the 3D bioprinting process, a cross-linker agent, able to maintain the shape of the 3D bio-printed scaffolds. Calcium chloride ($CaCl_2$) solution was used as cross-linker agent for the two collagen-based bio-blends in which alginate was added as thickener. $CaCl_2$ solution, improves the mechanical properties, particularly tensile strength, due to a crosslinking reaction between Ca^{2+} ions and carboxyl groups of sodium alginate *[Ibrahim S.F. et al., (2019)].*

The two blends developed, showed non-Newtonian behaviour, with an apparent viscosity (η) depending on the shear rate ($\dot{\gamma}$): increasing the shear rate, a shear-thinning behaviour was observed, while the viscosity value was influenced by the shear rate. This shear-thinning behaviour made the blends printable *[Bercea M., (2023)].* The blends were easily extruded for shear stress values above the yield stress, $\sigma_{y,}$ as reported in Table VIII *[Sakr M.A. et al., (2021)].*

Possible drawbacks of the 3D scaffold surface functionalization with post-processing treatments, as crosslinking treatments, are represented by potential side effects or change in the original morphology and shape of the scaffolds *[Camacho P. et al., (2021)].* In the present work, to verify a possible modification in shape or change in aspect, for instance a change in transparency of the blends after treatment with a crosslinking agent, the two bioblends were preliminary tested: the first 6 scaffolds 3D-bioprinted in a Falcon 6well plate, were put into the CELBIO incubator, at 37°C, and 5% CO_2 for 3 days, covered with culture medium (DMEM). At the control, the constructs were perfectly conserved and did not present any change in shape, loose of substance or modification in aspect, so the blends were considered adequate for the purpose.

The results and considerations above reported, derive from the analysis of the rheological properties of the two bio-blends, at 25°C, without cell laden. It is important to highlight that:

1. any assessments of a cell-free bioink may not hold complete relevance with respect to the equivalent bioink containing cells, as cells have an impact on the rheological properties of the mixture;

2. in this experimental work, was used a tumour cell-line, presenting different behaviour with respect to normal cells and capable, *in vivo*, to modify properties and composition of an ECM.

In the present work, an in vitro study and not a clinical application, was used a SK-LSM-1 tumour cell line obtained from the vulva of a 43-year-old, white female with leiomyosarcoma, furnished by ATCC group, biologically safe, fast to expand, used in cancer research.

When the 3D bioprinting is used for clinical application, the most critical issues is represented by the selection of an appropriate cell source, which should be safe, minimally invasive, fast and easy to expand *[Amler A.K. et al., (2021)].*

The tumour cells used in this work, were able to form spheroids, composed by tumour cells only and not by a multicellular ensemble; this can have a minor impact on the microenvironment and on cell behaviour because interactions between different cell-types are absent.

The capability of spheroid formation by the tumour cell-line used, is important to characterise the two bio-blends that represent the structural support, the ECM for the growth of tumour cells. In fact, for spheroid formation, it is necessary cell-cell interaction and cell-matrix interaction. The curves of growth, representing the total number of spheroids formed (Figg. 55, 60) and the total area occupied by spheroids (Figg. 56, 61) are self-explanatory, giving a picture of the matrix characteristics, also considering the results of the research studies reported. Furthermore, overlapping the curves of the number of spheroids (Figg. 55, 60), it is possible to observe the same trend of growth, even though a numerical difference is present (Fig. 62). On the contrary, the curves representing the area of spheroids (Fig.63), are quite different and, this difference could be due to the composition and consequently to the mechanical properties of the blends, representing the Tumour Micro Environment. Both the blends appear to support the spheroid formation, allowing cell-cell and cell matrix interaction, but at a certain moment there is a divergence in the cell growth behaviour.

The mechanical properties of the cellular microenvironment modulate the displacement of single cells and the formation and growth of tumour spheroids. Based on the composition of the extracellular matrix, its stiffness and architecture can significantly vary, consequently influencing cell displacement and tumour growth. Collagen density, which modulates the steric properties of the matrix, governs individual cell migration and, as consequence, leads to the formation of cell clusters of different sizes. Matrix stiffness, which characterises the resistance of matrix to deformation in

response to applied forces, is a well-known regulator of many biological processes, in particular cell motility *[Ehrbar M. et al., (2011); Lo C. et al., (2000); Pathak A. et al., (2012)].*

Different studies, mainly related to 2D conditions, have shown that the matrix stiffness may influence:

1. the direction of cell displacement, driving the cells along stiffness gradients [*Lo C. et al., (2000)*];
2. cell speed, producing higher cell velocity values with stiffer matrices [*Pathak A. et al., (2012)*].

In 3D configuration, has been observed that structural changes able to induce stiffness in matrix, can also affect the matrix architecture, which regulates migration by itself *[Pathak A. et al., (2011)].* Differently said, matrices with a higher fibre density may be stiffer, but may also present smaller pore sizes, which regulate the confinement levels. Confined microenvironments are commonly associated with restrained cell motility, as cells become unable to move through the matrix *[Charras G. and Sahai E., (2014)].* Consequently, the complexity of 3D cultures makes it difficult to dissociate the effects induced by matrix stiffness from those produced by matrix architecture.

Cell motility and its dependence on the physical properties of the ECM is particularly important in cancer biology and for the present work. The mechanical properties of the tumour microenvironment are diverse with respect to those found in normal tissues, depending on the ability of tumour cells to sense and modify their environment *[Yamaguchi H. et al., (2005)].*

In several studies, bioinks containing tumour cells, in 3D scaffolds were able to replicate the initial stages of growth in avascular solid tumours, creating a setting that can also reflect the initial stages of metastatic colonization in new tissue *[Nyga A., et al., (2011)].*

Several techniques to produce multicellular structures from tumour cells are available *[Lv D. et al., (2017)]:* in this thesis work, individual cells were directly mixed to the bio-blend and then printed to form 3D scaffolds to understand how cells organise on the base of the matrix characteristics [Cheng G. et al., (2009)].

Despite these advances and the various available experimental setups, it is still unclear how the mechanical properties of 3D scaffolds modulate tumour cell behaviour.

In experimental settings, hydrogels based on collagen, the most abundant component of the natural ECM *[Frantz C. et al., (2010)],* are commonly used. Collagen gives the possibility to produce

matrices with different mechanical properties simply changing their composition and preparation procedures *[Sapudom J. and Pompe T., (2018)].* For example, different collagen concentrations or changes in pH can modify the different matrix properties *[Roeder B.A. et al., (2002)].*

Gonçalves IG et al. (2021), in their study, replicated a set of experiments in which cells were seeded in collagen matrices of different collagen densities, producing matrices with different mechanical properties; tracking individual cell trajectories and speeds, was also analysed the formation of multicellular clusters and their size was measured. Overall, the results showed that cells seeded in matrices with low collagen density tend to migrate more. Accordingly, cells leave their original cluster and form small structures. In contrast, high collagen density reduces cell migration producing multicellular structures (spheroids) with increased volume.

In conclusion, not only exists a relation between matrix density and individual cell migration but also experimental data demonstrate how migration, or its inhibition, modulates tumour growth. The authors concluded that the effect of collagen density on cell migration was a key regulator in tumour spheroid formation and growth *[Gonçalves IG et al. (2021)].*

It is also necessary to consider the impact that cells can have on the physicochemical properties of the bioink: the impact of cells on bioink properties is manifold. Cells within a bioink occupy a specific volume, depending on their size and density. The volume taken up by cells is precluded to the hydrogel, potentially impacting on the cross-linking efficiency and viscoelastic properties *[Yamada K.M. and Cukierman E., (2007)].*

The metabolic state of the embedded cells is also important, as their subtype and the volume occupied, with potential difference when single cells, spheroids, or complex aggregates are processed. *[Pinto B. et al., (2020)].*

It is necessary to underline the importance of the cell type used in a bioink. In this work, were used vulva leiomyosarcoma cells, presenting a rapid rate of growth in favourable conditions.

In this study, as discussed before, was observed a difference in the area occupied by spheroids developed in the two diverse bioinks. Considering that the only difference between the scaffolds was the composition of the blends used to prepare the bioinks, can be supposed that the difference of mechanical properties, mainly due to a difference of rheological properties, had plaid a central role in the cell growth mode. As highlighted in many of the studies reported, in 3D environment, stiffness of the matrix can also modify the architecture of a matrix, first the porosity.

This aspect, in presence of tumour cells, can be translated into a change of the cell migration capability, with a change in cell velocity and displacement. These facts could explain the different total area occupied by spheroids observed into the scaffolds. A softer environment can promote cell migration leading to the formation of spheroids of smaller size; on the contrary, stiffer matrices, inducing a certain degree of confinement, can lead to a minor migration of tumour cells and a parallel increase of the spheroid dimension locally formed that tend to be bigger in size. This fact could also explain the different curves representative of the area of spheroids. Observing the curve obtained using alginate-gelatine-collagen, it is possible to notice a *Gomperztian* modality of growth, with an exponential phase followed by a log phase, that can be justified by the existence of the three layers of cells, outer proliferative, inner of necrotic cells, intermediate of quiescent cells, able of maintaining a steady state in cell growth representing a local reservoir of cells. Conversely, an environment promoting cell migration together with cell types presenting a high rate of growth can present a rapid increase in number and dimension of spheroids but also a rapid decrease in number and size of spheroids formed, followed by a new increase. This can be justified by a rapid growth followed by a sudden cell death rapidly washed out, allowing a new rise of the wave of growth when the availability of oxygen and nutrients is newly sufficient to grow up a new generation of cells.

A further important consideration is that the results obtained in this work with the use of cost-effective products available for alimentary use, are comparable with the results obtained by many authors, the studies of which have been carried on with the use of commercial bioinks.

About the blends characterization, the tube inverting test gave the expected results, with a sol->gel transition time shorter for collagen-gelatine (45min), longer for collagen-alginate (more than 4hours), intermediate for collagen gelatine alginate blend. These results were depending on the presence/absence of gelatine in the blends considered.

The swelling test demonstrated the capability of water absorption of both the blends: the collagen-alginate blend increased its water content to 77% after 72 hours vs the collagen-gelatine-alginate, whose water content augmented of about 55% after a week. The dehydration test gave extremely different results, showing that the collagen-gelatine-alginate bulk, left at room temperature and in the room air, did not change its weight in a week. These different properties of the two blends, that make them different, can be used in different contests, because does not exist the right material but exist materials with different properties, that allow the use of each material in the most adequate contest. It is important to underline that the hydration capability tested thanks

to the swelling test, represents a fundamental aspect of the hydrogels used in tissue engineering as, the “in vivo tissue” and extracellular matrices present an high water content, physiologically.

Morphological analysis of the blends developed, showed two materials extremely transparent, easy to be observed in microscopy to visualise fibre formation, reticulation, cross-linking event and the behaviour of the cell laden.

Optical analysis after haematoxylin/eosin staining, showed a matrix (formed by the blends), very similar to a living ECM, adequate for cell growth and spheroid formation.

A disadvantage of this technique of analysis with H&E staining, is represented by the fact that, histological procedure used in spheroid fixation, precludes the study of dynamic alterations in the spheroids overtime. In addition, sample fracture and deformation of morphology can occur during spheroid sectioning. Due to the delicate nature and small size of spheroids, the fixation time may need to be reduced, with respect to biopsies or organ fragments *[Vielreicher M. et al., (2013)].*

In this research of cost-effective biomaterials for the realization of tissue phantoms, were only included the simplest tests and techniques of analysis, widely available at a lower cost. The most expensive device used in the present work was represented by the Anton Paar MCR 702e MultiDrive Rheometer, available at the Department of Science and Engineering of Materials, Environment and Urban Planning (SIMAU) of the Engineering Faculty of Università Politecnica delle Marche.

About bioactive molecules and growth factors, representing the third element of a bioink, DNA is an essential biological macromolecule for the development and normal operation of organisms. It is widely used in modern biology and biochemistry, mainly in the field of genetic engineering. However, it can also be applied in 3D bioprinting to prepare gene-active bioinks and combine with bone marrow mesenchymal stem cells, providing a new idea for the treatment of bone defect regeneration *[Cunniffe G.M. et al., (2017)].* It is arguable that also in this area of research the use of tissue phantom can be extremely supportive.

8. Conclusions

In the past decades, 3D-printing has become an extremely popular multi-functional technology platform for the rapid manufacture of synthetic substitutes for tissue engineering (TE) *[Memarian P. et al., (2021)].*

3D-printing technology can precisely control the appearance and internal structure of printed objects through computer - aided design modelling (CAD*) [Palmara G. et al., (2021)].*

3D-bioprinting can integrate diverse types of living cells into 3D structures composed of traditional biomaterials, creating artificial grafts able to regenerate damaged tissues *[Cheng X. et al., (2021)].*

At present, the most common 3D-bioprinted artificial scaffolds for tissues or organs in the medical field include skin, nerves, blood vessels, cartilage and bones *[Lin J.et al., (2018); Setacci C. et al., (2018); Yan W.C. et al., (2018)].*

Almost all cells in the human body can be used for bioprinting. The main difficulty of 3D printing cells is still maintaining cell activity and their original functions and phenotype. This aspect requires further reformulation and improvement of 3D printing technology to achieve the desired therapeutic effect.

3D-bioprinting together with other biological manufacturing methods represent a set of tools for the use of materials, cells and molecules to construct *on-demand* customized structures in a reproducible way *[Prendergast M.E. and Burdick J.A., (2020)].*

This technology is also used for drug delivery *[Sandler N. and Preis M., (2016); van der Elst L. et al., (2021)]*: the advancement in technology has made it possible to realize personalized drug dosage regimens with 3D-printing technology, which has the characteristics of flexibility and precise control *[Sandler N. and Preis M., (2016)].*

The use of cost-effective biomaterials for the 3D-bioprinting of scaffolds able to support cell growth, represents an important tool in biology, medical, pharmacology, cancer research. The availability of simplified models, fast to prepare and obtained at low cost, can be used as tissue phantoms for the study of disease development and in preclinical trials for testing new drugs.

The development of preclinical models able to recapitulate patient solid tumour and microenvironment, can represent the possibility to improve the success rate in anticancer drug

development. Since the importance of the extracellular matrix (ECM) in cell behaviour become clear, three-dimensional (3D) cell culture systems were considered fundamental to replicate the avascular solid tumour, by allowing cancer cells to be cultured, either alone or in co-culture with other cell types, mimicking the structural architecture of the tumour, with its classical cell–cell and cell–ECM interactions *[Bissell M.J., (2007); Ravi M. et al. (2015); Białkowska, K. et al., (2020); Shehzad A. et al., (2019)].*

Based on the the final comment of the Biotechnologist who worked with the blends, who affirmed that *"The reticula formed can be used like a biopsy…. their structure appears intact",* and considering the results obtained in this work, perfectly coherent with the most recent advancements in this area of research, it is possible to conclude that, cost-effective biomaterials for 3D-bioprinted scaffolds, represent a valid option in different areas of research.

Tissue phantoms have also a great potential in the educational field: tissue engineering (TE) is becoming an important topic in different academic branches (medicine, biology, biotechnology, bioengineering, science of material, pharmacology and further sectors). The availability of tissue phantoms prepared with cost-effective materials, would make it possible the introduction of practical activities for the students in this new research area. The possibility to create low-cost tissue phantoms with the use of cheap materials largely available, could allow students to meet a new technology, in the present non widely known because of the high costs of the bioink cartridges commercially available. The possibility to create a library of these materials, classified on the base of composition and properties, would allow to practically demonstrate to a future generation of researchers what 3D-bioprinting means, the potential of this technology in many fields of research.

Acknowledgments

I wish to remember all those who gave me their help in this work with their suggestions, observations and criticises: my gratitude goes out to all of them.

Thank you to Prof. Francesca Tittarelli, Head of Laboratories at SIMAU Department, Faculty of Engineering, Università Politecnica delle Marche, where I developed my blends.

Thank you to Prof. Tiziano Bellezze, Microscope Room Manager at the SIMAU Department, Faculty of Engineering, Università Politecnica delle Marche, and to the laboratory technician Sig. Giampaolo Giuliani who trained me at the use of the microscopes I used to check the optical properties of the blends, reticulation and crosslinking formation.

Thank you to Prof. Pasquapina Ciarmela, Department of Experimental and Clinical Medicine, Università Politecnica delle Marche and Prof. Francesca Luzi, SIMAU Department, Faculty of Engineering, Università Politecnica delle Marche, both co-supervisors, the contribution of which allowed the realization of the present work.

Thank you to Dott.ssa Stefania Greco, Department of Experimental and Clinical Medicine, Università Politecnica delle Marche, and to Dott. Abel Duménigo González, PhD student at the same Department, with whom I worked in the printing stage of the scaffold developement, testing the printability of the bioblends selected at the 3D Cellink Incredible+ bioprinter, and the cell biocompatibility in the post printing stage.

Thank you to the student collegues of mine, present in the SIMAU Department, with which I shared for a period the work performed in this area of research.

Thank you to Dr. Orlando Favoni, the laboratory technician working with Prof. Alida Mazzoli, who was completely available with us, allowing the preparation of the home-made solutions necessary for our work, giving us reccomandations about safety and checking the full respect of the rules with the use of chemical products.

And, finally, my thank you and gratitude goes to Prof. Alida Mazzoli, SIMAU Department, Faculty of Engineering, Supervisor of mine, who allowed me to work in her Department for the realization of this thesis, following all the steps of the present work.

To all of them I wish to tell

Thank you

References

1. Agarwal, T., Chiesa, I., Presutti, D., Irawan, V., Vajanthri, K. Y., Costantini, M., et al. (2021). Recent Advances in Bioprinting Technologies for Engineering Different Cartilage-Based Tissues. Mater. Sci. Eng. C 123, 112005.
2. Akbarzadeh R, Yousefi AM. Effects of processing parameters in thermally induced phase separation technique on porous architecture of scaffolds for bone tissue engineering. J Biomed Mater Res B Appl Biomater 2014;102(6):1304–15.
3. Akkineni AR, Ahlfeld T, Lode A, Gelinsky M. A versatile method for combining different biopolymers in a core/shell fashion by 3D plotting to achieve mechanically robust constructs. Biofabrication 2016;8(4):045001.
4. Aldrich, A., Kuss, M. A., Duan, B., and Kielian, T. (2019). 3D Bioprinted Scaffolds Containing Viable Macrophages and Antibiotics Promote Clearance of Staphylococcus Aureus Craniotomy-Associated Biofilm Infection. ACS Appl. Mat. Interfaces 11, 12298–12307. doi:10.1021/acsami.9b00264
5. Amler, A. K., Dinkelborg, P. H., Schlauch, D., Spinnen, J., Stich, S., Lauster, R., et al. (2021). Comparison of the Translational Potential of Human Mesenchymal Progenitor Cells from Different Bone Entities for Autologous 3D Bioprinted Bone Grafts. Int. J. Mol. Sci. 22, 796. doi:10.3390/ijms22020796.
6. Apelgren, P., Amoroso, M., Säljö, K., Montelius, M., Lindahl, A., Stridh Orrhult, L., et al. (2021). Vascularization of Tissue Engineered Cartilage - Sequential In Vivo MRI Display Functional Blood Circulation. Biomaterials 276, 121002.
7. Ashammakhi, N., Ahadian, S., Pountos, I., Hu, S.-K., Tellisi, N., Bandaru, P., et al. (2019). In Situ Three-Dimensional Printing for Reparative and Regenerative Therapy. Biomed. Microdevices 21, 42. doi:10.1007/s10544-019-0372-2.
8. Atala A, Bauer SB, Soker S, Yoo JJ, Retik AB. Tissue-engineered autologous bladders for patients needing cystoplasty. Lancet 2006;367(9518):1241–6.
9. Alzahrani E.O., Asiri A., El-Dessoky M.M., Kuang Y. (2014). Quiescence as an explanation of Gompertzian tumor growth revisited. Mathematical Biosciences 254 (2014) 76–82.
10. Banks J. Adding value in additive manufacturing: Researchers in the United Kingdom and Europe look to 3D printing for customization. IEEE Pulse 2013;4(6):22–6.
11. Bedell, M. L., Navara, A. M., Du, Y., Zhang, S., and Mikos, A. G. (2020). Polymeric Systems for Bioprinting. Chem. Rev. 120, 10744–10792. doi:10.1021/acs. chemrev.9b00834.

12. Bercea, M. (2023). Rheology as a tool for finetuning the properties of printable bioinspired gels, Molecules 28 (2023) 2766, https://doi.org/10.3390/molecules28062766.
13. Bertassoni LE, Cardoso JC, Manoharan V, Cristino AL, Bhise NS, Araujo WA, et al. Direct-write bioprinting of cell-laden methacrylated gelatin hydrogels. Biofabrication 2014;6(2):024105.
14. Bhatt, A., and Anbarasu, A. (2017). Nanoscale Biomaterials for 3D Printing. Iosrjpbs 12, 80–86. doi:10.9790/3008-1203068086
15. Białkowska, K.; Komorowski, P.; Bryszewska, M.; Miłowska, K. Spheroids as a Type of Three-Dimensional Cell Cultures-Examples of Methods of Preparation and the Most Important Application. Int. J. Mol. Sci. 2020, 21, 6225.
16. Billiet, T., Gevaert, E., De Schryver, T., Cornelissen, M., and Dubruel, P. (2014). The 3D Printing of Gelatin Methacrylamide Cell-Laden Tissue-Engineered Constructs with High Cell Viability. Biomaterials 35, 49–62. doi:10.1016/j. biomaterials.2013.09.078.
17. Birgersdotter, A.; Sandberg, R.; Ernberg, I. Gene expression perturbation in vitro–a growing case for three-dimensional (3D) culture systems. Semin. Cancer Biol. 2005, 15, 405–412.
18. Birk D.E., Bruckner P.: Collagen Suprastructures. Collagen. Springer (2015) 185-205.
19. Bissell, M.J. Architecture Is the Message, The role of extracellular matrix and 3-D structure in tissue-specific gene expression and breast cancer. Pezcoller Found J. 2007, 16, 2–17.
20. Blaeser, A., Duarte Campos, D. F., Puster, U., Richtering, W., Stevens, M. M., and Fischer, H. (2016). Controlling Shear Stress in 3D Bioprinting Is a Key Factor to Balance Printing Resolution and Stem Cell Integrity. Adv. Healthc. Mat. 5, 326–333. doi:10.1002/adhm.201500677
21. Bose, S.; Vahabzadeh, S.; Bandyopadhyay, A. Bone tissue engineering using 3D printing. Mater. Today 2013, 16, 496–504.
22. Bouhadir, K. H., Lee, K. Y., Alsberg, E., Damm, K. L., Anderson, K. W., and Mooney, D. J. (2001). Degradation of Partially Oxidized Alginate and its Potential Application for Tissue Engineering. Biotechnol. Prog. 17, 945–950. doi:10.1021/bp010070p
23. Brodsky B. and Ramshaw J.: The collagen Triple – Helix Structure. Matrix Biology (1997) 545-554
24. Buttgereit A, Boccaccini A, Friedrich O. (2013). Taking a deep look: modern microscopy technologies to optimize the design and functionality of biocompatible scaffolds for tissue engineering in regenerative medicine. J R Soc Interface 10: 20130263. http://dpx.doi.org/10.1098/rsif.2013.0263

25. Cai R., Gimenez-Camino N., Xiao M., Bi S., Di Vito K.A. (2023). Technological advances in three-dimensional skin tissue engineering. De Gruyter: Reviews on Advanced Materials Science 2023; 62:20220289.
26. Camacho, P., Behre, A., Fainor, M., Seims, K. B., and Chow, L. W. (2021). Spatial Organization of Biochemical Cues in 3D-Printed Scaffolds to Guide Osteochondral Tissue Engineering. Biomater. Sci. 9, 6813–6829. doi:10.1039/ d1bm00859e
27. Campbell JJ, Husmann A, Hume RD, Watson CJ, Cameron RE. Development of three-dimensional collagen scaffolds with controlled architecture for cell migration studies using breast cancer cell lines. Biomaterials 2017;114:34–43.
28. Chan, G., and Mooney, D. J. (2013). Ca2+ Released from Calcium Alginate Gels Can Promote Inflammatory Responses In Vitro and In Vivo. Acta Biomater. 9, 9281–9291. doi:10.1016/j.actbio.2013.08.002.
29. Chang, R.; Emami, K.; Wu, H.L.; Sun, W. Biofabrication of a three-dimensional liver micro-organ as an in vitro drug metabolism model. Biofabrication 2010, 2, 045004.
30. Charras G, Sahai E. Physical influences of the extracellular environment on cell migration. Nature Reviews Molecular Cell Biology. 2014; 15(12):813–824. https://doi.org/10.1038/nrm3897.
31. Chatterjee, K., and Ghosh, T. K. (2020). 3D Printing of Textiles: Potential Roadmap to Printing with Fibers. Adv. Mat. 32, 1902086. doi:10.1002/adma.201902086.
32. Chen, X., Yue, Z., Winberg, P. C., Lou, Y.-R., Beirne, S., and Wallace, G. G. (2021). 3D Bioprinting Dermal-like Structures Using Species-specific Ulvan. Biomater. Sci. 9, 2424–2438. doi:10.1039/d0bm01784a.
33. Cheng YL, Chen YW, Wang K, Shie MY. Enhanced adhesion and differentiation of human mesenchymal stem cell inside apatite-mineralized/poly(dopamine)- coated poly(ε-caprolactone) scaffolds by stereolithography. J Mater Chem B. 2016;4(38):6307–15.
34. Cheng L., Suresh K, S., He, H., Rajput, R. S., Feng, Q., Ramesh, S., et al. (2021). 3D Printing of Micro- and Nanoscale Bone Substitutes: A Review on Technical and Translational Perspectives. Ijn Vol. 16, 4289–4319. doi:10.2147/ijn.s311001.
35. Cheng G, Tse J, Jain R, Munn L. Micro-Environmental Mechanical Stress Controls Tumor Spheroid Size and Morphology by Suppressing Proliferation and Inducing Apoptosis in Cancer Cells. PLoS ONE. 2009; 4(2):e4632.

36. Choudhury, D., Tun, H. W., Wang, T., and Naing, M. W. (2018). Organ-Derived Decellularized Extracellular Matrix: A Game Changer for Bioink Manufacturing? Trends Biotechnol. 36, 787–805. doi:10.1016/j.tibtech.2018.03.003.
37. Cowie J., Arrighi V. Polymers: Chemistry and Physics of Modern Materials, 3rd ed.; CRC Press, 2007.
38. Cheremisinoff, N. Introduction to Polymer Rheology and Processing; CRC Press, 1993.
39. Cunniffe, G. M., Gonzalez-Fernandez, T., Daly, A., Sathy, B. N., Jeon, O., Alsberg, E., et al. (2017). Three-Dimensional Bioprinting of Polycaprolactone Reinforced Gene Activated Bioinks for Bone Tissue Engineering. Tissue Eng. Part A 23, 891–900. doi:10.1089/ten.tea.2016.0498.
40. Demirtaş, T. T., Irmak, G., and Gümüşderelioğlu, M. (2017). A Bioprintable Form of Chitosan Hydrogel for Bone Tissue Engineering. Biofabrication 9, 035003. doi:10.1088/1758-5090/aa7b1d.
41. Derakhshanfar, S.; Mbeleck, R.; Xu, K.G.; Zhang, X.Y.; Zhong, W.; Xing, M. 3D bioprinting for biomedical devices and tissue engineering: A review of recent trends and advances. Bioact. Mater. 2018, 3, 144–156.
42. Dorishetty, Pramod, Rajkamal Balu, Amy Gelmi, Jitendra P. Mata, Naba K. Dutta, and Namita Roy Choudhury. "3D printable soy/silk hybrid hydrogels for tissue engineering applications." Biomacromolecules 22, no. 9 (2021): 3668-3678.).
43. Dzobo, K., Motaung, K. S. C. M., and Adesida, A. (2019). Recent Trends in Decellularized Extracellular Matrix Bioinks for 3D Printing: An Updated Review. Ijms 20, 4628. doi:10.3390/ijms20184628.
44. Ehrbar M, Sala A, Lienemann P, Ranga A, Mosiewicz K, Bittermann A et al. Elucidating the Role of Matrix Stiffness in 3D Cell Migration and Remodeling. Biophysical Journal. 2011; 100(2):284–293. https://doi.org/10.1016/j.bpj.2010.11.082 PMID: 21244824.
45. Frantz C, Stewart K, Weaver V. The extracellular matrix at a glance. Journal of Cell Science. 2010; 123 (24):4195–4200. https://doi.org/10.1242/jcs.023820.
46. Freeman S, Calabro S, Williams R, Jin S and Ye K (2022) Bioink Formulation and Machine LearningEmpowered Bioprinting Optimization. Front. Bioeng. Biotechnol. 10:913579. doi: 10.3389/fbioe.2022.913579.
47. Furth ME, Atala A, Van Dyke ME. Smart biomaterials design for tissue engineering and regenerative medicine. Biomaterials 2007;28(34):5068–73.

48. Garcia-Villen F, Guembe A, Rey JM, et al., 2023, Characterization and assessment of new fibrillar collagen inks and bioinks for 3D printing and bioprinting. Int J Bioprint, 9(3): 712. https://doi.org/10.18063/ijb.712.
49. Gattazzo, F., Urciuolo, A., and Bonaldo, P. (2014). Extracellular Matrix: a Dynamic Microenvironment for Stem Cell Niche. Biochimica Biophysica Acta (BBA) - General Subj. 1840, 2506–2519. doi:10.1016/j.bbagen.2014.01.010
50. Gelse K., Pöschl E., Aigner T.: Collagens – structure, function, and biosynthesis. Advanced Drug Delivery Reviews 55 (2003) 1531-1546.
51. Georgakoudi I, Rice WL, Hronik-Tupaj M, Kaplan DL. 2008 Optical spectroscopy and imaging for the noninvasive evaluation of engineered tissues. Tissue Eng. B, Rev. 14, 321– 340. (doi:10.1089/ten.teb. 2008.0248)
52. Ghasemi-Mobarakeh L, Prabhakaran MP, Morshed M, Nasr-Esfahani MH, Ramakrishna S. Electrospun poly(epsilon-caprolactone)/gelatin nanofibrous scaffolds for nerve tissue engineering. Biomaterials 2008;29(34):4532–9.
53. Gold, K. A., Saha, B., Rajeeva Pandian, N. K., Walther, B. K., Palma, J. A., Jo, J., et al. (2021). 3D Bioprinted Multicellular Vascular Models. Adv. Healthc. Mater 10, e2101141. doi:10.1002/adhm.202101141.
54. Goldhammer, N.; Kim, J.; Timmermans-Wielenga, V.; Petersen, O.W. Characterization of organoid cultured human breast cancer. Breast Cancer Res. 2019, 21, 141.
55. Gompertz B., On the nature of the function expressive of the law of human mortality, and on a new mode of determining the value of life contingencies, Philos. Trans. Royal Soc. London 115 (1825) 513–583.
56. Gonçalves IG, Garcia-Aznar JM (2021). Extracellular matrix density regulates the formation of tumour spheroids through cell migration. PLoS Comput Biol 17(2): e1008764. https://doi.org/ 10.1371/journal.pcbi.1008764.
57. Greco S, Pellegrino P, Giampieri F, Capocasa F, Delli Carpini G, Battino M, Mezzetti B, Giannubilo SR, Ciavattini A, Ciarmela P. The In Vitro Effects of Romina Strawberry Extract on 3D Uterine Leiomyosarcoma Cells. Nutrients. 2023 May 30;15(11):2557. doi: 10.3390/nu15112557. PMID: 37299521; PMCID: PMC10255497).
58. Groll, J., Boland, T., Blunk, T., Burdick, J. A., Cho, D.-W., Dalton, P. D., et al. (2016). Biofabrication: Reappraising the Definition of an Evolving Field. Biofabrication 8, 013001. doi:10.1088/1758-5090/8/1/013001.

59. Gross BC, Erkal JL, Lockwood SY, Chen C, Spence DM. Evaluation of 3D printing and its potential impact on biotechnology and the chemical sciences. Anal Chem 2014;86(7):3240–53.
60. Guarino V, Ambrosio L. The synergic effect of polylactide fiber and calcium phosphate particle reinforcement in poly epsilon-caprolactone-based composite scaffolds. Acta Biomater 2008; 4(6):1778–87.
61. Haaparanta AM, Järvinen E, Cengiz IF, Ellä V, Kokkonen HT, Kiviranta I, et al. Preparation and characterization of collagen/PLA, chitosan/PLA, and collagen/ chitosan/PLA hybrid scaffolds for cartilage tissue engineering. J Mater Sci Mater Med 2014;25(4):1129–36.
62. Hanahan, D.; Weinberg, R.A. Hallmarks of cancer: The next generation. Cell 2011, 144, 646–674.
63. Ho CM, Mishra A, Lin PT, Ng SH, Yeong WY, Kim YJ, et al. 3D printed polycaprolactone carbon nanotube composite scaffolds for cardiac tissue engineering. Macromol Biosci 2017;17(4):1600250.
64. Holmes D., Lu Y., Starborg T., et al.: Collagen Fibril Assembly and Function. Current Topics in Developmental Biology 130 (2018) 107-142.
65. Hospodiuk, M., Dey, M., Sosnoski, D., and Ozbolat, I. T. (2017). The Bioink: A Comprehensive Review on Bioprintable Materials. Biotechnol. Adv. 35, 217–239. doi:10.1016/j.biotechadv.2016.12.006.
66. Hribar KC, Soman P, Warner J, Chung P, Chen S. Light-assisted direct-write of 3D functional biomaterials. Lab Chip 2014;14(2):268–75.
67. Huang, K.; Ma, H.; Liu, J.; Huo, S.; Kumar, A.; Wei, T.; Zhang, X.; Jin, S.; Gan, Y.; Wang, P.C. Size-dependent localization and penetration of ultrasmall gold nanoparticles in cancer cells, multicellular spheroids, and tumors in vivo. ACS Nano 2012, 6, 4483–4493.
68. Hughes, F.J.; Turner, W.; Belibasakis, G.; Martuscelli, G. Effects of growth factors and cytokines on osteoblast differentiation. Periodontol. 2000 2006, 41, 48–72.
69. Ibrahim, S.F.; Azam, N.A.N.M.; Amin, K.A.M. Sodium alginate film: The effect of crosslinker on physical and mechanical properties. IOP Conf. Ser. Mater. Sci. Eng. 2019, 509, 012063).
70. Imamura, Y.; Mukohara, T.; Shimono, Y.; Funakoshi, Y.; Chayahara, N.; Toyoda, M.; Kiyota, N.; Takao, S.; Kono, S.; Nakatsura, T.; et al. Comparison of 2D- and 3D-culture models as drug-testing platforms in breast cancer. Oncol. Rep. 2015, 33, 1837–1843.

71. Itoh M, Nakayama K, Noguchi R, Kamohara K, Furukawa K, Uchihashi K, et al. Scaffold-free tubular tissues created by a Bio-3D printer undergo remodeling and endothelialization when implanted in rat aortae. PLoS One 2015;10(9):e0136681.
72. Jentsch, S., Nasehi, R., Kuckelkorn, C., Gundert, B., Aveic, S., and Fischer, H. (2021). Multiscale 3D Bioprinting by Nozzle-Free Acoustic Droplet Ejection. Small Methods 5, 2000971. doi: 10.1002/smtd.202000971.
73. Jones, N. Science in three dimensions: The print revolution. Nature 2012, 487, 22–23.
74. Kan Wang, Chia-Che Ho, Chuck Zhang, Ben Wang. A Review on the 3D Printing of Functional Structures for Medical Phantoms and Regenerated Tissue and Organ Applications. Engineering 3 (2017) 653–662.
75. Kang, D., Ahn, G., Kim, D., Kang, H.-W., Yun, S., Yun, W.-S., et al. (2018). Pre-Set Extrusion Bioprinting for Multiscale Heterogeneous Tissue Structure Fabrication. Biofabrication 10, 035008. doi:10.1088/1758-5090/aac70b
76. Kang, H.W.; Lee, S.J.; Ko, I.K.; Kengla, C.; Yoo, J.J.; Atala, A. A 3D bioprinting system to produce human-scale tissue constructs with structural integrity. Nat. Biotechnol. 2016, 34, 312–319.
77. Kao CT, Lin CC, Chen YW, Yeh CH, Fang HY, Shie MY. Poly(dopamine) coating of 3D printed poly(lactic acid) scaffolds for bone tissue engineering. Mater Sci Eng C Mater Biol Appl 2015; 56:165–73.
78. Kiernan J. 1999 Histological & histochemical methods: theory and practice, 3rd edn. Oxford, UK: Butterworth Heinemann;
79. Kim YB et al. Mechanically reinforced cell-laden scaffolds formed using alginate-based bioink printed onto the surface of a PCL/alginate mesh structure for regeneration of hard tissue. Journal of Colloid and Interface Science 461 (2016) 359–368.
80. Kitaeva, K.V.; Rutland, C.S.; Rizvanov, A.A.; Solovyeva, V.V. Cell Culture Based in vitro Test Systems for Anticancer Drug Screening. Front. Bioeng. Biotechnol. 2020, 8, 322.
81. Klein GT, Lu Y, Wang MY. 3D printing and neurosurgery—Ready for prime time? World Neurosurg 2013;80(3–4):233–5.
82. Knowlton, S., Anand, S., Shah, T., and Tasoglu, S. (2018). Bioprinting for Neural Tissue Engineering. Trends Neurosci. 41, 31–46. doi: 10.1016/j.tins.2017.11.001.
83. Kozusko F., Bajzer Z. Combining Gompertzian growth and cell population dynamics. Mathematical Biosciences 185 (2003) 153–167.

84. Kulkarni, P., Marsan, A., and Dutta, D. (2000). A Review of Process Planning Techniques in Layered Manufacturing. Rapid Prototyp. J. 6, 18–35.
85. Lee J, Cuddihy MJ, Kotov NA. 2008 Threedimensional cell culture matrices: state of the art. Tissue Eng. B, Rev. 14, 61– 86. (doi:10.1089/teb. 2007.0150).
86. Lee, J., Hong, J., Kim, W., and Kim, G. H. (2020). Bone-Derived Decm/Alginate Bioink for Fabricating a 3D Cell-Laden Mesh Structure for Bone Tissue Engineering. Carbohydr. Polym. 250, 116914. doi:10.1016/j.carbpol.2020. 116914.
87. Lin, J., Zhou, Z., Guan, J., Zhu, Y., Liu, Y., Yang, Z., et al. (2018). Using Three Dimensional Printing to Create Individualized Cranial Nerve Models for Skull Base Tumor Surgery. World Neurosurg. 120, e142–e152. doi:10.1016/j.wneu.2018.07.236.
88. Liu N, Zhang X, Guo Q, Wu T and Wang Y (2022) 3D Bioprinted Scaffolds for Tissue Repair and Regeneration. Front. Mater. 9:925321. doi: 10.3389/fmats.2022.925321.
89. Lo C, Wang H, Dembo M, Wang Y. Cell Movement Is Guided by the Rigidity of the Substrate. Biophysical Journal. 2000; 79(1):144–152. https://doi.org/10.1016/S0006-3495(00)76279-5
90. Lv D, Hu Z, Lu L, Lu H, Xu X. Three dimensional cell culture: A powerful tool in tumor research and drug discovery. Oncology Letters. 2017;
91. Ma, D., Gao, R., Li, M., and Qiu, J. (2022). Mechanical and Medical Imaging Properties of 3D-printed Materials as Tissue Equivalent Materials. J. Appl. Clin. Med. Phys. 23, e13495. doi:10.1002/acm2.13495.
92. Ma, H.L.; Jiang, Q.; Han, S.; Wu, Y.; Tomshine, J.C.; Wang, D.; Gan, Y.; Zou, G.; Liang, X.J. Multicellular tumor spheroids as an in vivo-like tumor model for three-dimensional imaging of chemotherapeutic and nano material cellular penetration. Mol. Imaging 2012, 11, 487–498.
93. Malda J., Visser J., Melchels F.P., Jüngst T., Hennink W.E., Dhert W.J.A., Groll J., Hutmacher D.W. (2013) 25th Anniversary Article: Engineering Hydrogels for Biofabrication. Adv. Mater. 2013, 25, 5011–5028
94. Mao, H., Yang, L., Zhu, H., Wu, L., Ji, P., Yang, J., et al. (2020). Recent Advances and Challenges in Materials for 3D Bioprinting. Prog. Nat. Sci. Mater. Int. 30, 618–634. doi:10.1016/j.pnsc.2020.09.015.
95. Marelli B, Ghezzi CE, Mohn D, Stark WJ, Barralet JE, Boccaccini AR, Nazhat SN. 2011 Accelerated mineralization of dense collagen-nano bioactive glass hybrid gels increases

scaffold stiffness and regulates osteoblastic function. Biomaterials 32, 8915–8926. (doi:10.1016/j.biomaterials.2011.08.016).

96. Matai, I., Kaur, G., Seyedsalehi, A., Mcclinton, A., and Laurencin, C. T. (2020). Progress in 3D Bioprinting Technology for Tissue/organ Regenerative Engineering. Biomaterials 226, 119536. doi: 10.1016/j.biomaterials.2019.119536
97. Mazzocchi, A., Devarasetty, M., Huntwork, R., Soker, S., and Skardal, A. (2018). Optimization of Collagen Type I-Hyaluronan Hybrid Bioink for 3D Bioprinted Liver Microenvironments. Biofabrication 11, 015003. doi: 10.1088/1758-5090/ aae543
98. Melchels FPW, Dhert WJA, Hutmacher DW, Mald J. Development and characterisation of a new bioink for additive tissue manufacturing. J Mater Chem B 2014;2(16):2282–9.
99. Memarian, P., Sartor, F., Bernardo, E., Elsayed, H., Ercan, B., Delogu, L. G., et al. (2021). Osteogenic Properties of 3D-Printed Silica-Carbon-Calcite Composite Scaffolds: Novel Approach for Personalized Bone Tissue Regeneration. Int. J. Mol. Sci. 22, 475. doi:10.3390/ijms22020475.
100. Meyer M.: Processing of collagen based biometrerials and the resulting materials properties. BioMedical Engineering OnLine (2019).
101. Mezger T. G., The Rheology Handbook, 3rd revised ed.; Vincentz Network, 2011.
102. Mickel W, Mu¨nster S, Jawerth LM, Vader DA, Weitz DA, Sheppard AP, Mecke K, Fabry B, Schroder-Turk GE. 2008 Robust pore size analysis of filamentous networks from three-dimensional confocal microscopy. Biophys. J. 95, 6072– 6080. (doi:10. 1529/biophysj.108.135939).
103. Mironov V, Boland T, Trusk T, Forgacs G, Markwald RR. Organ printing: Computeraided jet-based 3D tissue engineering. Trends Biotechnol 2003;21(4):157–61.
104. Mironov V, Visconti RP, Kasyanov V, Forgacs G, Drake CJ, Markwald RR. Organ printing: Tissue spheroids as building blocks. Biomaterials 2009;30(12):2164– 74.
105. Movilla N, Borau C, Valero C, Garcı´a-Aznar J. Degradation of extracellular matrix regulates osteoblast migration: A microfluidic-based study. Bone. 2018; 107:10–17. https://doi.org/10.1016/j.bone.2017.10. 025.
106. Munaz, A., Vadivelu, R. K., St. John, J., Barton, M., Kamble, H., and Nguyen, N.-T. (2016). Three-dimensional Printing of Biological Matters. J. Sci. Adv. Mater. Devices 1, 1–17. doi: 10.1016/j.jsamd.2016.04.001.

107. Murphy SV, Atala A. 3D bioprinting of tissues and organs. Nat Biotechnol. 2014 Aug;32(8):773-85. doi: 10.1038/nbt.2958. PMID: 25093879.12.

108. Nacu, Isabella, Maria Bercea, Loredana Elena Niță, Cătălina Anișoara Peptu, Maria Butnaru, and Liliana Vereștiuc. "3D bioprinted scaffolds based on functionalized gelatin for soft tissue engineering." Reactive and Functional Polymers (2023): 105636.)

109. Najafi, M.; Farhood, B.; Mortezaee, K. Extracellular matrix (ECM) stiffness and degradation as cancer drivers. J. Cell Biochem. 2019, 120, 2782–2790.

110. Neufurth, M., Wang, X., Schröder, H. C., Feng, Q., Diehl-Seifert, B., Ziebart, T., et al. (2014). Engineering a Morphogenetically Active Hydrogel for Bioprinting of Bioartificial Tissue Derived from Human Osteoblast-like SaOS-2 Cells. Biomaterials 35, 8810–8819.

111. Nyga A, Cheema U, Loizidou M. 3D tumour models: novel in vitro approaches to cancer studies. Journal of Cell Communication and Signaling. 2011; 5(3):239–248.

112. Oheim M, Beaurepaire E, Chaigneau E, Mertz J, Charpak S. 2001 Two-photon microscopy in brain tissue: parameters influencing the imaging depth. J. Neurosci. Methods 111, 29 – 37. (doi: 10.1016/ S0165-0270(01)00438-1)

113. Olague P. B. and Kreinovich V., "Why Growth of Cancerous Tumors Is Gompertzian: A Symmetry-Based Explanation" (2016). Departmental Technical Reports (CS). 1073. https://scholarworks.utep.edu/cs_techrep/1073

114. Orr SB, Chainani A, Hippensteel KJ, Kishan A, Gilchrist C, Garrigues NW, et al. Aligned multilayered electrospun scaffolds for rotator cuff tendon tissue engineering. Acta Biomater 2015; 24:117–26.

115. Ouyang L, Highley CB, Sun W, Burdick JA. A generalizable strategy for the 3D bioprinting of hydrogels from nonviscous photo-crosslinkable inks. Adv Mater 2017;29(8):1604983.

116. Owczarzy A., Kurasiński R., Kulig C., Rogóż W., Szkudlarek Z., Maciążek-Jurczyk M. COLLAGEN - STRUCTURE, PROPERTIES AND APPLICATION [Engineering of Biomaterials 156 (2020) 17-23] doi: 10.34821/eng.biomat.156.2020.17-23.

117. Palmara, G., Frascella, F., Roppolo, I., Chiappone, A., and Chiadò, A. (2021). Functional 3D Printing: Approaches and Bioapplications. Biosens. Bioelectron. 175, 112849. doi: 10.1016/j.bios.2020.112849.

118. Park, S., Shou, W., Makatura, L., Matusik, W., and Fu, K. (2022). 3D Printing of Polymer Composites: Materials, Processes, and Applications. Matter 5, 43–76. doi:10.1016/j.matt.2021.10.018.

119. Pathak A, Kumar S. Independent regulation of tumor cell migration by matrix stiffness and confinement. Proceedings of the National Academy of Sciences. 2012; 109(26):10334–10339. https://doi.org/10. 1073/pnas.1118073109.

120. Pinto B., Henriques A.C., Silva P.M., Bousbaa H. Three-Dimensional Spheroids as In Vitro Preclinical Models for Cancer Research Pharmaceutics 2020, 12, 1186; doi:10.3390/pharmaceutics12121186 www.mdpi.com/journal/pharmaceutics.

121. Pitt, J.M.; Marabelle, A.; Eggermont, A.; Soria, J.C.; Kroemer, G.; Zitvogel, L. Targeting the tumor microenvironment: Removing obstruction to anticancer immune responses and immunotherapy. Ann. Oncol. 2016, 27, 1482–1492.

122. Place ES, Evans ND, Stevens MM. Complexity in biomaterials for tissue engineering. Nat Mater 2009;8(6):457–70.

123. Prendergast, M. E., and Burdick, J. A. (2020). Recent Advances in Enabling Technologies in 3D Printing for Precision Medicine. Adv. Mater 32, e1902516. doi:10.1002/adma.201902516.

124. Rana, D., Kumar, T. S. S., and Ramalingam, M. (2017). Impact of Nanotechnology on 3D Bioprinting. J. bionanosci 11, 1–6. doi:10.1166/jbns.2017.1417.

125. Rastogi, P., and Kandasubramanian, B. (2019). Review of Alginate-Based Hydrogel Bioprinting for Application in Tissue Engineering. Biofabrication 11, 042001. doi:10.1088/1758-5090/ab331e.

126. Ravi, M.; Paramesh, V.; Kaviya, S.R.; Anuradha, E.; Solomon, F.P. 3D cell culture systems: Advantages and applications. J. Cell Physiol. 2015, 230, 16–26.

127. Raya-Rivera A, Esquiliano DR, Yoo JJ, Lopez-Bayghen E, Soker S, Atala A. Tissueengineered autologous urethras for patients who need reconstruction: An observational study. Lancet 2011; 377(9772):1175–82.

128. c Blokzijl M.M., Levato R., Visser C.W., Castilho M., Hennink W.E. Vermonden, T.; Malda, J. (2018). Assessing Bioink Shape Fidelity to Aid Material Development in 3d Bioprinting. Biofabrication 2018, 10, 014102.

129. Ricard-Blum, S. (2011). The Collagen Family. Cold Spring Harb. Perspect. Biol. 3, a004978. doi:10.1101/cshperspect.a004978.

130. Roeder BA, Kokini K, Sturgis JE, Robinson JP, Voytik-Harbin SL. Tensile Mechanical Properties of Three-Dimensional Type I Collagen Extracellular Matrices With Varied Microstructure. Journal of Biomechanical Engineering. 2002; 124(2):214–22. https://doi.org/10.1115/1.1449904.

131. Roma-Rodrigues C, Mendes, R.; Baptista, P.V.; Fernandes, A.R. Targeting Tumor Microenvironment for Cancer Therapy. Int. J. Mol. Sci. 2019, 20, 840.

132. Sakr M.A., Sakthivel K., Hossain T., Shin S.R., Siddiqua S., Kim J., Kim K. (2021). Recent trends in gelatin methacryloyl nanocomposite hydrogels for tissue engineering, J. Biomed. Mater. Res. A. 110 (2021) 708–724, https://doi.org/10.1002/jbm. a.37310).

133. Sandler, N., and Preis, M. (2016). Printed Drug-Delivery Systems for Improved Patient Treatment. Trends Pharmacol. Sci. 37, 1070–1080. doi:10.1016/j.tips. 2016.10.002.

134. Sangaletti, S.; Chiodoni, C.; Tripodo, C.; Colombo, M.P. The good and bad of targeting cancer-associated extracellular matrix. Curr. Opin. Pharmacol. 2017, 35, 75–82.

135. Sapudom J, Pompe T. Biomimetic tumor microenvironments based on collagen matrices. Biomaterials Science. 2018; 6(8):2009–24. https://doi.org/10.1039/C8BM00303C.

136. Schwab A., Levato R., D'Este M., Piluso S., Eglin D., Malda J. Printability and Shape Fidelity of Bioinks in 3D Bioprinting. Chem. Rev. (2020), 120, 11028−11055.

137. Shehzad, A.; Ravinayagam, V.; AlRumaih, H.; Aljafary, M.; Almohazey, D.; Almofty, S.; Al-Rashid, N.A.; Al-Suhaimi, E.A. Application of Three-dimensional (3D) Tumor Cell Culture Systems and Mechanism of Drug Resistance. Curr. Pharm. Des. 2019, 25, 3599–3607.

138. Smith LE, Smallwood R, Macneil S. 2010 A comparison of imaging methodologies for 3D tissue engineering. Microsc. Res. Tech. 73, 1123 – 1133. (doi:10.1002/jemt.20859).

139. Sorushanova A., Delgado L., Wu Z., et al.: The Collagen Suprafamily: From Biosynthesis to Advanced Biomaterial Development. Advanced Materials 31 (2019) 1801651.

140. Tesei, A.; Sarnelli, A.; Arienti, C.; Menghi, E.; Medri, L.; Gabucci, E.; Pignatta, S.; Falconi, M.; Silvestrini, R.; Zoli, W. In vitro irradiation system for radiobiological experiments. Radiat. Oncol. 2013, 8, 257.

141. Valot, L., Martinez, J., Mehdi, A., and Subra, G. (2019). Chemical Insights into Bioinks for 3D Printing. Chem. Soc. Rev. 48, 4049–4086.

142. van der Elst, L., Faccini De Lima, C., Gokce Kurtoglu, M., Koraganji, V. N., Zheng, M., and Gumennik, A. (2021). 3D Printing in Fiber-Device Technology. Adv. Fiber Mat. 3, 59–75. doi: 10.1007/s42765-020-00056-6.

143. van der Worp, H.B.; Howells, D.W.; Sena, E.S.; Porritt, M.J.; Rewell, S.; O'Collins, V.; Macleod, M.R. Can animal models of disease reliably inform human studies? PLoS Med. 2010, 7, e1000245.

144. Vielreicher M, Schurmann S, Detsch R, Schmidt MA, Buttgereit A, Boccaccini A, Friedrich O. 2013 Taking a deep look: modern microscopy technologies to optimize the design and functionality of biocompatible scaffolds for tissue engineering in regenerative medicine. J R Soc Interface 10: 20130263.

145. Wang H, Yu H, Zhou X, Zhang J, Zhou H, Hao H, Ding L, Li H, Gu Y, Ma J, Qiu J and Ma D (2022) An Overview of Extracellular Matrix-Based Bioinks for 3D Bioprinting. Front. Bioeng. Biotechnol. 10:905438. doi: 10.3389/fbioe.2022.905438

146. Wang K., Ho C.C., Zhang C., Wang B. (2017) A Review on the 3D Printing of Functional Structures for Medical Phantoms and Regenerated Tissue and Organ Applications. Engineering 3 (2017) 653–662.

147. Warnke PH, Springer IN, Wiltfang J, Acil Y, Eufinger H, Wehmöller M, et al. Growth and transplantation of a custom vascularised bone graft in a man. Lancet 2004;364(9436):766–70.

148. Watt, F. M., and Huck, W. T. S. (2013). Role of the Extracellular Matrix in Regulating Stem Cell Fate. Nat. Rev. Mo.l Cell. Biol. 14, 467–473. doi:10.1038/ nrm3620.

149. Whitcomb, KJ. (2021) Determining the Linear Viscoelastic Region in Oscillatory Measurements https://www. tainstruments.com/pdf/literature/RH107.pdf

150. Wu, Y. Yu, J. Tan, L. Huang, B. Luo, L. Lu, C. Zhou 3D bioprinting of gellan gum and poly(ethylene glycol)diacrylate based hydrogels to produce human-scale constructs with high-fidelity Mater. Des., 160 (2018), pp. 486-495, 10.1016/j.matdes.2018.09.040;

151. Wust, S.; Godla, M.E.; Muller, R.; Hofmann, S. Tunable hydrogel composite with two-step processing in combination with innovative hardware upgrade for cell-based three-dimensional bioprinting. Acta Biomater. 2014, 10, 630–640.

152. Xu M., Xingrou Chen, Jingjing Rui, Yan Yu, Dongshi Gu, Jennifer Jin Ruan and Benfang Helen Ruan: Cell Growth Measurement DOI: http://dx.doi.org/10.5772/intechopen.86835.

153. Xu J., Chen X., Rui J,Yu Y., Gu D, Ruan JJ, Ruan BH. Cell Growth Measurement DOI: http://dx.doi.org/10.5772/intechopen.86835)

154. Yamada, K.M.; Cukierman, E. Modeling tissue morphogenesis and cancer in 3D. Cell 2007, 130, 601–610.

155. Yamaguchi H, Wyckoff J, Condeelis J. Cell migration in tumors. Current Opinion in Cell Biology. 2005; 17(5):559–564.

156. Yan, W.-C., Davoodi, P., Vijayavenkataraman, S., Tian, Y., Ng, W. C., Fuh, J. Y. H., et al. (2018). 3D Bioprinting of Skin Tissue: From Pre-processing to Final Product Evaluation. Adv. Drug Deliv. Rev. 132, 270–295. doi:10.1016/j.addr.2018.07.016.

157. Yang, Y., Zhang, Q., Xu, T., Zhang, H., Zhang, M., Lu, L., et al. (2020). Photocrosslinkable Nanocomposite Ink for Printing Strong, Biodegradable and Bioactive Bone Graft. Biomaterials 263, 120378. doi:10.1016/j. biomaterials.2020.120378.

158. Yeo M, Lee JS, Chun W, Kim GH. An innovative collagen-based cell-printing method for obtaining human adipose stem cell-laden structures consisting of core-sheath structures for tissue engineering. Biomacromolecules 2016;17(4):1365–75.

159. Yue, B. (2014). Biology of the Extracellular Matrix. J. Glaucoma 23, S20–S23. doi:10.1097/IJG.0000000000000108.

160. Yue, K., Trujillo-De Santiago, G., Alvarez, M. M., Tamayol, A., Annabi, N., and Khademhosseini, A. (2015). Synthesis, Properties, and Biomedical Applications of Gelatin Methacryloyl (Gelma) Hydrogels. Biomaterials 73, 254–271. doi:10. 1016/j.biomaterials.2015.08.045.

161. Zamir E, Geiger B. (2001) Molecular complexity and dynamics of cell-matrix adhesions. 2001 Journal of Cell Science 114(Pt 20):3583-90

162. Zhang, J.; Wehrle, E.; Rubert, M.; Müller, R. 3D Bioprinting of Human Tissues: Biofabrication, Bioinks, and Bioreactors. Int. J. Mol. Sci. 2021, 22, 3971.

163. Zhang et al. Factors affecting thermal stability of collagen from the aspects of extraction, processing and modification. Journal of Leather Science and Engineering (2020) 2:19 https://doi.org/10.1186/s42825-020-00033-0.

164. Zhanga K, Fenga W, Jina C. Protocol efficiently measuring the swelling rate of hydrogels. MethodsX 7 (2020) 1007.

165. Zopf DA, Hollister SJ, Nelson ME, Ohye RG, Green GE. Bioresorbable airway splint created with a three-dimensional printer. N Engl J Med 2013; 368(21):2043–5.